Numerical models for thermochemical degradation of thermally thick woody biomass, and their application in domestic wood heating appliances and grate furnaces

Inge Haberle[a,*], Øyvind Skreiberg[b], Joanna Łazar[a,b], Nils Erland L. Haugen[a,b]

[a] Department of Energy and Process Engineering, Norwegian University of Science and Technology, NTNU, Kolbjørn Hejes vei 1 B, 7491 Trondheim, Norway
[b] Department of Thermal Energy, SINTEF Energy Research, Postboks 4761 Torgard, 7465 Trondheim, Norway

ARTICLE INFO

ABSTRACT

This paper reviews the current state-of-the-art of numerical models used for thermochemical degradation and combustion of thermally thick woody biomass particles. The focus is on the theory of drying, devolatilization and char conversion with respect to their implementation in numerical simulation tools. An introduction to wood chemistry, as well as the physical characteristics of wood, is also given in order to facilitate the discussion of simplifying assumptions in current models. Current research on single, densified or non-compressed, wood particle modeling is presented, and modeling approaches are compared. The different modeling approaches are categorized by the dimensionality of the model (1D, 2D or 3D), and the one-dimensional models are separated into mesh-based and interface-based models. Additionally, the applicability of the models for wood stoves is discussed, and an overview of the existing literature on numerical simulations of small-scale wood stoves and domestic boilers is given. Furthermore, current bed modeling approaches in large-scale grate furnaces are presented and compared against single particle models.

© 2017 Elsevier Ltd. All rights reserved.

Contents

* Corresponding author.
  E-mail address: inge.haberle@ntnu.no (I. Haberle), oyvind.skreiberg@sintef.no
(Ø. Skreiberg), nils.e.haugen@sintef.no (N.E.L. Haugen).

1. Introduction

Currently, intense research is concentrated on the thermal conversion of biomass, which is due to the more attractive character of biomass compared to traditional fossil fuels for technologies based on thermal conversion, such as combustion [1]. The superiority of biomass-based technologies compared to fossil fuel technologies is related to the environmentally friendly character of botanic biomass, also including lignocellulosic biomass. A plant can only release the carbon dioxide (while burning) that it has stored during growth. The net CO_2 emission is therefore zero, making biomass carbon-neutral [2]. Hence, more research within the field of thermal conversion of biomass can contribute significantly to a sustainable energy mix.

Biomass combustion is one of the main routes of biomass conversion [3]. Different combustion technologies require differently sized lignocellulosic biomass particles [4]. Wood pellets, logs and chips are usually used, and are considered to be thermally thick particles [5]. When modeling thermally thick wood particles, heat and mass transport have to be considered. Overall, there is a large difference between thermally thin and thermally thick particles, which is classified by the Biot (Bi) number. The Biot number is defined as [6]

$$Bi = \frac{h_{eff} d}{\lambda},\qquad(1)$$

where the thermal conductivity (λ), characteristic length (d) and effective heat transfer coefficient (h_{eff}) are used. The Biot number defines the ratio between heat transfer resistance in the interior of the particle and at the surface of the particle [7]. For low Biot numbers (< 0.1), a thermally thin regime is present, whereas large Biot numbers (> 0.1) indicate the presence of a thermally thick regime [8]. In thermally thick particles, intra-particle gradients of temperature are important [9]. Due to varying temperatures, different conversion stages occur simultaneously within the wood log or particle, and intra-particle transport phenomena also have to be considered. In contrast, thermally thin particles have a uniform temperature distribution. This results in sequential conversion stages [10]. Independent of the applied combustion technology, the conversion steps that occur during combustion are drying, devolatilization and char burnout.

In addition to the fundamental research on thermal conversion of biomass particles, the application of the corresponding models to wood-fired boilers and stoves has recently been intensively studied. The main aim of current research is to improve the combustion process with the aid of modeling tools to help yield an improved design and operation of boilers or stoves. Improvement is required since emissions of carbon monoxide, particulates, organic pollutants such as polycyclic aromatic hydrocarbons (PAH), soot and nitrogen oxides of current small-scale units may be very high [11]. Furthermore, the use of bioenergy will increase in the future, thereby highlighting the importance of optimized stove and boiler designs [12]. In Norway today, domestic heating applications such as wood stoves account for almost 50% of bioenergy use, and the use of wood logs in small-scale units, as well as the utilization of pellets in pellet stoves and boilers, is predicted to increase even further. The Norwegian objective is to increase the rate of energy conversion in wood and pellet stoves by a factor of 2 from 2008 until 2020 [13]. The need for optimization of wood log fired stoves is due to decreasing emission limits and changing market demands [14]. Modern simulation techniques, such as computational fluid dynamics (CFD), are an efficient way to reach these objectives [14]. CFD for the optimization of combustion systems is considered an alternative way of improvement (compared to experiments) that is usually less expensive [15]. Even though numerical simulations are a more time-saving and less expensive optimization route, experiments are needed for the validation of models applied [12].

In order to apply commercial CFD tools, numerical sub-models have to be developed [15]. The sub-models aim to fully describe the thermal conversion of the solid fuel, and eventually link these results

to gas phase modeling, which is commonly performed with commercial CFD tools. It is of importance to develop numerical models for drying, devolatilization and char burnout of wood particles that optimize the balance between the degree of accuracy and the required computational time [10]. Both aspects need to be considered when the purpose is to apply the model as an engineering tool for the optimization of wood heating appliances.

Currently, most of the research within the field of CFD-aided design and optimization of biomass combustion units is restricted to large-scale biomass fixed bed and grate furnace applications. Only a few works have been done on CFD models for wood log combustion in domestic heating appliances [14]. In this work, the domestic scale is limited to 30 kW, which is more accurately rather micro-scale than small-scale, but is referred to as small-scale in this review. This review focuses in part on such domestic applications, but further also discusses current single particle models. The third part of the paper focuses on large-scale grate furnaces and the corresponding bed models. With respect to large-scale grate furnaces, it is outlined how currently applied bed models are simplified when compared to detailed single-particle models. While large-scale grate furnaces have a moving bed and the fuel is transported through the furnace while undergoing different stages of conversion, the previously discussed domestic heating applications have a fixed bed, e.g. wood stoves.

The current state-of-the-art for large-scale grate furnace design and optimization is that also within this field furnace design is primarily based on experience or empirical data. However, experiments are difficult and expensive, which highlights the necessity for a CFD analysis [16]. CFD also gains increasing importance within this field, due to the constant improvement of computer performance [17]. Despite this increasing importance, simplifications are still needed in order to make large-scale grate furnace modeling affordable [16].

The purpose of this review is to convey theoretical knowledge of physical and chemical phenomena related to the thermal conversion of woody biomass. The focus is on drying, devolatilization and char conversion of thermally thick wood particles (incl. logs). The aim is to discuss current modeling approaches for single particles in detail, and to identify their strengths and weaknesses.

A number of reviews on thermochemical degradation of wood and related physical processes is already available. The current review does not only cover chemical and physical processes modeling for single particle applications but also discusses models for the solid phase that can be applied in small-scale heating appliances as well as large-scale furnaces. Anca-Couce [18] presented an extensive review on pyrolysis of wood and related chemical and also partly physical processes. The full thermal conversion of particles though has not been reviewed. Furthermore, no direct linkage between the single particle models and how solid phase is modeled in small-scale heating appliances has been discussed. A detailed review on pyrolysis of biomass was also presented by Neves et al. [19]. The focus was on factors influencing secondary pyrolysis of gases and the product distribution and composition. Furthermore an empirical model for the volatile composition was presented. Di Blasi [20] reviewed literature on modeling of chemical and physical processes of wood during pyrolysis. Primary devolatilization kinetics were discussed in detail, as well as secondary reaction modeling approaches. They also reviewed pyrolysis reactor models, even though they found that only very limited work had been done in that field. Fixed-bed reactors and fast-pyrolysis reactors were included in their review. However, no review on stove models was performed and we also found that a significant amount of work has been done since Di Blasi's review [20] in 2008.

The purpose of the small-scale furnace modeling section is to review the current state-of-the-art, and to identify which modeling aspects need more attention. The purpose of the large-scale grate furnace section is to outline how current bed models for grate furnaces deviate from single particle models. Such deviation is due to the complexity of large-scale grate furnaces, which requires simplifying assumptions in order to operate at a reasonable computational cost.

2. Chemistry of woody biomass

Wood is classified as lignocellulosic biomass, and can be split into hardwood and softwood [21]. Table 1 outlines the composition of typical Scandinavian wood species.

In Table 1, fractions of lignin, cellulose and hemicellulose are presented for some woody biomasses. Lignocellulose describes three-dimensional composites of polymeric substructures, and is primarily composed of lignin, a phenolic polymer, as well as carbohydrate macromolecules, namely cellulose and hemicellulose. Besides these main compounds, small percentages of proteins, acids, salts and minerals are also identified in lignocellulosic feedstock [24].

Lignin is the natural binding material in the cell walls of lignocellulosic plants [22]. It is amorphous, and its units are randomly linked [18]. Lignin is a co-polymer, including three types of phenylpropane monomeric units, which are p-coumaryl, coniferyl and sinapyl alcohols [25]. Lignin varies with respect to its O, C and H composition, and can therefore be either hydrogen-rich, carbon-rich or oxygen-rich [26]. As it is later outlined, such a detailed classification of lignin is only used by Ranzi et al. [27] for developing a detailed devolatilization reaction model. However, a detailed description of the reacting fuel is required if the purpose of the model is to accurately predict volatile species and their release rates.

Cell walls mainly contain cellulose [22]. The cellulose content in wood can vary depending on the age of the plant, as well as the plant type. Cellulose is built up by linear chains of 1,4-β-bonded anhydroglucose units. These units contain OH-groups, which form hydrogen bonds inside the macromolecule. Not only do these bonds connect within one macromolecule, but they also link different macromolecules [28]. Cellulose molecules are characterized by their linearity, which is one of the primary differences compared to hemicellulose and lignin. The degree of polymerization, describing the number of sub-units forming the entire polymer of cellulose (> 10000), is much higher than for hemicellulose (20−500) [22].

Hemicellulose is the third main component forming cell walls. It is less linear than cellulose, and has a more branch-like character [22]. In hardwoods, the main hemicellulose macromolecule is methylglucuronoxylan [29]. This differs from hemicellulose macromolecules found in softwood, which are mainly built up by galactoglucomannan and arabinomethylglucuronoxylan [29]. Therefore, reaction schemes in case of thermal degradation for

Table 1
Chemical composition of typical Scandinavian hardwoods and softwoods.

Wood type	Lignin	Cellulose	Hemicellulose	Extractives	Ref.
Hardwoods:					
Silver birch	22%	41%	30%	3.2%	[22]
American beech	22%	48%	28%	2%	[22]
Softwoods:					
Scandinavian spruce	29%	43%	27%	1.8%	[22]
Scandinavian pine	29%	44%	26%	5.3%	[22]
Douglas fir	29%	39%	23%	5.3%	[22]
Scots pine	28%	40%	25%	3.5%	[22]
Hardwood	20−22%	40−42%	30−35%	2−3%	[23]
Softwood	27−28%	40−43%	21−23%	3−5%	[23]

these two types of hemicellulose also differ. Modeling hemicellulose in hardwood is often done by modeling the chemical characteristics of xylan [26].

One can clearly see that wood is a mixture of many components, and an accurate description of its devolatilization accordingly includes numerous reactions. Such a broad range of reactions increases both the complexity of the model and the computational cost, since reactions will be of different stiffnesses, which require finer temporal resolution. Simplifying assumptions are therefore needed, which can be either modeling wood as a mixture of all components, or modeling cellulose, hemicellulose and lignin separately. Both modeling approaches have their strengths and weaknesses, which are discussed in a later chapter.

3. Physical characteristics of woody biomass

Woody biomass particles vary significantly in their physical characteristics. Table 2 illustrates the major differences between wood logs and densified wood particles, which can both be categorized as thermally thick woody particles.

Pellets are compressed biomass particles made from pulverized biomass, either with or without additives (binder). The shape is most commonly cylindrical and the particles have a length of 5−40 mm [31].

The allowed diameter for wood logs is rather narrow for birch wood with a nice appearance (8−15 cm), as suggested by the Norwegian quality standard for firewood [32]. For other wood species, including birch, oak, ash and maple (hardwoods), the minimum diameter is 4 cm, while the maximum diameter is 18 cm. This diameter range is applicable to almost all wood species, whereas the corresponding standard lengths of the wood logs vary between 20, 30 and 60 cm.

Pellets and briquettes have a lower water content than wood logs. More specifically, both wood pellets and briquettes typically have an average water content of approximately 8wt% on wet basis, even though bark briquettes can also have a higher water content (18wt% on wet basis). This variation in water content has an effect on net calorific value, combustion efficiency and temperature of combustion [30]. In contrast to densified wood, freshly harvested wood has a higher water content. However, small-scale units can only operate sufficiently well if the moisture content does not exceed a critical value, and wood logs should be used with a water content that is not higher than 12−20wt% wet basis [23].

A primary difference between wood pellets and wood logs is the density, which for wood pellets is commonly assumed to be about twice as high (1100 kg/m^3) as the density of wood logs (500 kg/m^3) [1]. It has to be added though that especially the wood species significantly affects the density of undensified wood. In addition to the variation in densities, wood pellets are also often considered isotropic, while wood logs are considered anisotropic [1]. Wood is formed by elongated cells, whose walls are formed by micro-fibrils aligned along the longitudinal axis of the cell [22]. These fundamentals of the wood structure explain the naturally anisotropic properties of wood. Therefore, e.g. the thermal conductivity of wood is smaller in the radial and the tangential direction to the grains

compared to the longitudinal direction [33]. Due to the analogies between heat and mass transfer, similar behavior is expected for permeabilities. The anisotropy of wood also affects shrinkage during drying and devolatilization. The highest degree of shrinkage occurs tangentially to the grains, which means in the direction of annual growth rings. Radial shrinkage is only half of tangential shrinkage but is still more significant than longitudinal shrinkage [33].

These physical differences between undensified and densified wood particles highlights that simplifying assumptions, required for modeling, have to be applied with caution as they might be suitable for describing pellets and briquettes, e.g. isotropy, but can lead to false predictions, when applied to undensified particles.

4. Particle degradation modeling

New modeling approaches for drying, devolatilization and char conversion of single wood particles and logs are continuously being developed. There is a vast variety of such models, and there may be large differences between them. The differences are primarily due to the simplifying assumptions that have been made. The purpose of the subsequent comparison is to outline the differences between current models, and to identify their strengths and weaknesses. The comparison of models in Table 3 is for thermally thick particles only.

Table 3 shows that a number of models only include certain stages of thermal conversion (e.g. only drying and devolatilization, while neglecting char conversion), instead of modeling the entire thermal conversion process. This can lead to inaccuracies if the purpose of the model is to predict overall conversion times and product yields, rather than only developing a model for the fundamental research on a certain conversion stage, since the conversion stages have an influence on each another.

The heating rate affecting the wood particle during thermal conversion has a signficant influence on the devolatilization product yields. At lower heating rates, more char is produced, while at higher heating rates depolymerization of the wood compounds to permanent gases and tar is enhanced [65]. This fundamental understanding of product yields was used by Pozzobon et al. [62] to outline how evaporation can influence char conversion. Pozzobon et al. [62] found that the char yield is largest at intermediate moisture contents. This is related to the fact that at very low moisture contents (about 1wt%), drying does not slow down the overall heating up significantly, such that char formation is not significantly enhanced, while it is enhanced at an intermediate moisture content (9wt%). At a moisture content of 50wt%, it was found that char yield decreases again. This is because water vapor is formed, which leaves via the porous structure of wood and char, and hereby heterogeneously reacts with char, such that the char yield decreases [62]. Nothing comparable has been found in earlier works, which again highlights that an accurate thermal conversion model of a thermally thick particle has to account for all three main conversion stages simultaneously, as they significantly influence one another.

With respect to Table 3, it has to be mentioned that some of the models have been applied to packed-bed modeling. However, they were added to the table if their single particle models were separately validated. It is therefore assumed that these single particle

Table 2
Different physical properties of commercially available woody biomass.

Wood	Diameter [cm]	Length [cm]	Anisotropy/Isotropy	Density [kg/m^3]	Ref.
Densified wood:					
Wood pellets:	0.59−1.02	0.5−4.0	Isotropic	1180	[1,30,31]
Wood briquettes:	5.2−9.3	7.4−31.3	Isotropic	1060	[30]
Wood log	8−15	20−60	Anisotropic	430−650 [a]	[22,32]

[a] Density given on oven-dry basis.

Table 3

Comparison of current single particle models. [a] refers to the one-step global mechanism, [b] refers to the three independent parallel reactions, [c] refers to the three independent competitive reactions and [d] refers to the every other devolatilization model. If a column in the table is marked with "−" this indicates that it was explicitly mentioned in the paper that this aspect was not considered. In case of column "Log/Particle" , "−" indicates that neither of them is modeled, but instead only densified particles are modeled. If a field is marked with ✓ it means that it has been considered. "K" in the drying column refers to kinetic rate model, "T" refers to thermal drying model and "E" refers to equilibrium model. "NA" stands for "not announced".

Author (year)	Dimension	Wood species/type	Log (=1)/Particle (=2)	Densified wood	Isotropic (=1)\Anisotropic (=2)	Volumetric shrinkage	Drying	Devolatilization: one[a]	Devolatilization: 3 i.p.[b]	Devolatilization: 3 i.c.[c]	Devolatilization: others[d]	Secondary reactions	Char oxidation	Char gasification	Interface (=I)/Mesh based (=M)
Alves and Figueiredo (1989)[34]	1D	Pine	2	–	1	–	K/E	–	–	–	✓	–	–	–	M
Koufopanos et al. (1991)[35]	1D	NA	2	–	1	–	–	–	–	–	✓	–	–	–	M
Di Blasi (1994)[36]	2D	Cellulose	2	–	2	–	–	–	–	–	✓	–	–	–	M
Di Blasi (1996)[37]	1D	Maple	2	–	1	✓	–	–	–	–	✓	–	✓	–	M
Melaaen (1996)[38]	1D	NA	2	–	1	–	E	–	–	–	✓	✓	–	–	M
Di Blasi (1998)[39]	2D	Cellulose	2	–	2	–	–	–	–	–	✓	–	–	–	M
Grønli and Melaaen (2000)[40]	1D	Spruce	2	–	1	–	–	–	–	✓	–	✓	–	–	M
Larfeldt et al. (2000)[41]	1D	Birch	1	–	1	✓	–	✓	–	✓	✓	–	–	–	M
Bryden et al. (2002)[42]	1D	Basswood/Poplar/Red oak/Southern Pine	2	–	1	✓	K	–	–	✓	–	✓	–	–	M
Hagge and Bryden (2002)[43]	1D	Poplar	2	–	1	✓	–	–	–	✓	–	✓	–	–	M
Thunman et al. (2002)[44]	1D	Birch/Spruce	2	–	1	✓	K	–	–	✓	–	–	✓	✓	I
Wurzenberger et al. (2002)[45]	1D	Beech	2	–	1	–	E	–	–	–	✓	✓	✓	✓	M
Bruch et al. (2003)[46]	1D	Beech	2	–	1	–	T	✓	–	–	–	–	✓	–	M
Bryden and Hagge (2003)[47]	1D	Poplar	2	–	1	✓	K	–	–	✓	–	✓	–	–	M
Babu and Chaurasia (2004)[48]	1D	NA	2	–	1	✓	–	–	–	–	✓	✓	–	–	M
de Souza Costa and Sandberg (2004)[49]	1D	NA	1	–	1	–	T	–	–	–	✓	–	✓	–	I
Galgano and Di Blasi (2006)[50]	1D	Poplar	1	–	1	–	T	✓	–	–	–	–	✓	✓	I
Galgano et al. (2006)[51]	1D	Poplar	1	–	1	–	T	✓	–	–	–	–	✓	✓	I
Porteiro et al. (2006)[52]	1D	Densified wood	–	✓	1	✓	T	–	–	✓	–	–	✓	–	I

Reference	Dim	Material													
Porteiro et al. (2007) [53]	1D	Densified wood	–	✓	1	✓	T	–	–	✓	–	–	✓	–	I
Shen et al. (2007) [54]	1D	Birch	2	–	1	–	K	–	–	–	✓	–	–	–	M
Yuen et al. (2007) [55]	3D	Beech	2	–	2	–	E	✓	–	–	–	–	–	–	M
Sand et al. (2008) [56]	2D	Birch	1	–	2	✓	T	–	–	✓	–	✓	–	–	M
Yang et al. (2008) [57]	2D	Willow	2	–	1	✓	T	✓	–	–	–	–	✓	–	M
Sadhukhan et al. (2009) [58]	1D	Casuarina wood	2	–	1	✓	–	–	–	–	✓	✓	–	–	I
Haseli et al. (2012) [59]	1D	Pine/ Red Oak/ Spruce/ Douglas Fir/ Redwood/ Plywood	2	–	1	–	–	–	–	–	✓	–	–	–	I
Mehrabian et al. (2012a) [7]	1D	Poplar/ Beech/ Spruce/ Spruce pellet	2	✓	1	✓	T	–	✓	–	–	–	✓	✓	I
Mehrabian et al. (2012b) [10]	1D	Poplar	2	–	1	✓	T	–	✓	–	–	–	✓	✓	I
Ström and Thunman (2013a) [8]	1D	Beech / Poplar	2	–	1	✓	T	–	–	✓	–	–	–	–	I
Ström and Thunman (2013b) [5]	1D	Beech	2	–	1	✓	T	–	–	✓	–	–	–	–	I
Galgano et al. (2014) [60]	1D	Oak	2	–	1	–	T	✓	–	–	–	–	✓	–	I
Kwiatkowski et al. (2014) [61]	3D	Pressed wood shavings	2	–	1	✓	E	–	–	–	✓	✓	–	✓	M
Pozzobon et al. (2014) [62]	2D	Beech	2	–	2	–	K	–	–	–	✓	✓	–	–	M
Seljeskog and Skreiberg (2014) [63]	1D	NA	1	–	1	–	T	–	✓	–	–	–	–	–	I
Biswas and Umeki (2015) [1]	1D	Katsura	1	–	1	✓	–	–	–	✓	–	✓	–	–	M
Biswas and Umeki (2015) [1]	1D	Pine and Spruce	–	✓	2	✓	–	–	–	✓	–	✓	–	–	M
Ding et al. (2015) [64]	1D	Birch	2	–	1	–	K	✓	–	–	–	–	✓	–	M

models can also be used to model single particles alone, as only boundary conditions have to be adjusted accordingly.

Moreover, it has to be added that independent of the choice of single particle model, the validation of models against experiments is very challenging due to various reasons [40]. The first problem is that chosen properties can vary a lot, and also show a significant dependency on wood species. Furthermore, the values for the properties of charred and partially charred solids are related to a significant uncertainty. The values of properties of the solid then also have to take into consideration the structural changes (e.g. cracking, fragmentation) and shrinkage that can occur during the entire thermal conversion process. It is also not possible to know the detailed chemical composition of each wood particle modeled. This is because the same sample cannot be produced twice, since it is expected that there always is a small variation in the percentage of contributing cellulose, hemicellulose and lignin fractions. Inorganic matter that is contained in the experimental wood sample, and which catalyzes primary devolatilization, is often not taken into consideration in modeling applications. Finally, the influence of chosen kinetic data is related to uncertainty, since the kinetic models themselves are also a gross simplification. In addition, the obtained kinetics are restricted to the operational conditions for which they were derived [40].

The models listed in Table 3 are of different complexity. The two most simplified models [49,59] in Table 3, were primarily based on pre-defined temperatures and geometrical relations. To a certain extent, they were based on interfaces moving through the wood particle, even though they included a higher number of simplifying assumptions compared to the rest of the listed interface-based models. Models of medium complexity listed in Table 3 are the interface-based models, where conversion fronts move through the particle from the surface to the center, and the highest complexity is related to the very detailed mesh-based models, where the full single particle is discretized. Nonetheless, more details on mesh-based and interface-based models are mentioned in the following sections. With respect to Table 3, however, it must be pointed out that, depending on the purpose of a model, simplistic models can be more suitable than very comprehensive mesh-based models. Even though mesh-based models result in higher accuracy, they might not be suitable for certain purposes (e.g. as a fast and simple engineering tool) due to increased computational cost.

4.1. Evolution equations

A model's accuracy and complexity increase with increasing detail in the mathematical description of physical and chemical processes. Therefore, the relevant evolution equations for thermochemical wood degradation and combustion modeling need to be discussed.

As shown in Fig. 1, the wood volume is formed by a solid matrix, and embedded in this solid matrix there are openings (pores) that contain gas and liquid phase. The dimensions of these pores can vary quite a bit. Pore size distribution, and consequently the overall porosity of wood, influence mass and heat transfer, which consequently affects thermal degradation [66]. This combined structure of solid matrix and gas- or liquid-filled pores leads to the assumption that wood can be described as a porous medium.

Based on the structure of wood, the describing equations need to include the influence of all current phases. Given the porous multi-phase structure of wood, the evolution equation for temperature is given by

$$\left(c_{P,s}\rho_s + c_{P,l}\rho_l + c_{P,b}\rho_b + \epsilon_g(c_{P,g}\rho_g^g)\right)\frac{\partial T}{\partial t}$$
$$+\left(\rho_l\mathbf{v}_l c_{P,l} + \rho_b\mathbf{v}_b c_{P,b} + \rho_g\mathbf{v}_g c_{P,g}\right)\nabla T \qquad (2)$$
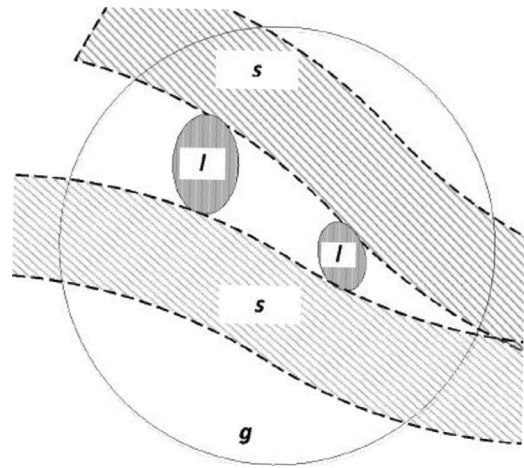$$= \nabla\cdot(k_{\text{eff}}\nabla T) + \Phi_{\text{evap}} + \Phi_{\text{dev}} + \Phi_{\text{char}}$$

Fig. 1. Wood as a porous medium. The lined areas illustrate the solid phase (marked with s), the crossed areas are occupied by the liquid phase (marked with l) and the plain white areas illustrate areas where the gas phase (marked with g) is present. The pores themselves can contain both liquid and gas phase. The circle illustrates a certain representative sub-volume of the entire wood log.

where the subscripts s, l and g refer to the solid, the liquid and the gas phase, respectively. In the case of ongoing devolatilization reactions in a thermally thick particle, the solid phase includes the virgin wood as well as the produced char. During the stage of char conversion, char and ash form the solid phase. The effective thermal conductivity, k_{eff}, includes the influence of virgin wood, char, free liquid and bound water, in addition to gases. A linear variation of thermal conductivity from virgin wood to char, based on the degree of conversion, is commonly assumed [22,34,36−40,42,43,54,55,58,61]. A general assumption is that material properties vary linearly from virgin wood to char, and this does not solely apply to thermal conductivity, but also to specific heat capacity and permeability. The last three terms on the right-hand-side of the equation are source and sink terms due to the heat of reactions of drying, devolatilization and char conversion. The specific heat capacities are given by $c_{P,i}$, where subscript i represents the phase, which can be either for solid (s), liquid (l), bound (b) or gas phase (g), respectively. One of the major simplifying assumptions that has been used in obtaining Eq. (2), and which is also applied by many researchers [1,7,10,22,34−43,45−55,57−62,64], is the assumption of thermal equilibrium between all the phases (solid, liquid and gas).

Large Peclet numbers, defined as

$$Pe = \frac{du\rho c_p}{\lambda} \qquad (3)$$

for heat transfer [67] justify the simplifying assumption of a local thermal equilibrium. Here, d is the characteristic length, u is the velocity, ρ is the density, λ is the thermal conductivity and c_p is the specific heat capacity. The Peclet number is the ratio of convective and diffusive transport. The assumption of thermal equilibrium reduces the number of required temperature equations to one, and consequently reduces the computational cost. Some deviation between modeling results and experimental results can be due to this assumption [68,69], as it results in longer conversion times, which increase by approximately 20%, compared to the case where separate temperature equations are solved for each phase.

Some authors neglect convection in the porous structure [48,64]. It has to be mentioned, however, that the gas phase that is flowing through the pores will result in a cooling of the solid particle, and that this effect cannot be modeled accurately if convection is neglected. Neglecting the convection should actually be considered

as a gross over-simplification because it is known that a high gas flow along the grain direction can limit the heating rate, and accordingly the entire temperature evolution is closely coupled to the gas flow within the pores. Another consequence is that a slower heating of the wood log, due to high gas flows out of the wood log center, yields different product yields and also gives a different conversion time comparable to what is obtained when neglecting convection. Di Blasi[39] identified an interesting dependency of particle size in relation to the influence of the convective term. With increasing particle size, the influence of the convective term decreases, as the maximum velocity is also reduced. This finding can therefore justify why the convective term in the temperature equation can by neglected in the case of very large wood particles.

Another common simplification is to neglect the influence of the heat capacity of the gas phase [34,42,43,47,50,51,60]. This is a fair assumption, since the thermal mass (defined as $m_i c_{P,\,i}$, with m being the mass of a species) of wood char is 650 times larger than the thermal mass of gases [47]. In Eq. (2), two different phase averages, the intrinsic average and the phase average, are used, which are explained hereafter.

The intrinsic phase average is the averaged value within a single phase. This means that the intrinsic average of the variable φ within the phase i, is defined as [22]

$$\phi_i^i = \frac{1}{V_i} \int_{V_i} \phi dV \tag{4}$$

where i can be l, g or s and V is the volume over which the average is performed, while V_i is the sub-volume of V occupied by phase i. In contrast to this, the phase average is defined as [22]

$$\phi_i = \frac{1}{V} \int_{V_i} \phi dV. \tag{5}$$

The relation between phase averaging and the intrinsic phase average is given as [22]

$$\epsilon_i \phi_i^i = \phi_i \tag{6}$$

where $\epsilon_i = V_i/V$ is the volume fraction of phase i. This relation is valid for all three phases present in wood. The continuity equation for the liquid free water is given as [38]

$$\frac{\partial \rho_l}{\partial t} + \nabla \cdot (\rho_l \mathbf{V}_l) = \dot{\omega}_{\text{evap,l}} \tag{7}$$

where ρ_l is the liquid free water density, $\dot{\omega}_{\text{evap,l}}$ is the rate of evaporation of the liquid-free water, and $\mathbf{V}_l$ is the velocity of the liquid free water.

The evolution equation of bound water is similarly constructed [22,38] as

$$\frac{\partial \rho_b}{\partial t} + \nabla \cdot (\rho_b \mathbf{V}_b) = \dot{\omega}_{\text{evap,b}} \tag{8}$$

where ρ_b is the bound water density, $\dot{\omega}_{\text{evap,b}}$ is the rate of evaporation of the bound water, and $\mathbf{V}_b$ is the velocity of the bound water. The velocities for liquid free water and bound water transportation are calculated differently, based on whether convective or diffusive transport is dominant.

The bound water movement is modeled as [22]

$$\rho_b v_{bx} = -\rho_{\text{wood,dry}} D_b \left(\frac{\partial \left(\frac{\rho_b}{\rho_{\text{wood,dry}}} \right)}{\partial x} \right) \tag{9}$$

where D_b is the bound water diffusivity, which depends on temperature and the bound water content itself. Commonly, one can assume $\rho_{\text{wood,\,dry}}$ to be constant during drying, which therefore cancels out and the equation is further simplified.

In contrast, the liquid free water transport is dominated by advection, which is commonly modeled by Darcy's law, such

that [22]

$$\mathbf{V}_l = -\frac{K_l K_{rl}}{\mu_l} \nabla P_l. \tag{10}$$

As can be seen from the equation, the permeability contains the influence of a relative permeability, K_{rl}, and the intrinsic (absolute) permeability, K_l. The liquid phase pressure is based on a correlation between the gas phase pressure, P_g, and capillary pressure, P_c, such that [22]

$$P_l = P_g - P_c. \tag{11}$$

A common approach for modeling the capillary pressure is based on experimental work by Spolek and Plumb [70]. The mathematical expression for capillary pressure as a function of temperature, T, and liquid free water content (M_l) was derived by Perre and Degiovanni [71] as

$$P_c = 1.364 \times 10^{-5} \sigma (M_l - 1.2 \times 10^{-4})^{-0.63}, \tag{12}$$

where σ is the surface tension between the gas phase and the liquid phase, which is defined as

$$\sigma = \frac{128 + 0.185T}{1000}. \tag{13}$$

The above expressions are, however, based on experiments, which reduces the validity of the mathematical expression not only to softwood species, but also to certain operational conditions that the experiments were performed with.

The gas phase continuity equation is given by [22]

$$\frac{\partial (\epsilon_g \rho_g^g)}{\partial t} + \nabla \cdot (\rho_g \mathbf{V}_g) = \dot{\omega}_{\text{evap}} + \dot{\omega}_{\text{dev}} + \dot{\omega}_{\text{char}} \tag{14}$$

where ϵ_g, ρ_g^g, $\mathbf{V}_g$ are the volume fraction of the gas phase, the intrinsic phase average density of the gas phase and the velocity of the gas phase, respectively. On the right-hand side in the above equations are the source terms due to water evaporation $\dot{\omega}_{\text{evap}}$, wood devolatilization $\dot{\omega}_{dev}$ and char conversion $\dot{\omega}_{char}$. The gas phase species continuity equation reads [38]

$$\frac{\partial (\epsilon_g \rho_i^g)}{\partial t} + \nabla \cdot (\rho_i \mathbf{V}_g) = \nabla \cdot \left[\rho_g^g D_{\text{eff}}^i \nabla \left(\frac{\rho_i^g}{\rho_g^g} \right) \right] + \dot{\omega}_i \tag{15}$$

where ρ_i^g is the intrinsic phase average density of a species i in the gas phase, and $\dot{\omega}_i$ is the source term of species i. The effective diffusion coefficient, D_{eff}, has to be used in the gas phase species continuity equation because it accounts for the constrictions due to diffusion in a porous medium, such as wood. It is suggested by Fogler [72] that it can be related to the binary diffusion coefficient, D, such that

$$D_{\text{eff}} = \frac{\epsilon_g \sigma_c D}{\tau}, \tag{16}$$

where τ is tortuosity, σ_c is a constriction factor and ϵ_g is the volume fraction occupied by the gas phase, which is equal to the porosity in the case of dry wood. In some works, diffusion of the gas species is neglected, since it is assumed that it is much smaller compared to convection [50,51,60]. The convective term of the volatile species equation was adjusted by Galgano et al. [60], such that the influence of the formation of cracks was partly considered in their work. They assumed that only a fraction of the entire gas phase is actually transported out by convection, and therefore has to pass the entire thickness of the hot char layer [60]. This means that a fraction of gases is modeled to leave the wood particle immediately along cracks and fissures.

The velocity of the gas phase is calculated such that [38]

$$\mathbf{V}_g = -\frac{K_g K_{rg}}{\mu_g} \nabla P_g, \tag{17}$$

where the effective permeability again is a combination of intrinsic, K_g and relative permeability, K_{rg}. Generally speaking, the intrinsic permeability is higher for softwoods than for hardwoods, and higher for sapwood than for heartwood [22]. Eq. (17) is also known as Darcy's law. Using Darcy's law to model gas phase advection is a common approach [1,22,36–43,45,55,61,62]. Since one expects a laminar flow in the pores, and since the viscous forces dominate over the inertial forces in the woody biomass structure, the computation of liquid and gas phase advection inside the wood with Darcy's law is reasonable [73].

It has been experimentally shown that significant pressure peaks can form inside a wood log [74]. It was also found that the pressure has an influence on the distribution of the devolatilization products within the solid, since the mass transfer is linked to the effect of pressure gradients on mass transfer velocity and thus also on residence times of products in the interior of the particle [75].

There are works in which the gas flow was not based on Darcy's law. Sand et al. [56] modeled gas phase behavior inside and outside of the wood log by fully solving the momentum equation, and were thereby able to identify a gas plume leaving the wood log. The influence of such a plume on the entire wood log degradation processes has not been investigated intensively so far, and accordingly, the importance of such a detailed description of the gas flow inside and outside the wood log needs to be investigated in more detail in the future.

The direction of the gas flow is often restricted, as it is common to assume that gases can only move away from the wet core [34,46,49,52,60]. Such a simplifying assumption neglects entirely the fact that gaseous products of thermal conversion can also move inwards, towards cooler regions and condense there. This would then require the modeling of tar and water vapor re-condensation, which is not commonly done. Only a few works model the inwards and outwards movement of produced gases [36,39,45,54], even though in those works, condensation reactions are still neglected. Wurzenberger et al. [45] experimentally found condensation reactions of gases moving inwards. It is therefore suggested that condensation reactions are relevant. It would also be interesting to see how an asymmetric flow field, due to the anisotropy of wood, affects the importance of tar condensation reactions during thermal conversion modeling. Additionally, it is not yet known how anisotropic heating affects the importance of tar re-condensation modeling.

In order to solve the previously discussed governing equations, suitable boundary conditions have to be chosen and the most common ones are discussed hereafter.

4.1.1. Boundary conditions

For temperature evolution in a wood particle, it is most common to consider the influence of radiation and convection at the boundaries [5,8,10,22,34,35,38,40,42,49,52–54]. Some works set a fixed uniform radiant heat flux to heat up the wood log, and assigned losses to the boundaries, which result from convection and re-radiation [22,37,50,54,60,62]. It is also a common approach to assign fixed background temperatures, either one single temperature [36,39,42,43,47,52,53] or a combination of radiation temperature (commonly furnace temperature), T_{rad}, and convective temperature (from the surrounding gas phase), T_{conv}, [7,10], which results in heating of the wood particle.

The value of the applied heat flux has a significant effect on the produced char, since at higher heat fluxes the char density will decrease at the boundaries, while it will be higher in the interior of the wood log, due to slower heating inside. Faster heating at the boundaries, as a result of applying high heat fluxes, yields enhanced tar production and reduced char production [40]. Seljeskog and Skreiberg [63] set their boundary conditions such that two different heat fluxes could be applied at the bottom and top surface of the wood log. Accordingly, this model grants the flexibility to its user to also model asymmetric heating conditions that are more realistic in stoves.

None of the works has considered that the steam, exiting from the interior of the particle primarily during drying, can build a layer around the particles outer surface and absorb some of the radiation that heats up the particle [52]. Consequently, it is of interest for future work to identify how large the influence of such a layer on the temperature history of the particle really is.

The radiative heat flux from the flame was only mentioned in a limited number of works [64]. Even though this was a first step towards considering the back-radiation of the flame to the wood particle surface, it has to be pointed out that the validity is restricted, as a constant uniform heat flux was applied [64]. However, in the case of a real flame, the radiant heat flux will fluctuate significantly, mainly due to the highly transient thermal conversion process.

The particle emissivity is an important parameter that couples the exterior conditions of the solid with the drying, devolatilization and char burnout processes occurring inside the particle. Particle emissivity has been assigned a value of 0.85 [7,10,40,52,53,55] but also higher values of 0.9 [1,38,42,43] and 0.95 [48] and 1 [37,39] have been applied. A comparably low particle emissivity of 0.78 [54] has rarely been used. Surprisingly, some works even assume the emissivity of wood to exceed the emissivity of char [56]. In addition, some works did not account for significant changes of emissivity as wood converted to char [62,64] which is considered a weakness of a model, as one expects the emissivities to vary, because there is a significant change in elemental composition as wood degrades to char.

The applied emissivities do not follow a certain trend (a dependency on the composition of the initial wood species) or a dependency on the degree of conversion. It seems that the value of the emissivity is fitted in order to obtain better agreement between numerical and experimental results. It is also assumed that the ambiguous choice of emissivity values is due to the overall limited range of values for different wood species available in literature.

For external heat and mass transfer, heat and mass transfer coefficients have to be defined. Some authors therefore assume constant values [34,37,40,54,59], while others have started to work on a more detailed description of heat and mass transfer to the particle surface. A primary influence on these two coefficients is due to outflowing gases, which will reduce the transfer coefficients. This indicates that the gases leaving the particle act as a convective barrier [52,53]. One of the effects of the outflowing gases is also that they tend to react with oxygen before it can reach the active char sites. Porteiro et al. [52,53] considered such a reaction only for the exiting hydrogen. They corrected heat and mass transfer coefficients due to the blowing by the model suggested by Moffat and Kays [76]. In this correlation, a geometrical parameter and a blowing factor are related to the Stanton number with blowing, and a Stanton number without blowing. From the adjusted Stanton number the heat transfer coefficient can be calculated. De Souza Costa and Sandberg [49] also considered the blowing effect of exiting gases by the following expression of the heat transfer coefficient

$$h_s = h_0 \frac{ln(1 + B_s)}{B_s} \tag{18}$$

where B_s is the smoldering transfer number, which is a function of mass fractions of oxygen [49]. Transpiration effects influencing heat and mass transfer coefficients are accounted for in some works [50,51].

Bruch et al. [46] took this outflow of gases into consideration by using the Stefan correlation. The Stefan correlation corrects the transfer coefficients for mass and heat, which are not influenced by blowing of gases, by the influence of the mass flow of gases exiting

the particle such that [77]

$$h_c = \frac{\dot{m}_g c_{P,g}}{\exp\left(\frac{\dot{m}_g c_{P,g}}{h_{c0}}\right) - 1} \tag{19}$$

and

$$h_m = \frac{\dot{m}_g / \rho_g}{\exp\left(\frac{\dot{m}_g}{\rho_g h_{m0}}\right) - 1} \tag{20}$$

where $\dot{m}_g$ is the mass flux of gases, h_{c0} is the not-influenced heat transfer coefficient and h_{m0} is the not-influenced mass transfer coefficient. The corrected mass and heat transfer coefficients are h_c and h_m, respectively [77].

The influence of blowing factors on the temperature profile of a particle significantly depends on whether radiation or convection dominate the heat transfer to the particle. It is acceptable to neglect the influence of the blowing factor with respect to heat transfer phenomena if radiation dominates the heat transfer to the particle [78]. However, if convection dominates, the blowing factor has to be considered, as it can slow down the particle devolatilization process by about 20% [78]. The conclusion is that depending on the choice of boundary conditions, the blowing effect on heat and mass transfer has to be considered (convection dominates) or can be neglected (radiation dominates).

The pressure at the boundary is handled in such a manner, that it is commonly set equal to the atmospheric pressure, e.g. [37,40,43].

The layer model, applied by a number of researchers [7,10,44,52,53], used homogeneous boundary conditions for its implementation. The original work by Thunman et al. [44] was based on an Eulerian discretization, which does not require homogeneous boundary conditions as such. In fact, the boundary conditions can vary and instead of relating conversion to the external surface of the particle it was related to the surface area per unit volume. A significant spatial variation in boundary conditions can only be accurately modeled if the discretization is finer than the size of the particle.

However, in order to include highly diverse boundary conditions, it is recommended to develop a multi-dimensional mesh-based model in order to yield sufficient accuracy.

After having discussed how the particle is linked to its exterior, it is now of further interest to discuss how the thermal conversion processes in the interior of the particle are modeled.

4.2. Drying

This section describes the theory of drying of thermally thick woody biomass. Water is present as bound water, liquid free water and water vapor in the porous structure of wood. Bound water is attached to cell walls as OH-groups bound to structures of cellulose and hemicellulose (and not that many attachments to lignin). The presence of bound water is considered to be significant due to the hygroscopic nature of wood materials. Free water is liquid water in voids in the biomass, which is held in place due to capillary forces. Water vapor is considered as a species in the gas phase resulting from evaporation [18].

Drying is an endothermic process [23] that is prolonging the heat-up time [5]. There will not be any mass loss of the organic solid fuel until devolatilization starts. Water evaporates and leaves the wood as vapor, and if the heating rates are sufficiently high, the cell walls might be affected by higher pressures due to vapor formation in the pores. In special cases, extractives, such as resins, can melt and block the pores. The result is that the convective transport of the gas phase through the pores is slowed down or entirely hindered, which explains such a pressure increase in the porous body as previously mentioned. Physical changes in the wood related to drying can also be explained with respect to different dilatation rates along and across the wood fibers. Due to this variation of dilatation in different spatial directions, the resulting tension increase can lead to cracking of wood structures. These cracks can eventually help to accelerate the drying process, since the surface of the wood log exposed to the heat source is increased [23] and also permeability increases.

During evaporation, water vapor can move towards higher temperature regions, but it can also move towards cooler regions and condense there [79]. The simplifying assumption of negligible re-condensation of water vapor is a common approach when drying is modeled. Only a very limited number of works considered re-condensation of water vapor [42,47,78]. It is said that the effect of re-condensation on the overall modeling results of thermal conversion is negligible. However, since hardly any works include re-condensation, it is not fully known how such a re-condensation of water vapor affects the overall heating-up of the wood log and the conversion time, in comparison to the modeling of an ideal irreversible evaporation of water vapor. This should be studied for anisotropic heating of large wood particles.

One highly interesting aspect has been discussed by Lu et al. [78], who split water into bound water and liquid free water when modeling the drying of a poplar wood particle. Lu et al. [78] found that bound water and liquid free water do not vaporize in the same manner, which outlines that the present liquid water has to be split accordingly. They assumed that bound water can only be irreversibly reduced in heterogeneous Arrhenius expressions reflecting the evaporation of water, while liquid free water evaporation can be reversible and re-condensation reactions can also increase the amount of present liquid free water.

One expects the pressure distribution within the wood log to vary if water vapor re-condenses, so it therefore seems reasonable to assume that the convective transport of gaseous species out of the porous medium, and accordingly the entire heat and mass transfer within a wood log, are likewise affected. However, the identification of the degree of this influence is recommended to be an objective of future work. In the case of biomass with a lower moisture content, the influence of re-condensation reactions is also less compared to woody particles with a significantly higher moisture content.

Shrinkage is also occurring during drying, though in modeling it is mostly neglected [10] since it occurs to a significantly smaller extent compared to the volumetric shrinkage occurring during devolatilization, or even the particle size reduction due to heterogeneous reactions taking place during char conversion.

The reason for shrinkage during drying is that the cell walls lose the bound water that has been attached to hydroxyl-groups of cellulose and hemicellulose via hydrogen bonds. In comparison, the free water does not have any influence on shrinkage, as it only affects the density of the wood particle [10]. This relation indicates that wood does not show any change in size if moisture above the fiber saturation point is evaporated, while it is affected by shrinkage if moisture is lost below the fiber saturation point [33]. Shrinkage during drying accounts for 5–10% of size reduction of the entire particle [43]. Shrinkage related to the stage of drying is reversible, since the particle can swell again if exposed to humidity [10].

What is most interesting is that due to various shrinkage rates in longitudinal, radial and tangential direction, the wood particle can be distorted. This is also valid for shrinkage during devolatilization, and any comparable physical change of the wood particle results in an influence on heat and mass transfer, and accordingly the overall thermal conversion. It is a natural consequence that such a diversity of shrinkage, which varies significantly with direction, can only be accurately replicated in a multi-dimensional model, while 1D models focus on shrinkage in only one preferential direction.

Shrinkage during drying, often defined as the percentage of the green dimension, depends on the wood species [33]. The green
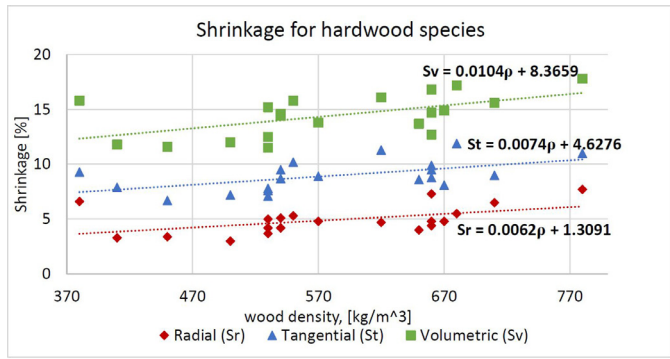
(a) Shrinkage, radial, tangential and volumetric, dependency on hardwood species.
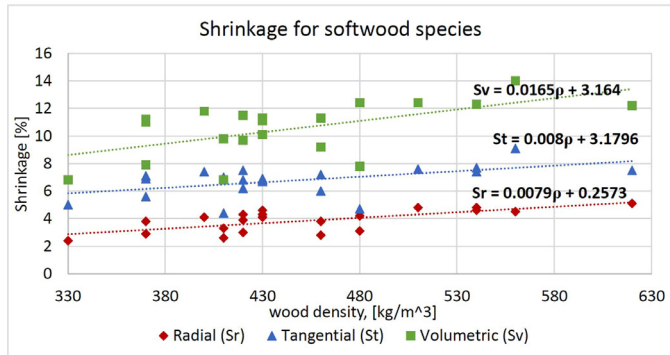
(b) Shrinkage, radial, tangential and volumetric, dependency on softwood species.

Fig. 2. Shrinkage dependency on wood species. The figure illustrates the shrinkage for a range of different hardwood and softwood species. Shrinkage occurs when green wood is dried to an oven-dry basis. Trend lines have been added to indicate that the shrinkage values increase as the density of certain wood species increases (= higher shrinkage for wood species of a higher density). More detailed information on shrinkage for different hardwood and softwood species can be found elsewhere [33]. The figure was based on data provided in a reference work for the various properties of wood [33]. (For interpretation of the references to color in this figure legend, the reader is referred to the web version of this article.)

dimension relates to the dimension of the green wood particle. Moreover, the shrinkage is also affected by the moisture content [33] such that

$$S = S_0 \frac{M_{\mathrm{fsp}} - M}{M_{\mathrm{fsp}}} \tag{21}$$

where S is shrinkage, %, from green wood to wood of a certain residual moisture content (M), S_0 is the total shrinkage, and M_{fsp} is the moisture content at the fiber saturation point is fulfilled. The fiber saturation point, M_{fsp}, is defined as the critical point where the cell walls of the wood contain the maximum quantity of bound water but no liquid free water is yet present. This relation is only valid if $M < M_{\mathrm{fsp}}$.

When comparing shrinkage for different hardwood species and softwood species, it was found that the shrinkage also depends on the wood species. It appears to be the case that radial, tangential and volumetric shrinkage tend to increase for wood species of higher densities, even though it has to be pointed out as well that the dependency is modest. Fig. 2 shows the dependency of shrinkage, %, on different hardwood and softwood species.

In current models, shrinkage during drying is usually neglected. One can therefore conclude that an enhanced modeling focus on physical changes during drying can be a field of interest in future research.

4.2.1. Mathematical modeling of drying

Due to evaporation, the source term in the energy equation Eq. (2) is given by

$$\phi_{\mathrm{evap}} = -\Delta h_{\mathrm{vap}} \dot{\omega}_{\mathrm{evap}} \tag{22}$$

where h_{vap} represents the vaporization enthalpy of water. The rate of evaporation, $\dot{\omega}_{\mathrm{evap}}$, is determined based either on a thermal, kinetic rate or an equilibrium drying model [10]. Attention has to be paid when modeling the heat of evaporation. Only in a limited number of works [22,38,40] have the influences of bound water and liquid free water been explicitly modeled. Depending on whether the available moisture content exceeds the fiber saturation point or not, the heat of evaporation has to be calculated differently. If the moisture content exceeds the fiber saturation point, the heat of vaporization Δh_{evap} is calculated such that [22]

$$\Delta h_{\mathrm{evap}} = \Delta h_{\mathrm{l}} \tag{23}$$

where Δh_{l} is the latent heat of vaporization of water, which is independent of the porous material. If the moisture content drops below the fiber saturation point, the heat of vaporization is calculated as a combination of the latent heat of vaporization of water and the differential heat of sorption, Δh_{sorp}, such that [22]

$$\Delta h_{\mathrm{evap}} = \Delta h_{\mathrm{l}} + \Delta h_{\mathrm{sorp}}. \tag{24}$$

The differential heat of sorption mainly depends on the structure of the wood, and is hence important in a regime lacking liquid free water but with bound water present [38].

Also, only limited works [22,38,40] have introduced an additional source term in the temperature equation

$$\Phi_{\mathrm{sorp}} = \rho_{\mathrm{b}} \mathbf{v}_{\mathrm{b}} \Delta h_{\mathrm{sorp}}, \tag{25}$$

which highlights that the level of enthalpy of the bound water depends on the bound water itself [22]. The consideration of bound water in current models is very limited, and the water is not commonly split into liquid free water and bound water. This is considered a weakness since the transport of bound water and liquid free water have to be modeled differently. It is also not uncommon to neglect both the diffusion and convective transport of water all together [5,7,8,10,52,53].

Based on the available literature, it seems that the scientific world is in favor of the thermal drying model [5,7,8,10,46,50−53, 56,60,63]. This method is based on the assumption that drying occurs at a fixed boiling temperature at atmospheric pressure, 373.15 K, and that any amount of heat above this temperature will be consumed by the drying process in order to vaporize the moisture [10]. The advantage of thermal drying models is that they are easy to implement in numerical codes. However, the robustness of the thermal model is limited because it results in a step-function, which can result in numerical instabilities. The operational conditions, under which the thermal model can be applied, require that a high-temperature environment is given, and also that the size of the drying front is comparably small in contrast to the entire particle dimension [10]. Furthermore, it was found that the assumption of evaporation at exactly 373 K is wrong, since due to significant water vapor formation the pressure in the wood log interior increases, such that the actual pressure significantly differs from atmospheric pressure [77]. This suggests that higher boiling point temperatures are given and it is recommended to model the actual evaporation temperature as a function of wood internal pressure.

The equilibrium model employs the assumption of a thermodynamic equilibrium between the liquid water and the water vapor in the gas phase. The difference between the equilibrium concentration and the current vapor concentration in the gas phase is the driving force for the drying process. The equilibrium method is usually considered in low-temperature drying models [10]. This approach has been employed by several researchers [22,55,61]. Alves and

Figueiredo [34] assumed that drying based on the equilibrium model is only valid for a moisture content below 14.4%, while above this value, the thermal model is applied.

Even though it has been stated that the equilibrium model is generally applicable in low-temperature processes, it has also been applied in these works in a high-temperature environment, such as in combustion and gasification processes. It is considered that especially at lower heating rates, where the time to reach the boiling point temperature is significantly long, the influence of an accurate modeling of drying below the boiling point temperature is significant; even so, it is presumed that for most combustion processes, a high-temperature environment can be assumed, which justifies the neglecting of drying below 100 °C.

Based on these strengths and weaknesses of the present drying models, it can be concluded that a combination of equilibrium and a thermal model can result in a good prediction of drying over a broad temperature range, because the implementation of such a combined model results in a good description of both low-temperature and high-temperature drying.

An alternative to the thermal drying model is the kinetic rate model, which has the primary advantage that it is more numerically stable, since it lacks the discontinuity. Furthermore, one can model drying to occur over a broader temperature range (depends on how kinetic data is adjusted), and therefore also consider drying below the boiling point temperature to some extent by fitting the kinetic data. In addition one can account for bound water, which evaporates at higher temperatures than 373 K. In the kinetic rate models, the drying is considered a heterogeneous reaction, and an Arrhenius equation is used to calculate its rate [44]. The pre-exponential factor and activation energy are set such that the evaporation mainly occurs around the water boiling temperature [10]. In contrast to the common application of thermal models, there is a smaller number of papers that apply the kinetic rate model [42,44,47,54,62,64]. Three different combinations of activation energy and pre-exponential factor were found. Bryden et al. [42,47], Shen et al. [54] as well as Ding et al. [64] used 5.13×10^{10} s^{-1} as a pre-exponential factor and an activation energy of 88 kJ/mol. Pozzobon et al. [62] used the same activation energy but applied a lower pre-exponential factor of 5.13×10^6 s^{-1}. Thunman et al. [44] used an activation energy of approximately 207 kJ/mol, while the pre-exponential factor was set to 10^{27} s^{-1} by Thunman et al. [44]. With respect to the pre-exponential factors applied in these works, one can identify a clear discrepancy between the chosen values, since Thunman et al. [44] modeled a layer model, in which infinitely fast reactions, in this case phase change, are expected, such that the zone where reactions occur is very narrow (= infinitely thin) and high pre-exponential factors are required. This model is based to a certain degree on assuming very fast conversion stages, while Bryden et al. [42,47] developed a mesh-based model, where reaction zones can also be thicker and accordingly phase change due to drying does not have to be infinitely fast.

Finally we will now discuss the numerical efficiency of the thermal drying model and the kinetic rate model. The equilibrium model is not included in the discussion, since it is only relevant for low-temperature drying conditions, while the combustion environment in wood stoves requires models that are suitable for high-temperature conditions. Due to the fact that it has frequently been pointed out that the thermal drying model is lacking numerical robustness, the authors aimed to investigate this drawback of the drying model by comparing it to the more stable kinetic rate model.

For this comparison, a model, based on the one developed by Di Blasi [37] is used. Kinetic data was taken from Font et al. [80] (K3 in Di Blasi's work [37]). Because Di Blasi only discussed a dry particle, we just added the two drying models, after having successfully validated the dry particle modeling against Di Blasi [37]. The transport equations for drying were taken from Melaaen [38]. The moisture content was 5 wt%, wet basis. For both the thermal drying and

kinetic rate model, the tolerance of the iterative solver defining the convergence criteria of the model was set to 10^{-4}. Time discretization was done with a backward differentiation formula (BDF). It was found that using the kinetic rate model with kinetic data by Chan et al. [81] (pre-exponential factor being 5.13×10^6 s^{-1} and the activation energy being 88 kJ/mol), resulted in the applicability of a significantly larger temporal resolution compared to the thermal drying model. The chosen time step using the kinetic rate model was as large as 2.5×10^{-4} s, whereas the thermal drying model required time steps as small as 1×10^{-6} s. Most interesting was also that by increasing the external heat flux, the numerical stability of the thermal drying model was significantly affected. The temporal resolution had to be refined from 1×10^{-6} s to 5×10^{-7} s when increasing the external heat flux from 70 kW/m^2 to 100 kW/m^2.

When increasing the stiffness of the kinetic drying model, by using a higher pre-exponential factor (5.13×10^{10} s^{-1}) as suggested by Bryden et al. [42], the temporal resolution had to be refined. In this case, the time step size had to be reduced to 7.5×10^{-6} s. Such an increase in stiffness mimics the reduction of the size of the drying zone, because it concentrates evaporation reactions in a more narrow temperature region. Accordingly, by increasing the pre-exponential factor, the kinetic rate model approaches the principle of very thin drying zones, as commonly implemented in layer models.

It was found that the choice of drying model has a significant influence on the numerical efficiency of the overall thermal conversion model of a thermally thick wood particle. This is the case, since the time step size is determined by drying and not by devolatiliztion reactions. It was also found that the low robustness of the thermal drying model is a key weakness of this model, and that the kinetic rate model is less complex to implement in a code.

Besides these numerical aspects all three models are capable of demonstrating that the overall heating time of wet wood is greatly affected by the amount of moisture in the wood log.

4.3. Devolatilization

Devolatilization is a thermochemical degradation process that occurs by definition in the absence of oxygen. While tar and permanent gases are formed and leave the wood log via the pores, oxygen can only enter the wood log via diffusion, since these gas compounds build up a convective barrier to inflow.

In some works, there is a clear differentiation between pyrolysis and devolatilization, as pyrolysis is assumed to occur in a reducing environment, while devolatilization is related to thermochemical degradation in oxidizing environment. However, most particles that are thermochemically degrading are within a volatile cloud that to some extent mimics a reducing atmosphere, so these two expressions can be used interchangeably [78].

Chemical reactions, as well as physical processes that occur during thermal conversion, have to be modeled simultaneously since they influence one another [82]. The fresh green wood (=moist wood) is primarily heated by conduction. After drying, the heated part subsequently undergoes thermochemical degradation and the release of volatiles starts. In thermally thick particles, drying and devolatilization can overlap, even though they never overlap in space. The permanent gases that are formed during devolatilization include a vast variety of chemical species, with the main compounds being CO, CO_2, CH_4 and H_2. Produced in lower quantities are also light hydrocarbons such as ethene, propene and nitrogenous compounds [18]. In addition tar is formed, which is organic compounds that are liquid at ambient temperature [18]. This broad range of different gas phase compounds makes it clear that modeling all the species related to devolatilization reactions is a challenge, and the so-called lumping procedure has therefore been introduced. As part of this method, various products of thermochemical biomass

degradation are collected in different product categories, namely char, tar and permanent gases [83].

After all the gases have been removed, only a char layer remains [82]. Mostly due to higher pressure inside the particle (and due to a higher char permeability), the flow of the gases is directed towards the heated surface. In the high-temperature region, which the gases have to pass, secondary tar reactions, cracking or re-polymerization, occur. These reactions may occur homogeneously in the gas phase, or might also be heterogeneous and occur on the char surface. The gases can also be directed towards the virgin wood, which has a lower temperatures, leading to condensation. However, only a small fraction of the entire gases will be directed towards the colder wood region. As a result, the convective inward transport of heat and mass is often neglected in models. The condensed gas phase compounds can evaporate again if the temperature at the spatial location in the wood log increases over a critical value due to ongoing heat transfer phenomena [82].

The char layer forming on the biomass tends to build up on the non-devolatilized wood as devolatilization continues. This leads to an increased residence time of tar, thereby enhancing cracking or re-polymerization. As thermal degradation continues, the physical parameters of wood logs change due to shrinkage and cracking of the solid fuel, which again have to be considered in cases of heat, mass and momentum transfer [82]. During devolatilization, mass loss of wood will be around 80% due to the formation of gaseous products [23].

Furthermore, shrinkage becomes more important during devolatilization compared to its relevance during drying. This process is not reversible, and its degree depends on wood species, peak temperature and temperature history. It is also interesting that lignin can swell during devolatilization, which adds even more complexity to numerical modeling [43]. Shrinkage is influenced by the anisotropic properties of wood. The theoretical discussion of devolatilization underscores that considering detailed chemistry and detailed changes in wood structure yields a high-complexity model. Consequently, it is of interest to review all the chemical and physical aspects of devolatilization and identify the most relevant ones and some additional simplifications, such that future models can easily find the balance between accuracy and complexity, and therefore save computational time.

4.3.1. Mathematical modeling of wood devolatilization

The modeling of devolatilization of wood requires the description of chemical and physical phenomena in a mathematical form. Therefore, the most relevant governing equations for devolatilization modeling are discussed in this chapter. When modeling gas phase continuity Eq. (14) the devolatilization source term $\dot{\omega}_{\mathrm{dev}}$ occurs, which is defined as [37]

$$\dot{\omega}_{\mathrm{dev}} = (k_1 + k_2)\rho_{\mathrm{wood}} - \epsilon_{\mathrm{g}} k_5 \rho_{\mathrm{tar}} \qquad (26)$$

where k_i with i = 1,2,5 are reaction rate constants modeled with Arrhenius expressions. This is only an exemplary reaction pathway where three independent competitive reactions describe wood degradation. However, in a more generic way one can state that the first term in Eq. (26) represents primary devolatilization reactions and the second term describes secondary devolatilization reactions. Reaction rate constants k_1 and k_2 are due to permanent gases and tar formed from wood, respectively, whereas k_5 refers to the reaction where tar is converted to char again. The mass change of solid wood is defined as [1]

$$\frac{\partial M_{\mathrm{wood}}}{\partial t} = R_{\mathrm{wood}} = -(k_1 + k_2 + k_3)M_{\mathrm{wood}}, \qquad (27)$$

where k_3 is due to the formation of char from wood. The species mass fractions are calculated from Eq. (15) and the corresponding

source terms are given as [37]

$$\dot{\omega}_{\mathrm{tar}} = k_2 \rho_{\mathrm{wood}} - \epsilon_{\mathrm{g}}(k_4 + k_5)\rho_{\mathrm{tar}} \qquad (28)$$

for tar, where k_4 is the reaction rate constant for the cracking of tar to permanent gas. The source term of permanent gas is modeled similarly as

$$\dot{\omega}_{\mathrm{vol}} = k_1 \rho_{\mathrm{wood}} + \epsilon_{\mathrm{g}} k_4 \rho_{\mathrm{tar}}. \qquad (29)$$

The permanent gas phase includes a broad range of different species and the range of compounds that form this product group [19] is discussed hereafter. A detailed discussion on gas phase products from devolatilization is found in Neves et al. [19].

Commonly, one lumps together CO, CO_2, H_2 and CH_4, as well as other light hydrocarbons, when modeling permanent gases. Additional light hydrocarbons are C_2 species, as well as C_3 species. It was found that the main compounds of the permanent gas phase species are CO and CO_2, and light hydrocarbons and H_2 are also commonly present in lower amounts. This composition is little influenced by heating rate. In fact, CO, CH_4 and H_2 show similar temperature dependencies as far as their formation trends are concerned. It is also found that the higher light hydrocarbons (mostly C_2 species) increases linearly with methane, thereby suggesting that they have similar reaction pathways. However, the formation of CO_2 with respect to temperature changes deviates from what is observed in the case of the other compounds [19]. If the temperature is approximately 500 °C, it is expected that the major contribution of volatile species is derived from primary devolatilization reactions. In such cases, CO and CO_2 are the main compounds while small amounts of CH_4 are also present. At approximately 450 °C, 2/3 of the entire mass of dry gas species are CO_2, while the residual fraction is primarily CO. It has also been found that at temperatures below 500 °C the composition of the volatile species does not show a strong temperature dependency. However, as temperatures increase and exceed 500 °C, the yields of combustible gases in the volatile species become strongly temperature-dependent. Such a change in composition above 500 °C is mainly related to secondary reactions. As the temperature increases from about 500 °C to 850 °C, the mass fraction of CO increases from 2 to 15% to 30−55% (based on dry and ash-free fuel) [19]. Accordingly, the tar yield decreases. Some tars are also converted to light hydrocarbons (including CH_4), which thereby increases from 1% at around 500 °C to 10% at temperatures higher than 850 °C. Hydrogen shows a similar temperature dependency, and increases from < 0.2% at around 500 °C to > 1% at above 850 °C. It is therefore suggested that if a significant increase in CO and H_2 can be found in experiments, the presence of secondary tar reactions is highly relevant for an accurate prediction of permanent gas phase species product distribution. As mentioned earlier, the temperature dependency of CO_2 deviates from the temperature dependency of the residual species forming the volatile fraction. In the case of CO_2, no significant change with respect to an increasing temperature is found. This highlights that CO_2 is a main product of primary reactions [19].

The change of char mass due to devolatilization reactions is modeled as being influenced by primary and secondary devolatilization reactions, but also gasification reactions $\dot{\omega}_{\mathrm{gasif}}$ and oxidation reactions $\dot{\omega}_{\mathrm{oxid}}$ influence the char yield

$$\frac{\partial M_{\mathrm{char}}}{\partial t} = R_{\mathrm{char}} = k_3 M_{\mathrm{wood}} + k_5 V_{\mathrm{gas}} \rho_{\mathrm{tar}} - \dot{\omega}_{\mathrm{gasif}} - \dot{\omega}_{\mathrm{oxid}}. \qquad (30)$$

The overall mass change of char, Eq. (30), is modeled similarly to wood degradation in Eq. (27). Here, V_{gas} is the volume occupied by pores, which equals the volume occupied by the gas phase, since liquid water has entirely been evaporated as char conversion initiates [37]. The porosity of the dry wood can be expressed as the

ratio between the volume occupied by the gas phase and the total volume, as shown in Eq. (31)

$$\epsilon_{\mathrm{g}} = \frac{V_{\mathrm{gas}}}{V}. \tag{31}$$

Modeling the degradation of wood occurring during devolatilization is a vast field of research. Di Blasi [84] stated in her work that the field of chemical kinetics of biomass is highly debated. The complexity is that wood is a mixture of many different compounds that degrade differently. Not only does the raw material differ, but also a high number of different products needs to be modeled, which even further challenges researchers. Mathematically, this indicates a high number of required equations. The kinetics of these models can vary a lot in their stiffness, so the computational efficiency is also affected [85]. However, the computational cost and accuracy need to be balanced, and researchers inevitably have to apply simplified models to overcome this challenge [86]. The most common models are discussed in the following sections.

Finally the influence of devolatilization reactions on the temperature of the wood log has to be modeled. Due to devolatilization, the source term in the energy equation Eq. (2) is given by

$$\Phi_{\mathrm{dev.}} = \sum_{k=1,2,3} r_k \Delta h_k + \sum_{k=4,5} \epsilon_{\mathrm{g}} r_k \Delta h_k \tag{32}$$

where Δh_k is the heat of reaction, due to devolatilization reactions, with the first term representing primary devolatilization and the second term secondary reactions. As will be outlined later, it is a challenge to define accurate values for the heat of reaction for devolatilization, since it tends to vary from endothermic to exothermic reactions as conversion proceeds. We will go more into detail on how heat and mass source terms related to devolatilization reactions are modeled in those governing equations, and which challenges arise with certain model approaches.

4.3.2. One-step global mechanism model

The reaction mechanism of a one-step global mechanism can be illustrated as [20]

$$\text{dry woody biomass} \rightarrow \text{gases} + \text{char}. \tag{33}$$
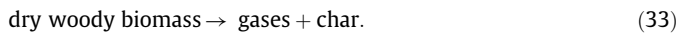
This is the most simplified reaction scheme applied in a number of works as shown by the number of different kinetic data used in the models (see Fig. 3). The temperature dependency of the Arrhenius expression defining kinetic rate constants is plotted in Fig. 3.

The kinetic rate constant by Ding et al. [64] seems to be inconsistent with the rest of the data used to model the one-step global reaction mechanism. It shows a steep increase of the reaction rate with respect to temperature increase, and eventually highly exceeds all the other values for reaction rate constants already at 500 K. It is therefore suggested that this set of data predicts too fast devolatilization. The inconsistency of kinetic data in the case of Ding et al. [64] is also highlighted by the fact that for the devolatilization modeling of birch wood, Larfeldt et al. [41] used a much lower kinetic rate constant, which agrees with what has been used for other hardwoods [46,55,57]. There is also a slight discrepancy in kinetic data used for beech devolatilization modeling by Yuen et al. [55] and Bruch et al. [46]. However, none of those two reaction rates increase unreasonably fast, and therefore both models are assumed to yield reasonable conversion rates.

The primary disadvantage of the one-step global model is that the produced gas phase is not automatically split into tar and permanent gases [22]. In order to clearly split the gaseous fraction, a stoichiometric coefficient for tar has to be known prior to modeling [22]. It is expected that the mass fractions of these two products are inversely linked, and that the ratio between the two products depends on operational conditions. In this approach, the reactant (wood) is considered to be homogeneous [37]. Considering only one
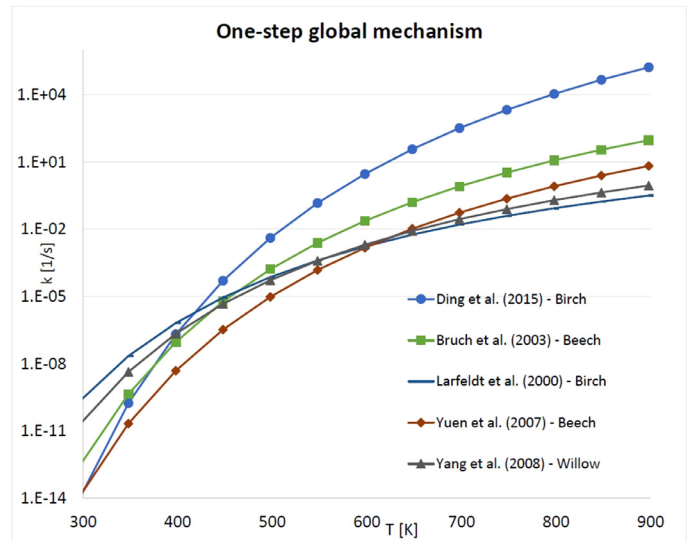
Fig. 3. Reaction rate constants of one-step global reaction mechanisms. In this plot the reaction rate constant, k [1/s] is plotted against the temperature, [K]. Kinetic data, used in a number of independent models in which different wood species were modeled, are plotted.

reactant, and consequently only defining kinetics with respect to a single reaction rate constant is often considered to be a rather crude approximation, even though the justification of this model is that the thermal behavior of biomass reflects the behavior of the sum of its compounds and tt is not the response of every single compound [37].

Many researchers work with single first-order reactions (one-component mechanism) when modeling devolatilization [41,50,51,55,57,60,64]. Some works [50,51] fitted the modeled mass losses and therefore the kinetics to experiments, such that surface reactions could be used to model devolatilization. This was done, since the model was based on an interface-based approach, and it was assumed that devolatilization only occurs at the surface of the dry wood layer. Such a fitting can be considered a weakness.

Even so, the primary advantage of the one-step global mechanism is that product yields, as well as overall decomposition rates, can be predicted accurately enough at a reasonable computational cost [10]. It is suggested that this is acceptable for most engineering applications. However, one might think that for larger particles this does not apply, since there is a large temperature difference in the particle and in one-step global reaction mechanisms, such a temperature influence on the char yield cannot be modeled precisely [20,87]. Furthermore, it is concluded that for the purpose of fundamental research on devolatilization, a more detailed devolatilization reaction model is recommended.

4.3.3. Independent competitive reactions model

In the three independent competitive reactions model, the solid input material degrades competitively to char, tar and permanent gases. The principle scheme of the independent competitive reaction model is presented in Fig. 4. The only linkage between the product
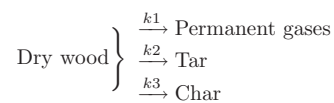
$$\text{Dry wood} \left\}\begin{array}{l} \xrightarrow{k1} \text{Permanent gases} \\ \xrightarrow{k2} \text{Tar} \\ \xrightarrow{k3} \text{Char} \end{array}\right.$$

Fig. 4. Independent competitive reactions scheme. This reaction model describes the thermochemical degradation of wood to tar, permanent gases and char via three independent competing reactions.

yields is through the mass fraction (the sum of all mass fractions at a certain time equal unity) [88].

A broad range of kinetic data for the three independent competitive reactions model is currently available and used in wood particle degradation modeling. Some of the most commonly applied kinetic data is discussed hereafter.

Thurner and Mann [89] present kinetics that are commonly used and that are derived from experiments with oak. The main disadvantage of this set of kinetic data is that the experiments were only conducted in a temperature range from 300−400 °C, which is very narrow and low. It is known that e.g. devolatilization reactions for cellulose can start below 300 °C, and overall devolatilization is expected to be finished at approximately 500 °C. The experiments were conducted with oak sawdust, which suggests that the kinetic data is mainly applicable to hardwood species. The influence of secondary reactions was aimed to be avoided during these experiments by keeping the temperature low. This suggests that if the kinetic data by Thurner and Mann [89] is to be used for modeling thermally thick particles, the modeling approach always has to be coupled with secondary reactions in order to predict the thermal conversion of a thermally thick particle with an acceptable accuracy. In general, it is more accurate to include secondary reactions as particle size increases.

A second set of commonly applied kinetic data was presented by Font et al. [80], who conducted experiments in a temperature range from 400 to 605 °C. This therefore leads to the conclusion that the kinetic data may not be valid in the temperature range from 200 to 400 °C, in which the degradation of holocellulose (combined cellulose and hemicellulose) in particular will occur. Furthermore, almond shells were tested, and no specific wood species can thus be directly related to this set of kinetic data.

The third very common set of kinetics was presented by Chan et al. [81], who based their kinetic model on two references. The kinetics for char formation were estimated from a previous work by Shafizadeh (obtained via personal communication, see [81]). The modeling results are highly sensitive to the kinetic data of char formation. Permanent gas and tar formation reactions and corresponding kinetic data were taken from Hajaligol et al. [90]. In this work, the rapid pyrolysis of cellulose was tested (1000 °C/s), and the temperature range of the experiments was between 300 and 1100 °C.

These three sets of kinetics are very often used when modeling thermochemical degradation of a single particle with the three independent competitive reactions scheme. The three independent competitive reactions model is commonly coupled to secondary tar reactions. If secondary tar reactions are neglected, this is linked to the simplifying assumption of produced gases exiting the wood particle or log immediately as they are formed. Such a simplifying assumption has been the basis for a number of works [44,52,53,59]. Bruch et al. [46] claimed that in the particle size range they were modeling (5 to 25 mm), only less than 10 % of the primary tars are cracked or re-polymerized, and accordingly, secondary reactions can be neglected.

One can also assume that without a correct inclusion of secondary charring or tar cracking reactions, the pressure field in the interior of the wood log is not predicted accurately, hence influencing the calculation of the gas phase velocity. However, this influence on the pressure prediction is assumed to be less important, since the overall prediction of the pressure is related to a number of uncertainties. These uncertainties include the common neglect of the formation of cracks in the char, in addition to a high uncertainty concerning commonly used permeability values.

Tar condensation reactions can also occur in a second stage after primary devolatilization, but such condensation reactions are commonly neglected (all works listed in Table 3 have neglected tar condensation). It is said that their influence on the thermal conversion process is somewhat limited, and in 1D simulations, where this was investigated in detail, it was found that the influence of tar condensation on overall conversion is negligible [91]. However, it is assumed that if asymmetric heating at the boundary of the wood log is given, the gaseous tar can flow to cooler regions and condense there. One can then expect that this will lead to a blocking of the pores, and a subsequent hindering of the convective transport of gaseous species, which can affect the pressure field in the wood interior. However, since the majority of the gases is transported outwards, this tar condensations can be neglected without significantly affecting modeling accuracy. The dependencies of devolatilization models on the temperature are shown in Fig. 5 a−c.

The mass loss rate of the center cell volume of the wood log versus the temperature in the center cell volume for different sets of kinetic data is shown in Fig. 6.

Fig. 6 shows that wood mass starts degrading fastest with the kinetic data suggested by Biswas and Umeki [1], while the kinetic data of Chan et al. [81], Thurner and Mann [89] and Font et al. [80] follow, respectively exhibiting lower mass loss rates. The modeled wood mass loss rate by Biswas and Umeki [1] increases steeply until it reaches a certain peak (a peak much higher compared to the other models). The mass loss behavior is comparable to what has been found for the other three sets of kinetic data, but occurs at a lower temperature range. The conversion is over at about 580 °C, when applying kinetic data by Biswas and Umeki [1]. This is a fast devolatilization compared to the other kinetic models resulting in devolatilization being finished at approximately 600 to 620 °C. It is also interesting that the models by Chan et al. [81], Thurner and Mann [89] and Font et al. [80] show a maximum mass loss rate at approximately 480 °C, which is close to what is commonly assumed to be the temperature where most of the devolatilization reactions should be finished (500 °C). With the kinetic data used by Biswas and Umeki, the peak in the mass loss rate occurred at slightly lower temperatures, around 460−470 °C. With respect to the data used by Biswas and Umeki, it has to be added that they used data originally derived by Di Blasi and Branca [92], who tested thermally thin particles and comparably high heating rates. It can also be seen from Fig. 7 that Biswas and Umeki predicted the lowest residual solid mass, which is consistent with the test conditions for the originally derived data. With respect to the kinetics found by Font et al. [80], where almond shells were tested, it has to be added that this data is assumed relevant for wood degradation modeling, since it is similar to the kinetic data obtained by Nunn et al. [93] for hardwood.

Fig. 7 shows that the kinetic data suggested by Font et al. [80] yields the highest residual solid. It is interesting to see that the amount of residual solid decreases as mass loss rates shown in Fig. 6 speed up, and also have their peak at lower temperatures. Thus, one explanation is that the mass loss rates with a peak at a lower temperature suggest that most of the mass losses are related to the degradation of cellulose and hemicellulose. In the case of Font et al. [80], the mass loss peaks at a slightly higher temperature, which agrees more with the devolatilization temperature of lignin.

A disadvantage of the three independent competitive reactions model is that wood as a reactant is not described in detail. Therefore, the validity of this reaction model is limited, since only wood species similar to the experimentally tested wood species for obtaining the kinetic data can be used. The main advantage of the this reaction scheme is, that one can predict char, tar and permanent gas yields, without pre-defining a stoichiometric coefficient that is required to split the product yields.

Overall, it can be concluded that the three independent competitive reaction scheme is a well-established concept that yields good results compared to experimental work, even though it misses a very detailed prediction of the product species.

Commonly, the secondary tar cracking reactions, which are often coupled with the three independent competitive reaction model, are of first order [94]. There are also models where the primary tar does
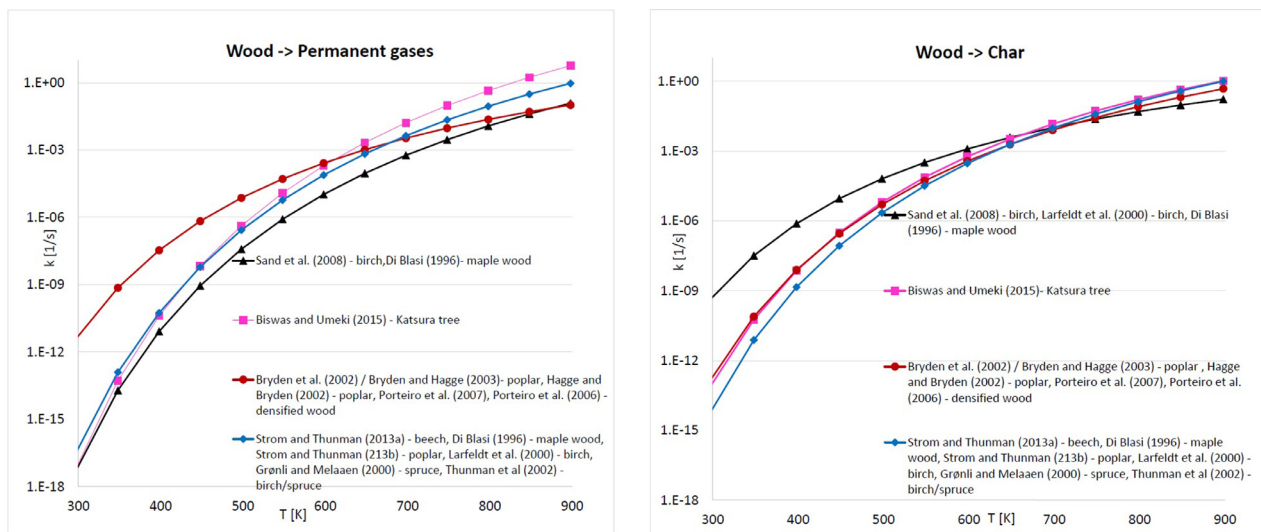
(a) Reaction rate constants of applied three independent competitive reaction schemes for the reaction of wood degrading to permanent gases.

(b) Reaction rate constants of applied three independent competitive reaction schemes for the reaction of wood degrading to char.
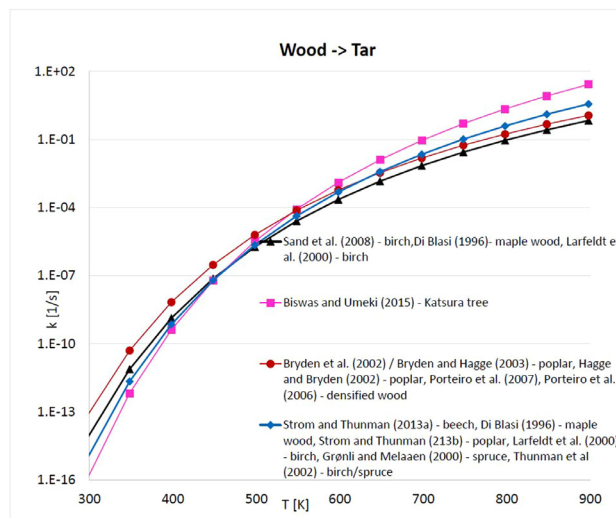
(c) Reaction rate constants of applied three independent competitive reaction schemes for the reaction of wood degrading to tar.

Fig. 5. Reaction rate constants of three independent competitive reaction schemes. The applied kinetic data was plotted also considering which wood species was modeled. The red lines having circles as markers refer to kinetic data originally derived by Thurner and Mann [89], the black lines having triangles as markers refer to kinetic data originally derived by Font et al. [80], the magenta colored lines having rectangles as markers refer to kinetic data used by Biswas and Umeki [1] and the blue colored lines having diamonds as markers refer to kinetic data originally derived by Chan et al. [81]. In the figures the lines are then related to the models that used these sets of kinetic data. (For interpretation of the references to color in this figure legend, the reader is referred to the web version of this article.)

not directly form char due to re-polymerization reactions and permanent gas phase compounds due to cracking, but instead yields secondary tar and permanent gases [22]. Various researchers have recently extended their kinetic models of thermal wood degradation to include secondary tar cracking [1,5,22,37,40,42,43,56,58,61].

The kinetic data used in their work is plotted against the temperature in Fig. 8a and b.

Fig. 8a shows the range of variation between the maximum reaction rate constant applied by Di Blasi [37] are the minimum reaction rate constant used by Kwiatkowski [61].

Fig. 8b shows that the reaction rate constant used by Kwiatkowski [61] is much slower than the reaction rate constant applied by other researchers [1,37,42,43,47,56,57,62]. Comparing Fig. 8a and b shows that heterogeneous reactions of tar to char are slower

compared to homogeneous gas phase reactions of tar to permanent gas phase compounds.

Furthermore, different values for the heat of reaction of pyrolysis were used. A common value for all primary reactions is -418 kJ/kg, and the heat of pyrolysis of the two competing secondary reactions is commonly set to 42 kJ/kg, e.g. [37,56]. Slight deviation from these values is common [42,43,47]. Accordingly, it is a common assumption to define primary devolatilization as endothermic reaction and secondary devolatilization as exothermic reaction. Grønli and Melaaen [40] chose different values (primary reactions endothermic with –150 kJ/kg and secondary reactions exothermic with 50 kJ/kg). By comparing all these previously mentioned values, it is suggested that there is no common consensus on heat of reactions. This lack of common consensus can even be illustrated by the heat of pyrolysis
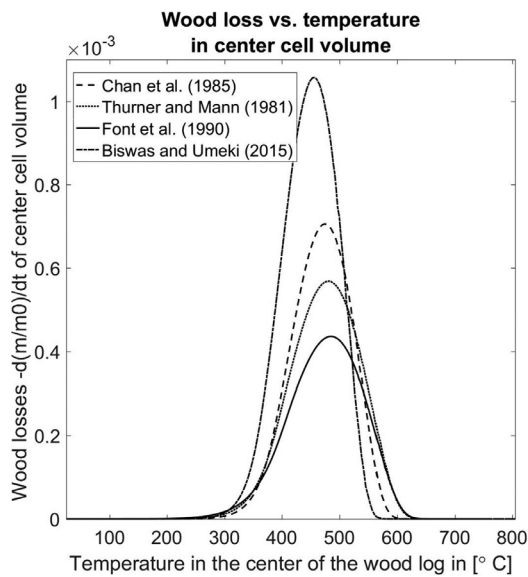
Fig. 6. Mass loss rate versus temperature of the center cell volume of a wood log. This is based on a mesh-based model, developed by the authors. The model is based on work by Di Blasi [37], and the same conditions and properties have been used; except a lower density of 410 kg/m³, a smaller particle size (1 × 1 × 3 cm³) and the varying set of kinetic data tested for three independent competitive reaction scheme models. The external heat flux heating up the wood log is 70 kW/m² (perpendicular to the grain). The heat flux to the boundary of the wood log was constant. The permeability was set to 1×10^{-15} m², and was therefore lower compared to Di Blasi, although it was found here that the influence of the convective term on the presented results was negligible.

of the primary devolatilization reaction of beech wood, which was found to vary between –156.1 and 145.3 kJ/kg [95]. The range of variation for the secondary pyrolysis reaction for beech wood is more narrow, only ranging from –65.7 to 17.3 kJ/kg [95]. Since beech wood can be assumed to represent hardwoods, one can also discuss the variation in the heat of pyrolysis for the degradation of spruce as a softwood species. In this case, the heat of pyrolysis of the primary degradation reactions ranges from 41.9 to 387.3 kJ/kg, while the secondary reactions range from –60.8 to –23.8 kJ/kg [95]. One of the reasons for these significant spans of values is that the experimental determination of heat of reaction of devolatilization reactions is very
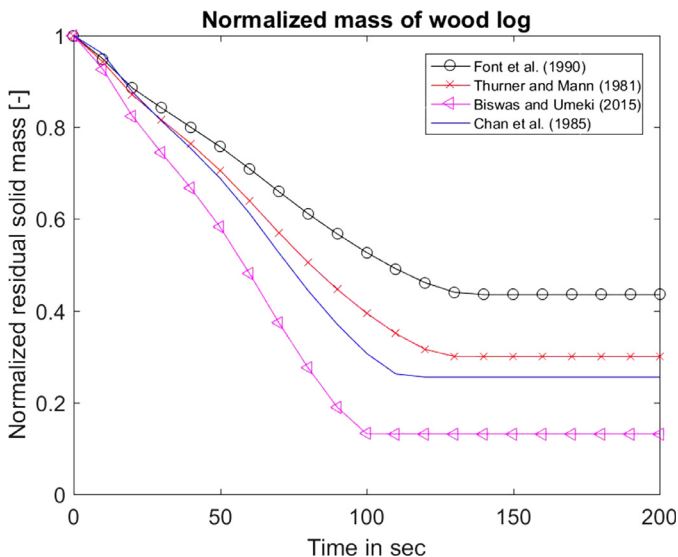

Fig. 7. Normalized residual mass of a wood particle based on most common kinetic data used in current three independent competitive reactions models. This is based on a mesh-based model, developed by the authors (description was provided earlier).

sensitive to the conditions under which the experiments are performed [19,95,96]. Moreover, it is also the case that many values for the heat of reaction for primary and secondary devolatilization reactions have been obtained by fitting the heat of pyrolysis to the measurements [8]. This instead suggests that the applied values are again based on a series of modeling assumptions, rather than being taken from realistic experiments.

4.3.4. Independent parallel reactions model

According to Papari and Hawboldt [94], many researchers prefer to predict the products of pyrolysis by modeling three independent parallel reactions. This means that they independently model the degradation of lignin, cellulose and hemicellulose [94]. The reaction scheme is illustrated in Fig. 9.

Mehrabian et al. [7,10] have implemented the three independent parallel reactions model, using pre-exponential factors of 2.202×10^{12}; 1.379×10^{14} and 2.527×10^{11} s⁻¹ for lignin, cellulose and hemicellulose degradation, respectively [97]. The corresponding activation energies for lignin, cellulose and hemicellulose decomposition were 181; 193 and 147 kJ/mol, respectively, experimentally obtained by Branca et al. [97].

The basic assumption for the three independent parallel reactions mechanism is that components in the mixture degrade the same way they would if they were decomposing separately [98]. Many authors have claimed that the degradation processes for hemicellulose and cellulose should be modeled as first-order reactions, whereas lignin degradation is modeled as a higher order reaction [99]. However, this is not a common consensus, since it is more commonly assumed that the degradation reactions of all pseudo-components are first-order reactions [98].

Furthermore, there are only a few studies that also include extractives in the independent parallel reaction model [20]. One advantage of such a split into three independent parallel reactions is that such a model can be applied to a variety of biomass types, since they differ by mass fractions of lignin, cellulose and hemicellulose. Because these compounds are all handled individually, it is relatively easy to adjust their fractions and take into account their influence in the model [100]. However, a more practical point of view causes the criticism that the modeling of three independent parallel reactions needs more input parameters (e.g. activation energy, pre-exponential factors, etc.) than the one-step global mechanism, which are primarily obtained by experiments or previous assumptions [22].

A main disadvantage of this model is that the interaction between cellulose and lignin, as well as hemicellulose and cellulose, is entirely neglected, even though such interactions have been found within certain temperature ranges [101]. Before being able to state whether ongoing cross-reactions limit the applicability of the three independent parallel reactions model with respect to the thermal degradation modeling of thermally thick wood particles in combustion environments, it is recommended to experimentally test the relevance of potential cross-linking reactions.

4.3.5. Broido—Shafizadeh scheme

In the Broido—Shafizadeh scheme, an activated intermediate is formed, which continues to degrade into tar, char and permanent gases [102]. The Broido—Shafizadeh scheme was originally developed for cellulose only, thereby suggesting that the initiation reaction leads to the generation of activated cellulose from cellulose. The activated cellulose will then competitively react to permanent gas, tar and char in first-order reactions [102]. It is very important to realize that the formation of the activated intermediate from the reactant (such as cellulose) is not related to any mass loss [103]. The principle of the reaction is shown in Fig. 10.

The Broido—Shafizadeh scheme, which was originally established for cellulose, has been used for modeling thermochemical wood degradation, even though in some works pure cellulose was
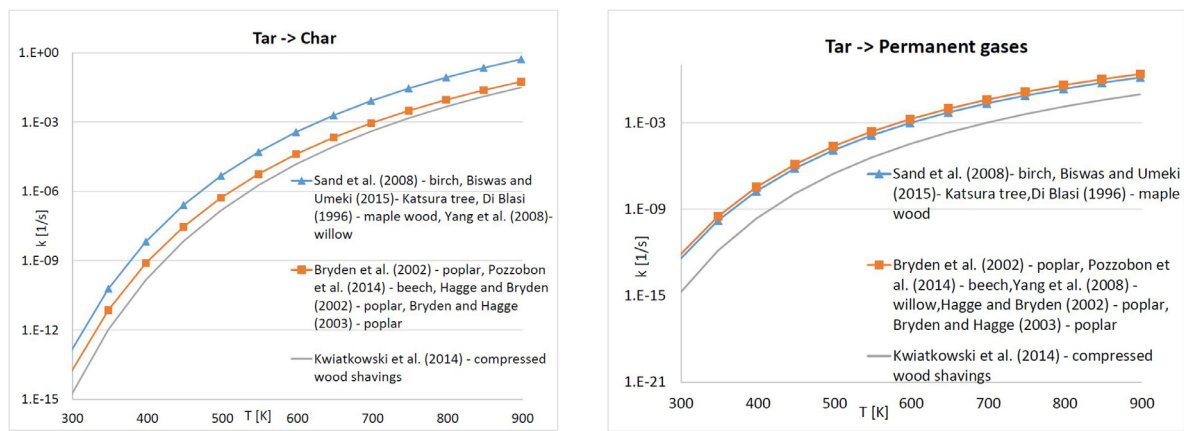
(a) Reaction rate constants of applied secondary reactions of tar reacting to char.

(b) Reaction rate constants of applied secondary reactions of tar reacting to permanent gases.

Fig. 8. Common kinetic data used for modeling secondary tar reactions. The kinetic rate constants applied in certain models are illustrated, and it is shown how the reaction rate constant increases as the temperature increases. The kinetic data discussed was applied for modeling different wood species. Even though there will most commonly not be a differentiation between tars derived from certain parent biomass fuels, the relation is still mentioned in the legend.

modeled [36,39]. This model is typically applied based on the assumption that wood can be modeled as pure cellulose, since holo-cellulose accounts for 75% of the wood [39], and it has already been applied for modeling thermochemical degradation of birch [41]. The typical reaction products resulting from lignin decomposition, which are mostly phenolic compounds, cannot be predicted with this model. One instead expects that even a more simplified scheme, based on the actual degradation of wood as a mixture of cellulose, hemicellulose, lignin and extractives results in a more accurate model of thermal conversion than the Broido−Shafizadeh scheme.

Furthermore, it is considered a main disadvantage that the reaction forming the activated intermediate, is considered less important at low temperatures, since based on new kinetic measurements, it has been found that such reactions are superfluous at 250 to 370 °C [37].

Furthermore, the kinetic parameters required for deriving the chemical reaction rate constant for the conversion stage of wood to the activated intermediate can hardly be derived experimentally. This conclusion agrees with what has been stated by Mamleev et al. [103], who claimed that the reactions related to the Broido−Shafizadeh scheme cannot be easily found experimentally, and interpretations of experimental results are difficult, since there is no mass loss related to the conversion to activated intermediate and it seems arbitrary to define when the activated intermediate has been created. From a more practical point of view, the Broido−Shafizadeh scheme also does not provide advantages compared to the more suitable three independent parallel reactions scheme or the three independent competitive reactions scheme, since in all cases three kinetic rate constants have to be determined. Due to these
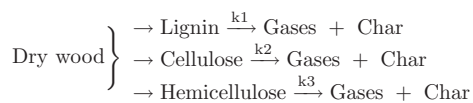
$$\text{Dry wood} \begin{cases} \rightarrow \text{Lignin} \xrightarrow{k1} \text{Gases } + \text{ Char} \\ \rightarrow \text{Cellulose} \xrightarrow{k2} \text{Gases } + \text{ Char} \\ \rightarrow \text{Hemicellulose} \xrightarrow{k3} \text{Gases } + \text{ Char} \end{cases}$$

Fig. 9. Independent parallel reactions model. This reaction model describes the thermochemical degradation of wood as three independent parallel reactions of its main components.
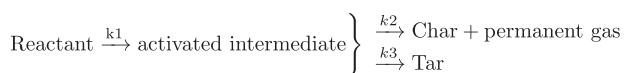
$$\text{Reactant} \xrightarrow{k1} \text{activated intermediate} \begin{cases} \xrightarrow{k2} \text{Char} + \text{permanent gas} \\ \xrightarrow{k3} \text{Tar} \end{cases}$$

Fig. 10. Broido−Shafizadeh scheme. This reaction model assumes the formation of an intermediate that eventually forms the final products char, permanent gas and tar.

facts, one cannot identify any major advantages or strengths of the Broido−Shafizadeh scheme.

4.3.6. Ranzi scheme

A multi-step lumped mechanism for the pyrolysis of woody biomass has also been developed by Ranzi et al. [27]. The most important aspects of this model are a detailed description of the parent biomass fuel, the devolatilization of it and its products. A simplifying assumption of the model is that similar components are grouped together, and related reactions are lumped together but in more detailed sub-groups of educts, products and reactions than the previously discussed models. This aims to sufficiently well balance the computational cost of modeling devolatilization and the accuracy of the predictions [27].

Cellulose reacts to activated cellulose, levoglucosan, hydroxy-acethaldeyde (HAA, $C_2H_4O_2$), glyoxal ($C_2H_2O_2$), CO, CH_2O, CO_2 and char, as well as H_2O in a number of reactions [27]. Levoglucosan is the main product at lower temperatures. At higher temperatures, the formation of other products such as HAA is dominant. Hemicellulose reacts to intermediates that subsequently decompose with different activation energies and charring propensities. One of the intermediates can form xylose, which is one of the primary components of the tar fraction. In addition, a number of species contributing to the permanent gas fraction are also released from the intermediates. Lignin is described by three sub-categories, which are either rich in carbon, oxygen or hydrogen, while the main products from lignin degradation are phenol and phenoxy species [27].

Advantages of the Ranzi scheme are that a broad range of volatile species can be predicted, with levoglucosan being the main product, due to high percentages of cellulose in both hardwood and softwood. Additionally, permanent gases such as CO, CO_2, H_2, CH_4 and C_2H_4 can be predicted. Alcohols, carbonyls, phenolics and water vapor can also be predicted. Moreover, the model can be applied to describe hardwood or softwood devolatilization, since the parent fuel can also be described in detail based on defining the contributions by its three main pseudo-components. It is also claimed that the model is applicable for a broad range of operational conditions, which enhances is applicability. One disadvantage is that secondary gas-phase reactions forming char are not included in the model, since char is only derived either from lignin or cellulose in the chemical wood structure, or the activated intermediates of cellulose and hemicellulose. Another weakness of this model is that the presence of extractives or inorganics, and their catalytic effect, are neglected.

Nevertheless, it is known that minerals contained in the parent fuel have an effect on the char yield, and can even catalyze cellulose and hemicellulose fragmentation [18]. Moreover, no nitrogen-containing species are included in the list of predicted products, i.e. the presence of fuel-bound nitrogen is also entirely neglected. The interaction between cellulose and lignin, as well as hemicellulose and cellulose, is neglected, even though, as previously mentioned, at temperatures comparable to temperatures in wood stoves, cross-linked reactions cannot be fully excluded. With respect to numerical efficiency it is also assumed that this model has its drawbacks. It is concluded that due to the increased number of modeled equations (compared to e.g. three independent competitive reactions model or the three independent parallel reactions model), the CPU time per time step is larger.

4.3.7. Other schemes

In Table 3, there is an extra column for "other schemes" and in this category some less common reaction schemes are listed. Alves and Figueiredo [34] modeled six parallel reactions. They provided kinetic data for cellulose and hemicellulose degradation, and further provided kinetic data for four additional reactions describing degradation of parts of the phenolic lignin macromolecule. Their kinetic data was obtained from isothermal TGA experiments performed with pine wood sawdust, with a particle size range of 180−595 μm. The temperature range was very broad (265-650 °C), and accordingly the kinetic data obtained is less restricted in its validity. One has to consider though, when using this set of kinetic data for large wood log modeling, that this set of kinetic data has originally been derived for thermally thin particles, and that experimentally derived correlations are needed to validate this model for thermally thick particles. Because the kinetics were originally derived for pine sawdust, a correlation was implemented [34] that was aimed to convert the mass loss obtained with the kinetics for thermally thin particles to the mass loss of large particles. The experimentally determined final char yield of large particle conversion entered this correlation as an empirical factor.

Wurzenberger et al. [45] based their devolatilization model on work by Alves and Figueiredo [34], and therefore also split the solid into various species that react in parallel. However, the kinetics for those reactions were taken from a TGA test, with a heating rate of 5 K/min and a beech wood particle of 1 mm, where the peak temperature of the tests was 1173 K [104]. The heat of pyrolysis was chosen such that it was correlated with a final char yield, as it was said that the actual value of heat of pyrolysis depends on wood species, particle size and the final char yield [45]. This broad dependency emphasizes again that it is very challenging to apply suitable values for the heat of reaction, and that the model is rather sensitive to this input data.

Larfeldt et al. [41] also implemented a reaction scheme with four independent parallel reactions, but it is not clearly stated which wood compounds are described by this degradation mechanism. They showed that a scheme with four independent parallel reactions was able to predict the correct devolatilization temperature for their application, while other models (one-step global mechanism, Broido−Shafizadeh and three independent competitive reactions scheme) over-predicted the initiation temperature of the devolatilization process. Even though the three independent competitive reactions scheme can be considered as an advanced devolatilization model, it is less advanced than the four independent parallel reactions model.

Babu and Chaurasia [48], as well as Sadhukhan et al. [58], based their devolatilization model on two competing reactions. In case of Sadhukhan et al. [58] the frequency factors and activation energies for secondary tar reactions were obtained by fitting the measured mass loss data of the tested wood sphere. The definition of the heat of reaction for secondary tar reactions was done in the same manner.

Therefore, doubt arises concerning the broad applicability of this model, as it appears to be significantly attached to the experiments it was validated against. Furthermore, this two-competitive reactions model only splits between gases and char, and even though changing operational conditions will affect the predicted yields of gases and char, such a variation in operational conditions cannot be linked to varying yields of tar and permanent gas. In order to know the yields of tar and permanent gases, one has to set a predefined ratio that does not vary with operational conditions.

Shen et al. [54] also modeled two independent competitive reactions yielding char and gases. It is not specified if this gas fraction included permanent gas and tar, but based on the applied kinetic data, one assumes that only permanent gas is modeled. Kinetic data by Thurner and Mann [89] was used, which was originally derived for the three independent competitive reactions scheme. In the work by Shen et al. [54], tar formation was therefore neglected. For this reason, it is concluded that both product yields and conversion times cannot be computed correctly. The same reaction principle was used by Koufopanos et al. [35], who added one consecutive secondary reaction, in which primary char and gases could react to secondary char and gases. For modeling secondary reactions they required a deposition coefficient that described the fraction of gas species deposited on char sites. This coefficient is a function of residence time inside the degrading particle, so it is also dependent on particle dimensions.

Melaaen [38] used a devolatilization model suggested by Glaister [105], which differs slightly from the common three independent competitive reactions scheme. In the model by Glaister, the solid parent fuel can also react to water vapor. In this model, the formed tar does not exit the particle immediately, since consecutive tar cracking reactions occur. However, the disadvantage of these secondary reactions is that one has to predefine a factor defining how much permanent gas, tar and water vapor are produced by such a consecutive cracking reaction. This again limits the applicability of the model, since such values do not consider changing operation conditions well enough. In addition to the predefined coefficient for splitting the products of the secondary tar cracking reactions, even more empirical values are required, since the other two reaction pathways forming permanent gas or char also produce water vapor simultaneously. Hence, one can conclude that this model, even though a broader range of products can be predicted, has to be applied with caution, since the application of such a predefined coefficient for conditions different from what they have been obtained in, can lead to false predictions.

Kwiatkowski et al. [61] assumed that wood does not react directly to char, but instead is converted to an intermediate solid, also referred to as temporary char, which then reacts to form the final char. However, since there is no clear definition of what is defined as char and how it differs from temporary char, such a classification seems ambiguous. One also cannot evaluate how the correlating kinetic data has been obtained if there was no clear differentiation between temporary char and char. A reaction model, following the same concept as suggested by Kwiatkowski et al. [61], has been introduced by Pozzobon et al. [62]. Kwiatkowski et al. [61] performed their own experiments on compressed wood shavings in order to obtain kinetic data. However, according to the given material properties, e.g. a density of 750 kg/m³, it is found that the sample of compressed wood shavings behaves comparably to an undensified wood sample.

Very simplified devolatilization models of a dry wood particle, also available in the current literature [59], model the devolatilization based on the assumption of a constant devolatilization temperature. The rate of devolatilization was accordingly linked to a constant pre-defined temperature, which acted as a boundary value between virgin dry wood and char. The decomposition rate was linked to the initial biomass density and the time-dependent evolution of the

char layer thickness. The disadvantage of this model is that detailed knowledge about the devolatilization products cannot be obtained, since only the overall thermal conversion time and the final residue can be obtained as model results. Moreover, the choice of pyrolysis temperature is ambiguous as this value highly varies with wood species, as well as heat flux [59].

A large number of devolatilization models are available. All of them are related to simplifications, but the degree of simplification differ significantly. It is clear that an extensive research focus, both modeling and experimental, is on devolatilization. The research within the field of devolatilization is more intense than within the other thermal conversion stages; drying and char conversion.

4.4. Char conversion

The solid product of the devolatilization process is a mixture of ash and mainly carbon, which further reacts as combustion proceeds. Modeling char conversion is challenging since heterogeneous reactions, which are influenced by mass transfer and kinetics, have to be modeled. When a particle with a low ash content, such as wood, is reacting, it will also shrink in size as the reactions proceed [106]. The gaseous products of char conversion will exit the reaction surface, and are transported into the freeboard by convection and diffusion. The carbon will primarily react with oxygen and form CO_2 and CO. Depending on the temperature and pressure conditions and the gas composition, the following reactions can be related to gasification and char oxidation [23]

$$C + O_2 \rightarrow CO_2 \tag{R1}$$

$$C + 0.5\ O_2 \rightarrow CO \tag{R2}$$

$$C + H_2O \rightarrow CO + H_2 \tag{R3}$$

$$C + CO_2 \rightarrow 2\ CO \tag{R4}$$

$$C + 2\ H_2 \rightarrow CH_4 \tag{R5}$$

Commonly applied kinetic data for the previously discussed char oxidation and gasification reactions are mentioned in Table 4.

The stoichiometric ratio, Ω, in Table 4 relates the moles of carbon to the moles of oxygen. Oxidation reactions of various ratios can be generically described by the reaction in Table 4 (listed in the first and fifth column). As one can see from Table 4, the same kinetic data is commonly used for char conversion. However, this entirely neglects that char reactivity is affected by operational conditions of a thermal conversion process. A higher heating rate would result in a highly porous and reactive char, with an extremely damaged structure, which is due to a fast and sudden gas phase release [107] compared to slower heating rates, as in the case of large particle heating. Such

a variation in reactivity cannot currently be reflected well enough, as in current models similar kinetic data is used for the most common oxidation and gasification reactions independent of the previous drying and devolatilization history of the particle. Yang et al. [57] stated that the kinetics will vary with the potassium content in the wood. It is also interesting to note, that in their approach the diffusion of oxygen is implicitly included in the kinetic expression.

The kinetics of char conversion are one of the most significant uncertainties in the current modeling of thermal conversion of thermally thick woody biomass particles. Using always the same kinetic data for char conversion does therefore not allow the consideration of the influence of varying operational conditions, e.g. pressure or residence time of char at certain temperatures, in a model. Furthermore, the influence of catalytic ash elements can hardly be correctly modeled. Because the diversity of available literature on single biomass particle combustion data is limited [78], this is recommended as a field of future research.

4.4.1. Mathematical modeling of char conversion

Char conversion is either kinetically or mass transfer controlled. The kinetically controlled regime is predominant at low temperatures, whereas the mass transfer controlled regime is dominant at higher temperatures. In addition to this, the mass transfer controlled regime is more important for larger particles, because intra-particle and external mass transfer are much slower than chemical reactions [52,53,61]. A limited mass transfer means that the gas reactant penetration into the particle is limited. Char conversion is heterogeneous and the rate at which conversion occurs is calculated based on intrinsic kinetics, the oxygen diffusion rate as well as the evolution of the specific surface area that is available for reactions [60]. The mass fraction of oxygen, Y_{O_2} is required to be determined if the rate of char conversion is aimed to be determined. Mathematically this can be expressed as [60]

$$k_m(\rho_{e,O_2} - \rho_{O_2}) = \dot{\omega}_C \frac{n_{O_2}}{n_C} \frac{M_{O_2}}{M_C} \tag{34}$$

with n_i being the moles of oxygen or char, M_i being the molecular masses of oxygen or char, k_m being the mass transfer coefficient, and $\dot{\omega}_C$ being the reaction rate of char oxidation. The oxygen densities are calculated as [60]

$$\rho_{O_2} = \frac{P\overline{M}}{RT_s} Y_{O_2} \tag{35}$$

if the oxygen density at the surface is calculated, since the temperature at the surface, T_s, is used to define the density. If the external oxygen density is calculated, it is defined as [60]

$$\rho_{e,O_2} = \frac{P\overline{M}}{RT_e} Y_{e,O_2} \tag{36}$$

Table 4
Comparison of kinetic parameters for char conversion. The most commonly applied kinetics for char conversion modeling (either gasification or oxidation reactions) are listed in this table. Models from Table 3 were only included here, if intrinsic kinetic data was given for char conversion modeling.

Ref.	$\Omega C + O_2 \rightarrow 2(\Omega-1)CO + (2-\Omega)CO_2$	$C + H_2O \rightarrow CO + H_2$	$C + CO_2 \rightarrow 2CO$	$C + 2H_2 \rightarrow CH_4$	$\Omega C + O_2 \rightarrow 2(\Omega-1)CO + (2-\Omega)CO_2$	$C + H_2O \rightarrow CO + H_2$	$C + CO_2 \rightarrow 2CO$	$C + 2H_2 \rightarrow CH_4$
	Pre-exponential factor				**Activation energy**			
[10]	1.715 [a]	3.42 [a]	3.42 [a]	3.42×10⁻³ [a]	74.8287	129.703	129.703	129.703
[53]	3.01×10^2 [b]	–	–	–	149.38	–	–	–
[52]	3.01×10^2 [b]	–	–	–	149.38	–	–	–
[51]	–	4.45×10^4 [c]	6.51×10^3 [c]	–	–	217	217	–
[60]	1.73×10^8 [c]	–	–	–	160	–	–	–
[50]	–	4.45×10^4 [c]	6.51×10^3 [c]	–	–	217	217	–
[7]	1.715 [a]	3.42 [a]	3.42 [a]	3.42×10⁻³ [a]	74.8287	129.703	129.703	129.703
[44]	1.715 [a]	3.42 [a]	3.42 [a]	3.42×10⁻³ [a]	74.8287	129.703	129.703	129.703
[46]	2.71×10^5 [d]	–	–	–	149.38	–	–	–
[57]	10.3 [c]	–	–	–	74.9	–	–	-

[a] indicates that values are given as m/sK. [b] marks the unit of 1/s. [c] indicates that the pre-exponential factor is given in m/s. [d] indicates that the pre-exponential factor has the unit m²/kg. E_a is given in kJ/mol.

where temeprature, T_e, and mass fraction Y_{e,O_2}, are taken from the external surrounding gas phase. Gasification, e.g. (R4) and (R3) is often modeled as an Arrhenius expression [50]

$$\dot{\omega}_{gasif,1} = S_{char} A_1 \exp\left(\frac{-E_{a,1}}{RT}\right) \rho_{char} y_{s,CO_2}^{n,1} \tag{37}$$

which describes reaction (R4), while reaction (R3) is described as

$$\dot{\omega}_{gasif,2} = S_{char} A_2 \exp\left(\frac{-E_{a,2}}{RT}\right) \rho_{char} y_{s,H_2O}^{n,2}. \tag{38}$$

where y_{s,H_2O} and y_{s,CO_2} are the surface mole fractions of the corresponding gasifying agent and S_{char} is the char specific surface area. The superscripts "n,1" and "n,2" mark the reaction orders of the corresponding reactions. The expressions in Eqs. (37) and (38) enter the equation for char mass loss calculations Eq. (30) as source terms, $\dot{\omega}_{gasif}$ Eqs. (37) and (38) show one approach on how gasification modeling can be done. However, the authors agree more with the char gasification and oxidation source term definition that was used by Fatehi and Bai [77].

The reaction of char with oxygen is faster than the gasification reactions for most practical applications. Hence, a common modeling assumption is that as long as residual oxygen is in the gas phase, char gasification reactions can be neglected [5,52,53,60]. Low oxygen supply rates to the particle result in a complete consumption of oxygen by the char and the leaving gas phase. A higher oxygen supply rate means that the reactions are limiting [108]. Accordingly, a model has to be flexible, such that it is valid over a broad range of operational conditions, which indicates the importance of a simultaneous consideration of both mass transfer and kinetic limitations for char conversion.

Despite this significant influence of operational conditions on char conversion, several authors modeled the char oxidation reaction as only diffusion controlled [46,50–53]. More flexible works are available where char conversion is a function of both reaction rate and mass transfer rate [7,10,44,60], which suggests that these models are more flexible to varying operational conditions.

Even though it is theoretically true that char oxidation is always faster than gasification reactions, which could therefore be neglected, it is not possible to pre-define when the critical oxygen mass fraction in the gas phase will be reached in practical applications. As a consequence, it is concluded that in order to be able to model a broad range of operational conditions and possible combustion conditions in a combustion unit, the implementation of both gasification and oxidation reactions is required. The model is then recommended to be able to freely model the most dominant reaction pathway depending on operational conditions.

In models where only the reaction of carbon and oxygen with carbon dioxide as a product (R1) is assumed to describe the char burnout process; e.g. [5,50,51], the production of CO from char conversion is entirely neglected. This assumption restricts char conversion to a temperature where CO_2 formation is dominant. By far, the char combustion in the majority of models is based on the reaction of carbon and oxygen, with both carbon monoxide and carbon dioxide as products [7,10,44–46,52,53,60]. The ratio between CO and CO_2, η, is commonly modeled as a function of temperature [52,53]

$$\eta = \frac{2\left(1 + 4.3 \exp\left(\frac{-3390}{T}\right)\right)}{2 + 4.3 \exp\left(\frac{3390}{T}\right)}. \tag{39}$$

It is assumed that modeling such a temperature dependency of CO/CO_2 increases the model's accuracy, and also broadens its applicability to a vast range of operational conditions.

Especially for large wet particles, it is suggested that the importance of gasifying reactions with H_2O is significant. In a thermally thick particle, the char layer will build up in the outer zones of the particle, even though in the core of the wood particle, evaporation still occurs. The formed water vapor has to pass through the hotter char layers, so it is reasonable to assume that the water vapor will react with the char. This of course also applies to CO_2 and H_2, which are products of wood devolatilization. These permanent gas phase species are also formed in the interior of the wood particle, and accordingly have to pass the hot char layer. A detailed modeling of leaving water vapor and permanent gas phase reactions with char are therefore considered essential for accurate prediction of product yields, both solid and gaseous.

However, gasification reactions described by reactions (R3) and (R4) have only been taken into consideration in some of the papers [7,10,44,61]. The formation of methane due to reactions of char with hydrogen have been included by even fewer works [7,10,44].

A further assumption in several models is that char only contains pure carbon [45,46,49–53,57,60,61,64]. In reality, char will also include ash and some reduced mass fractions of H, N and O, which remain after all the carbon has been consumed. The ash can build up an additional layer surrounding the particle, which results in an increasing resistance to mass and heat transfer. When this is taken into account, additional computations for the ash layer must be performed [7,10,44].

Furthermore, besides the influence of ash on mass transfer modeling, the catalytic influence of impurities on char conversion has not been modeled in any of the reviewed works. A general conclusion on whether considering impurities in a model is hard to draw, since there will be significant variations between different biomass species and also the extent to which specific inorganics are present will vary. However, one can expect that neglecting impurities is acceptable in the case of large woody biomass particles, because in larger particles diffusion is primarily controlling char conversion.

It was further found that there is no common approach on how the specific surface area available for heterogeneous reactions is modeled. However, the prediction of char conversion is highly dependent on the specific surface area. Because the formation of cracks and fissures leads to changes in the surface area, this also significantly affects heterogeneous reactions. Galgano et al. [60] considered the influence of cracks and fissures by introducing an enhancement factor when describing heterogeneous char conversion reactions. This enhancement factor is rather ambiguous, since it is not related to any detailed information concerning external and internal structural changes of a wood particle. Furthermore, it does not account for the fact that not all gas species can penetrate into any size of a newly formed opening (less relevant for cracks but more relevant for pore size), even though an increase of surface area enhances heterogeneous reactions.

It is common in current models to neglect the change in physical structure of the wood log and therefore the change in specific surface area. Overall, the change of specific surface area during thermal conversion, especially during char conversion, is very complex.

In the case of biomass char, it is likely that the pore size increases monotonously [109]. This contradicts with what is expected from coal char pore size evolution, since in such a case it is more likely that pores grow and also suddenly merge, which again results in a reduction of the specific surface area. It is therefore suggested to model the specific surface area of the biomass char to continuously increase during thermal conversion [110]. This can be achieved by modeling the evolution of the specific surface area which is defined as [110]

$$S_{char} = S_{char,0} \sqrt{1 - X\left(1 - \frac{1}{\epsilon_0}\right)} \tag{40}$$

where $S_{char,0}$ is the initial specific surface area and ϵ_0 is the initial porosity. Furthermore, S_{char} is the actual specific surface area and X

is defined as [110]

$$X = \frac{\rho_{char}}{\rho_{char,0}}. \tag{41}$$

The specific surface area is closely linked to the char porosity and the pore size seems to be a crucial parameter. One can distinguish between three main pore size groups, which are macro-pores ($d_p > 50$ nm), meso-pores ($d_p = 2-50$ nm) and micro-pores ($d_p < 2$ nm). However, even though the micro-pores contribute greatly to the specific surface area, they do not influence the overall conversion significantly, since reactants cannot enter these pores sufficiently well. The complexity in their case is that even though this pore size category is initially negligible, pore size will increase such that these pores will eventually become big enough to significantly contribute to conversion. It also has to be pointed out that for different reactions, different pore sizes are relevant [110]. Hurt et al. [111] also found that char and CO_2 mainly react outside of the micro-pores network. Furthermore, it was found that O_2 cannot enter micropores [112], while H_2O can penetrate into this pore size category [113]. It is therefore suggested that pore sizes also evolve differently and that an accurate description of heterogeneous reactions requires a good enough description of the available specific surface area.

A change of availability of reactive surface during reactions was considered by Wurzenberger et al. [45]. In their definition of reaction rates of char conversion, the amount of unreacted char was linked to an experimentally defined exponent, which expressed the change of reactive sites [114,115]. This experimentally defined exponent is highly dependent on operation conditions.

A detailed description of the evolution of the specific surface area evolution is lacking in current works. In order to reduce uncertainties related to char conversion modeling, a detailed knowledge of time dependent change of active sites and specific surface area is required.

After having focused on the main chemical processes of thermal conversion, the required data for physical characterization of woody particles are reviewed.

4.5. Dimensionality

Describing the thermal conversion of a single thermally thick biomass particle with a one-dimensional model is a very common simplification [1,5,7,8,10,34,35,37,38,40−54,58−60,63,64]. Utilizing a one-dimensional modeling approach effectively reduces both the complexity and required computation time of the model. On the other hand, the anisotropic structure of wood cannot be taken into account by 1D approximations, as this aspect has to be managed by multi-dimensional modeling approaches. Two-dimensional [36,39,56,57,62] and three-dimensional [55,61] single particle numerical models exist in the literature, but they are rare. A more detailed discussion on dimensionality of models follows hereafter.

4.5.1. One-dimensional interface-based models

In so-called interface-based models, the chemical reactions and phase changes take place at the boundaries between different layers in the particle. The layers are composed of either wet virgin wood, dry wood, char or ash, and the thickness of these layers is defined by the available mass of these solid compounds. A pre-requisite for the interface-based models is that chemical reactions, as well as phase changes, are much faster than the intraparticle diffusion of heat and mass. Only then can one assume very sharp fronts, thus indicating that the reactions are limited to very narrow regions only. These models can only be applied if the Biot number and thermal Thiele modulus describing the ratio between characteristic heat penetration time and devolatilization reaction time are large [8].

In the layer model, due to conversion of the fuel particle, solid matter leaves one layer to enter the layer assigned to the next

conversion stage and the drying, devolatilization and char combustion fronts move from the surface to the center of the particle [44]. Thunman et al. [44] adapted the concept of infinitely thin reaction fronts from Saastamoinen et al. [79] (only done for drying in their work), and assumed that devolatilization (and char conversion) also occurs in such infinitely thin reaction zones. This modeling work [44] has been the basis for a number of following models [5,7,8,10,52,53]. Galgano et al. [60], called their approximation a "front-based model", which still describes the same phenomena as all interface-based models.

The layer models are related to a high numerical efficiency and rather decreased computational cost, mainly due to the fact that only a somewhat limited number of governing equations is solved, and also partly due to a rather coarse spatial discretization in the interior of the wood particle. In fact, only equations for temperature and mass have to be solved in the layer model. Mehrabian et al. [10] found that the layer model resulted in the same accuracy as the much more extensive model by Lu et al. [78,116], who solved a set of 14 governing equations, whereas the layer model by Mehrabian et al. [10] only contains the energy and the mass equation. At the same time, their layer model was significantly faster.

A conclusion is that if the main purpose of the solid phase model is to be coupled with CFD simulations of large-scale furnaces, in which a bed has to be modeled, a reduced computational cost is the most relevant aspect and the layer model is considered a suitable choice. The solid phase models are also used to describe large wood log conversion in a heating unit. However, if the purpose of the wood degradation model is to predict crack formation and the transportation of species inside the pores, the interface-based models are not suitable. In such cases, mesh-based models are recommended.

However, the low robustness of the interface-based model can still be considered as a weakness of the model, independent of its application purpose. The sharp fronts where reactions occur result in mathematical discontinuities, which may cause numerical instabilities [8].

4.5.2. One-dimensional mesh-based models

In a mesh-based model, the equations for thermal conversion are related to grid points. The particle is therefore fully discretized. One-dimensional mesh-based models are applied by many authors [1,34,35,37,38,40−43,45−48,54,64] and solve a higher number of governing equations than the layer model, which inevitably leads to higher computational costs. Accordingly, these models need to be significantly simplified if coupled to CFD simulations, and if they are aimed to be able to compete with the numerical efficiency of layer models. Nevertheless, if reasonable simplifying assumptions can be found and computational costs are low, it is assumed that mesh-based models provide much more information than the layer model, e.g. since also liquid and gas phase can be modeled in detail.

4.5.3. Two-dimensional models

Sand et al. [56] as well as some other researchers [36,39,62] developed a higher dimensionality model, which is rarely done as the current focus is on 1D. They also considered anisotropy to some extent and modeled wood logs of very large sizes, which are comparable to what is used in wood stoves. Di Blasi [36,39] has also accomplished work within the field of 2D modeling of wood degradation. By considering anisotropy, one expects an asymmetric velocity field that affects heat and mass transfer. Di Blasi [39] found that heat conduction, both across and along grains, differs. It was found that the propagation of a devolatilization front inwards is first faster across the grain direction, because a larger surface heat flux occurs in that direction. However, the difference between across and along the grain continuously decreases with time, since for longer times the influence of convective transport values decreases (less cooling along the grains). Furthermore, the thermal conductivity across the grain directions is smaller than the thermal conductivity along the

grain direction. Di Blasi [39] found that 2D and 1D models yield results that are quantitatively relatively similar. 1D models showed slightly lower temperatures and velocities of gases in the pores of the wood particle in the cross-grain direction compared to 2D models. Consequently, the propagation of a conversion front was predicted to be slower, the final char density higher and the conversion times longer. Along the grain direction, 1D models over-predicted temperatures and velocities, which resulted in faster propagation speeds and reduced char densities [39].

Overall, it is important to consider that the discrepancy between 1D and 2D modeling results increased with an increasing particle size, so it is suggested that large wood log modeling requires 2D or even 3D models [39].

4.5.4. Three-dimensional models

The three-dimensional model of Kwiatkowski et al. [61] was based on the discretization of a wood cylinder in a mesh composed of hexahedral elements of 0.1 mm, which was found to be sufficient for solving the temperature gradient inside the particle. Yuen et al. [55] developed a three-dimensional model for the pyrolysis of wet wood with a detailed consideration of the drying process, anisotropy and pressure-driven internal convection of gases. The main disadvantage of 3D models is the higher computational cost, compared to 1D and 2D models. Higher dimensionality models are recommended if anisotropy is investigated or the influence of highly varying boundary conditions is considered. Furthermore, due to the fact that radial and tangential properties do not vary significantly, 3D models will not necessarily result in a significantly higher accuracy compared to 2D models. However, no comparison between 2D and 3D models has yet been made, and it is therefore recommended that future research investigates the difference between these two approaches.

4.6. Feedstock

Feedstock can vary in many aspects, such as particle size, shape, density, wood species and therefore also thermo-physical properties. Different values for certain properties of wood, relevant for thermal conversion, are used in current models. Some models are derived for the combustion of wood logs [1,41,49−51,56,63] or smaller wood particles [5,7,8,10,34−40,42−48,54,55,57−62,64] and others for densified wood [1,52,53]. Even though densified wood models are partially relevant, since intra-particle gradients are modeled, they are less relevant for wood log-fired heating applications. Most of the differences between densified and non-densified wood are due to different fuel properties, such as a higher density for compressed wood, as well as a lower porosity, lower water content and anisotropy. The thermochemical degradation process of densified wood will therefore be different from what is expected in wood log applications.

4.6.1. Isotropy

The assumption of isotropy is rather obvious when the conversion of densified wood is modeled. The densification process, including grinding of the wood to sawdust size particles, which is required for pellet formation, leads to homogeneity in the physical-mechanical characteristics of solid fuels [23]. Models for densified wood are commonly based on the assumption of isotropic conditions [1,7,10,52,53]. Raw wood should be considered an anisotropic material. For undensified wood particles and logs, the isotropic assumption is nevertheless applied in many models [5,7,8,10,34,35,37,38,40−51,54,57−64]. In other works, the anisotropy of wood is taken into consideration by using a bridge factor [1,56]. This simplified consideration of anisotropy of wood is based on averaging between parallel-to-the-grains- and perpendicular-to-the-grains-properties, and does not account for actual properties that depend on different directions. This consideration can be considered as an intermediate step

between the fully isotropic and fully anisotropic modeling of a wood log. Only a very limited amount of work has been done by actually implementing anisotropy, and consequently developing a higher dimensionality model without the usage of the bridge factor [36,39,55]. E.g. Yuen et al. [55] developed a 3D model, while Di Blasi [36,39] as well as Pozzobon et al. [62] implemented a 2D model. Due to this, it is of interest to focus on the influence of anisotropy on modeling predictions in the future.

4.6.2. Particle shape

It has been found that the particle shape has a significant influence on thermal conversion and that spherical particles have a lower mass loss rate than non-spherical particles. This is related to the smaller surface to mass ratio of spherical particles, which results in lower heat and mass transfer [10]. In the case of the layer model, a geometrical shape factor is used to model different shapes of the particle, and it was found that the layer model can sufficiently well describe the thermal conversion of particles of various shapes [10].

However, there is no model currently available that works with an irregular shaped particle, and the influence of cracks on thermal conversion is hardly ever included in a model. The particle shape is commonly assumed to be well-defined, though this is not the case, since wood particles are very irregular in most combustion applications. Therefore, it is of interest to identify how a more realistic description of particle shape affects the accuracy of the model.

It is not only that the virgin wood particles do not have ideal spherical or cylindrical shapes; the shape of the biomass char particles can be even more irregular. They are highly affected by the influence of the lignin structure of parent wood species, and by the mechanical process applied to form the wood particle [57].

It is therefore suggested to include the irregular shape of a particle undergoing thermal conversion. However, a very detailed description of the irregular shape of a particle and its evolution over time is expected to result in high computational cost as this will also require multi-dimensional models. Consequently, future models are challenged to find a balanced approach, including the description of high irregularity of particles while being computational low-cost models.

4.6.3. Particle size

The size of the particles varies from application to application, however, all the modeling approaches presented here are derived for predicting the thermal conversion of thermally thick wood particles and logs. Sadhukhan et al. [58] investigated a range of different particle sizes (the maximum being 10 cm and the minimum 1 cm). Their purpose was to identify the influence of the particle size on the entire devolatilization process. They found that the particle size has a significant influence on the history of the residual solid mass fraction, and accordingly the devolatilization time. The particle size influences when certain conversion stages are reached, even though the final residue mass fraction does not vary significantly.

In a particle thickness range of 0.1 cm - 2.0 cm it was found that for smaller particles, a high enough heat flux can result in a fast production of tar and permanent gas, and the leaving gases leave immediately, resulting in a single peak of leaving mass flow [64]. For larger particles, two peaks were found for the mass flow leaving the particle, which is related to an increasing influence of the char layer, which prevents the pyrolysate from exiting immediately [64].

Very few numerical simulations [41,56] have been performed on the thermochemical degradation and combustion of wood logs with sizes of the order of what is used in domestic wood stoves. Future work is therefore also encouraged to enhance research within the field of large wood log modeling. It is of interest to investigate how such comparably large particles and their shrinkage affect thermal conversion times and above all product yields, as it is expected that in case of such large particles the impact of the

char layer building up around the unreacted wood particle center has a significant influence. It is also assumed that leaving tar has a much longer residence time within hot char layers, so it is of interest to investigate to what degree the tars are converted within the char layer.

4.6.4. Density

Various wood species, and therefore also varying densities, are found in the existing literature. This variation limits the potential comparison of the modeling results (Table 5).

Based on a reference literature [33], that provides detailed information about wood and its properties, including density, the authors now investigate if the applied densities, used in current models are consisted. By investigating if the density is suitable for modeling a certain wood species, the authors were able to present a database for different wood species, that can be used for future model development. Furthermore, inconsistent values can outline that the model

was fitted to agree with experiments. Bryden et al. [42] modeled basswood with a density of 420 kg/m^3, which deviates slightly from the reference density of American basswood, which is defined to be 380 kg/m^3 [33]. However, it has been concluded that the chosen density is still suitable for modeling basswood, since it is assumed that the choice of other fuel properties, e.g. thermal conductivity, will have a more significant effect on thermal conversion times and product yield predictions.

For beech wood, the values for dry wood density ranged from 680 kg/m^3 [7] to 750 kg/m^3 [46]. Overall, this span is comparably narrow, with American beech, as a representative of beech wood, having a density of 680 kg/m^3 [33].

In the case of birch wood, it was found that a much broader range of densities was applied. The value span reached from 410 kg/m^3 [41,56] to a maximum of 740 kg/m^3 [54,64]. Based on reference values from the literature for sweet birch and yellow birch, having densities of 710 and 660 kg/m^3 [33], respectively, it is concluded that

Table 5
Comparison of wood densities.[a] states that this is the specific density (oven dry cell-wall substance); [b] aims to differ between the density for different charcoal samples with different diameters. If no superscript is given, the apparent density is given, which is the density of wood, if porosity is taken into consideration. If "−" is in one cell of the table, this highlights that the information was not mentioned in the paper. Structuring of the table was done by wood species.

Ref.	Name and year	Wood species and/or type	$\rho_{dry,\ wood}$[kg/m^3]	ρ_{char}[kg/m^3]
[42]	Bryden et al. (2002)	Basswood	420	−
[46]	Bruch et al. (2003)	Beech	750	200
[7]	Mehrabian et al. (2012a)	Beech	680	−
[62]	Pozzobon et al. (2014)	Beech	701	−
[8]	Ström and Thunman (2013)	Beech and poplar	−	−
[55]	Yuen et al. (2007)	Beech	700	91.56
[64]	Ding et al. (2015)	Birch	740	−
[41]	Larfeldt et al. (2000)	Birch	410	150/ 100[b]
[56]	Sand et al. (2008)	Birch	410	125
[54]	Shen et al. (2007)	Birch	740	−
[44]	Thunman et al. (2002)	Birch/ spruce	540 (± 40)/ 420 (± 40)	1950[a]
[58]	Sadhukhan et al. (2009)	Casuarina wood	682	−
[36]	Di Blasi (1994),			
[39]	Di Blasi (1998)	Cellulose	420	−
[61]	Kwiatkowski et al. (2014)	compressed wood shaving	750	170
[1]	Biswas and Umeki (2015)	Densified wood (Pine and Spruce)	1100	1950[a]
[10]	Mehrabian et al. (2012b)	Densified wood (spruce)	1200	−
[52]	Porteiro et al. (2006),			
[53]	Porteiro et al. (2007)	Densified Wood	1480[a]	1957[a]
[59]	Haseli et al. (2012)	Douglas fire	504	50
[1]	Biswas and Umeki (2015)	Katsura tree	500	1950[a]
[37]	Di Blasi (1996)	Maple wood	650	−
[42]	Bryden et al. (2002)	Red oak	660	−
[60]	Galgano et al. (2014)	Oak	670	−
[59]	Haseli et al. (2012)	Oak	753	75
[34]	Alves and Figueiredo (1989)	Pine	590−640	−
[42]	Bryden et al. (2002)	Southern Pine	508	−
[59]	Haseli et al. (2012)	Pine	380	60
[59]	Haseli et al. (2012)	Plywood	462	60
[42]	Bryden et al. (2002)	Poplar	504	−
[47]	Bryden and Hagge (2003)	Poplar	504	−
[50]	Galgano and Di Blasi (2006)	Poplar	460	−
[51]	Galgano et al. (2006)	Poplar	460	−
[43]	Hagge and Bryden (2002)	Poplar	504	−
[7]	Mehrabian et al. (2012a)	Poplar	545	200
[10]	Mehrabian et al. (2012b)	Poplar	545	200
[59]	Haseli et al. (2012)	Redwood	354	50
[40]	Grønli and Melaaen (2000)	Spruce	450	−
[59]	Haseli et al. (2012)	Spruce	450	60
[7]	Mehrabian et al. (2012b)	Spruce	420	−
[57]	Yang et al. (2008)	Willow	820	−
[48]	Babu and Chaurasia (2004)	−	650	−
[35]	Koufopanos et al. (1991)	−	650	−
[49]	de Souza Costa and Sandberg (2004)	−	360	−
[38]	Melaaen (1996)	−	550	−

the very low values of $410\,\mathrm{kg/m^3}$ [41,56] are not consistent with what has been reported elsewhere.

The higher density of compressed wood compared to uncompressed wood is a good assumption, since a lower porosity is also expected in densified wood particles due to the densification process. The comparably low density found by Kwiatkowski et al. [61] makes it hard to identify a clear differentiation between uncompressed and compressed wood, as the density is rather typical for uncompressed wood, while still compressed wood shavings were tested.

Maple wood was modeled [37] with a density of $650\,\mathrm{kg/m^3}$, which lies within the range of reasonable maple densities, whereby the maximum density is $660\,\mathrm{kg/m^3}$ (maple, sugar) and the minimum value $500\,\mathrm{kg/m^3}$ (maple, silver) [33]. The density for oak used in models [60] is also considered a suitable choice, since the overall values for oak densities found in the reference literature range from 660 to $720\,\mathrm{kg/m^3}$ [33].

When comparing the pine density chosen for different models [34], it was found that the value agrees well with the reference pine densities [33]. Still, the overall range of potential pine densities is significant, with a minimum value of $370\,\mathrm{kg/m^3}$ and a maximum value of $620\,\mathrm{kg/m^3}$. In case of pine wood modeling, one must therefore specify the type of pine wood in more detail and choose the properties for modeling thermal conversion accordingly.

When modeling poplar, the applied densities range from 460 [50,51] to $545\,\mathrm{kg/m^3}$ [7,10]. When compared to reference data [33], the lower density limit agrees with the density of yellow poplar.

Modeling spruce was done by assuming a density of $450\,\mathrm{kg/m^3}$ [40], which exceeds the maximum reference value by $20\,\mathrm{kg/m^3}$ [33]. However, it is assumed that this deviation is not very significant, since the density range of different spruce types ranges from 370 to $430\,\mathrm{kg/m^3}$, such that the difference between chosen and maximum reference value is comparably small. The modeled Redwood densities [59] agree well, with the reference value for young growth Redwood being $370\,\mathrm{kg/m^3}$ [33].

With respect to porosity, the documentation of applied values in the literature is scarce. Most commonly, only apparent densities of wood are given, and because there is no detailed information on either the porosity or true density of wood, no back-calculation or proper discussion can be performed. However, the conclusion is that if acceptable wood densities are used in the model, both for hardwood and softwood, a proper porosity has been chosen as well. Accordingly, one would expect that since the densities previously discussed agree well with literature data from the reference literature [33], the porosities applied in current models are within reasonable ranges. Fig. 11 shows what porosity is expected when assuming a true density of $1500\,\mathrm{kg/m^3}$ [117] and relating it to the previously listed apparent densities, such that

$$\epsilon = 1 - \frac{\rho_{\text{wood apparent}}}{\rho_{\text{wood true}}} \tag{42}$$

is fulfilled and the corresponding porosity, ϵ, can be calculated. The true density, which is the density of the cell walls, is considered to be the same for different wood species [117], and accordingly the same true density was used for both hardwoods and softwoods. In Fig. 11, the porosities listed in some works were also plotted.

It is shown in Fig. 11 that porosity increases as density decreases, which fits with the theoretical understanding of the wood structure, containing a solid matrix and pores filled with gas (in case of oven-dry wood). A higher porosity indicates a higher volume filled with gas phase, which leads to a reduction in apparent density. As stated earlier, by discussing the agreement of chosen apparent densities in models with literature data, it was found that porosities also agree well with what can theoretically be expected for certain wood species. It was also found that the applied porosities, given in a limited number of works, agreed well with what would have been theoretically expected. When it comes to finding values for densities of different wood species, a broad range of values is available in the open literature. Accordingly, less uncertainties are expected to be introduced to models, by the choice of wood densities.

4.6.5. Thermal conductivity

The characteristics of wood vary along, across and tangential to the grains, which also affects heat and mass transfer. Thermal conductivity across- and tangential to the fiber direction is approximately one-third of the thermal conductivity along the grains [39]. The effective thermal conductivity of green wood is defined as [22]

$$k_{\text{eff,s}} = k_{\text{cond}} + k_{\text{rad}} \tag{43}$$

where k_{cond} and k_{rad} are the conductive and radiative contributions, respectively. The conductive part is a function of the thermal properties of the fibers, bound and liquid free water and gas [22]

$$k_{\text{cond}} = f(k_{\text{fiber}}, k_{\text{bound, liquid free water}}, k_{\text{gas}}). \tag{44}$$
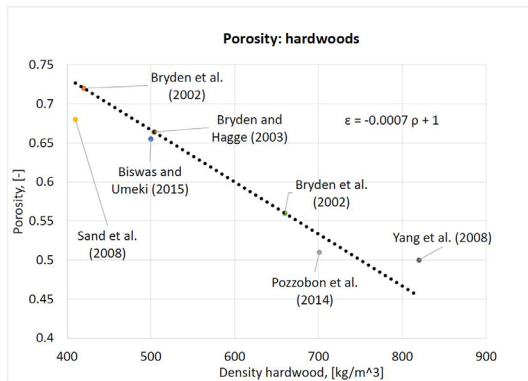
(a) Porosities of hardwoods. The plot shows the calculated porosities, obtained when using the apparent densities listed in models and a certain true density taken from the literature [117]. Given values for porosities found in literature were also added to the plot (single dots).
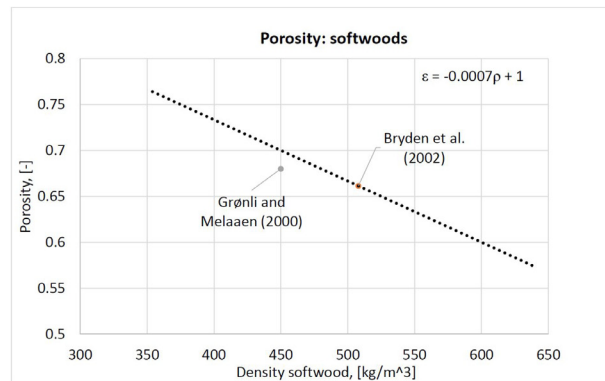
(b) Porosities of softwoods. The plot shows the calculated porosities obtained when using the apparent densities listed in models and a certain true density taken from literature [117]. Given values for porosities found in literature were also added to the plot (single dots).

Fig. 11. Porosities of different wood species plotted against the typical wood species density. (The calculated porosities are illustrated by the corresponding trendline (blue line)). (For interpretation of the references to color in this figure legend, the reader is referred to the web version of this article.)

The radiative term in the effective thermal conductivity is less important in green wood but becomes more influential as pore size increases, which is the case in the char layer. Furthermore, the radiative term in the effective thermal conductivity definition is influenced by the temperature to the power of three, and accordingly in the stage of char conversion, and for conditions where higher temperatures are expected, this term becomes significant.

Biswas and Umeki [1] use high conductivity values, but these values are given for cell walls. Multiplication with porosity leads to the actual thermal conductivity of dry wood

$$k_{\text{wood}} = k_{\text{cell wall}}(1-\epsilon_{\text{g}}). \tag{45}$$

It is also relatively common to combine the parallel and perpendicular thermal conductivities into one effective thermal conductivity, which is based on a fraction term that indicates the amount of material perpendicular to the heat flow $(1-\xi)$ and parallel to the heat flow (ξ). Here, ξ is often referred to as a bridge factor. This modeling approach has already been discussed when discussing anisotropy modeling in 1D. The mathematical expression for this correlation is given as [22]

$$k_{\text{eff,s}} = \xi k_{\text{parallel}} + (1-\xi)k_{\text{perpendicular}}. \tag{46}$$

One of the weaknesses of the bridge factor is that it is actually often only used to fit modeling results to experimental results.

The choice of bridge factor has a significant influence on the temperature profile and conversion time, as shown in Fig. 12.

The bridge factor weights the actual thermal conductivity between a maximum value (parallel to the fiber direction, $\xi = 1$) and a minimum value (perpendicular to the fiber direction, $\xi = 0$). The faster heating related to pure thermal conductivity along the grains leads to faster conversion times and a lower residual solid mass. This significant influence highlights that not only does the value chosen for thermal conductivities have an influence on model accuracy, but also that the corresponding direction (parallel and perpendicular) influence heating to a certain extent. The bridge factor is a value that is found to fit model results to experiments, and a broad range of values is actually found in the literature [22]. Moreover, the bridge factor does not provide a detailed description of anisotropy, and is therefore considered a less complex method that can still provide reasonable predictions for temperature profiles and mass losses. Concerning a velocity field this bridge factor is however assumed to result in errors.

The most common dependencies of thermal conductivities are discussed hereafter, which includes the influence of densities and therefore wood species and temperature

As suggested by Simpson and TenWolde [33], it can be seen in Fig. 13 that the thermal conductivity (across the grain) increases with the wood density, which is the case for both softwood and hardwood. This correlates well with the general understanding that an increasing density is related to decreasing porosity, and accordingly the influence of the cell wall thermal conductivity increases, which as such is higher than the thermal conductivity of the apparent wood. Furthermore, one can clearly see that the dependency of the thermal conductivity on wood density is similar for hardwoods and softwoods. When comparing thermal conductivities across the grain used in models (listed in Table 3, plotted in Fig. 13 in dark blue diamonds) with values found for oven-dry wood in the reference literature [33] (light blue rectangles), the overall agreement was acceptable. Even though, especially at higher densities, the values deviate significantly, they were found to be acceptable, as it was claimed in the reference data [33] that the actual thermal conductivities can deviate by about 20% from the listed values ($k_{\text{ref, perp}}$ plotted in Fig. 13 (light blue rectangles)). The brownish line presents the trend line for thermal conductivities along the grain commonly used in models. One can clearly see that those values are significantly higher than the thermal conductivity across the grain [33]. The effective thermal conductivities applied in 1D models (see Table 3; marked by orange triangles in Fig. 13), mostly has a value between the thermal conductivity across and the thermal conductivity along the grain.

However, because there is no clear trend visible on how the thermal conductivities in the modeling works were chosen, it is suggested that they were chosen in such a way that modeling results fitted well with the experimental data.

Only a limited number of works [36,39,55,62] is available in which the anisotropy of wood was considered by setting different values for the thermal conductivity of wood and char, depending on the actual direction of heat flow with respect to the fiber structure in a multi-dimensional model.

The difference between perpendicular and parallel values is significant, as shown in Fig. 14.

2D models, e.g. [62], are based on the simplifying assumption that the radial and tangential values for thermal conductivity do not differ significantly. Accordingly, it was said that a 2D model will yield an acceptable accuracy. This difference in thermal conductivity depending on the direction in the wood log, suggests that accurate consideration of this property can only be done by multi-dimensional models.
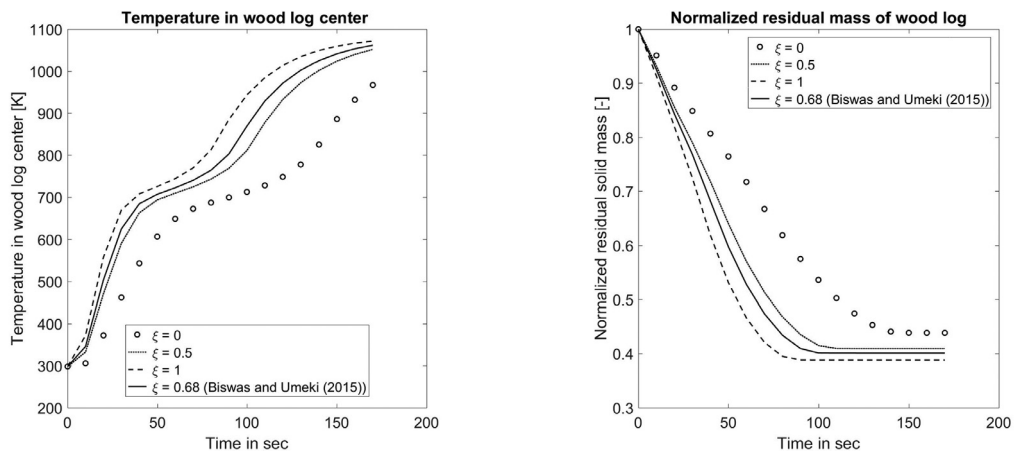

(a) Influence of bridge factor on core temperature profile.

(b) Influence of bridge factor on normalized residual mass and overall conversion time.

Fig. 12. Influence of different bridge factors on temperature and normalized residual mass. Different bridge factors were chosen to outline that the choice of bridge factor can significantly influence the accuracy of a model. The tested model was developed by the authors.
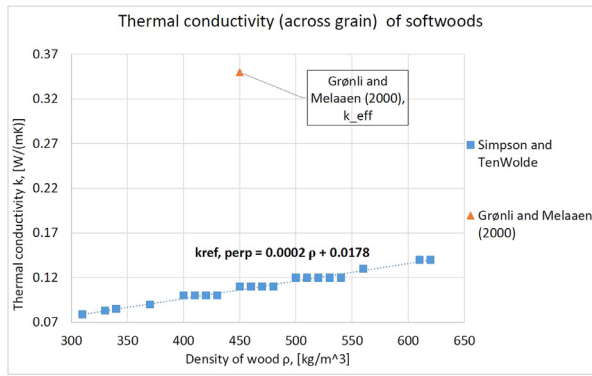
(a) Thermal conductivity of softwoods. Comparison of $k_{\text{eff.}}, k_{\text{perp.}}, k_{\text{parall.}}$
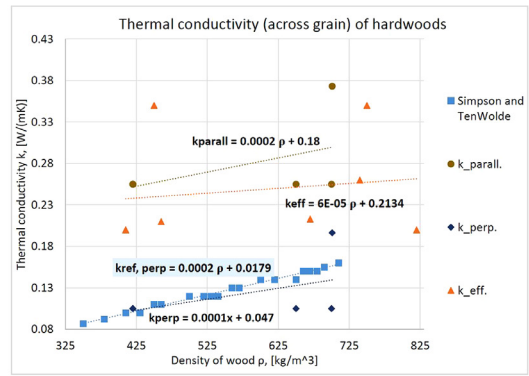
(b) Thermal conductivity of hardwoods. Comparison of $k_{\text{eff.}}, k_{\text{perp.}}, k_{\text{parall.}}$

Fig. 13. Thermal conductivity dependency on wood density for hardwood and softwood. The reference data used in this figure has been taken from Simpson and TenWolde [33] ($k_{\text{ref, perp}}$, light blue rectangles and trend-line). The residual data has been collected from models where it was given together with a wood species, listed in Table 3. If the wood species was not given, or no constant value of thermal conductivity of virgin wood was used, the value was not added to the figure. The thermal conductivities used in models plotted here were taken from [22,36,37,39−41,46,50,51,55−57,60,62,64]. (For interpretation of the references to color in this figure legend, the reader is referred to the web version of this article.)

The thermal conductivity of wood has quite often been described as a function of temperature, while other dependencies are neglected. Density dependencies have only been added by Bryden et al. [42,47] and Hagge and Bryden [43]. It has, however, not been modeled how this relation between thermal conductivity and wood density changes as wood density changes due to thermochemical degradation. Still, it can be assumed that it is a fair enough approximation in that case to model the change of thermal conductivity, as a linear interpolation between the thermal conductivity of wood and char such that the actual value is only defined by the degree of conversion. Further dependencies of the thermal conductivity of wood on either extractives or structural irregularities, which have been found for wood material [33], have not been included in any of

the applied thermal conductivities for wood used in models listed in Table 3. Future research could therefore investigate how extractives and structural irregularities influence the modeling results, and whether the increased complexity due to their incorporation is balanced by the enhanced accuracy.

Furthermore, little information is given on the thermal conductivity of the pyrolysis gas. In [37,40,48,52,53], a thermal conductivity of 0.026 W/mK for the gas phase was used. In contrast to this, Sand et al. [56] used the thermal conductivity of propane (0.0176 W/mK) for modeling the gas phase. Reviewing a number of modeling works has shown that the thermal conductivity is commonly not adjusted based on the chemical composition of the gas phase. However, this simplifying assumption is reasonable, as the influence of the gas
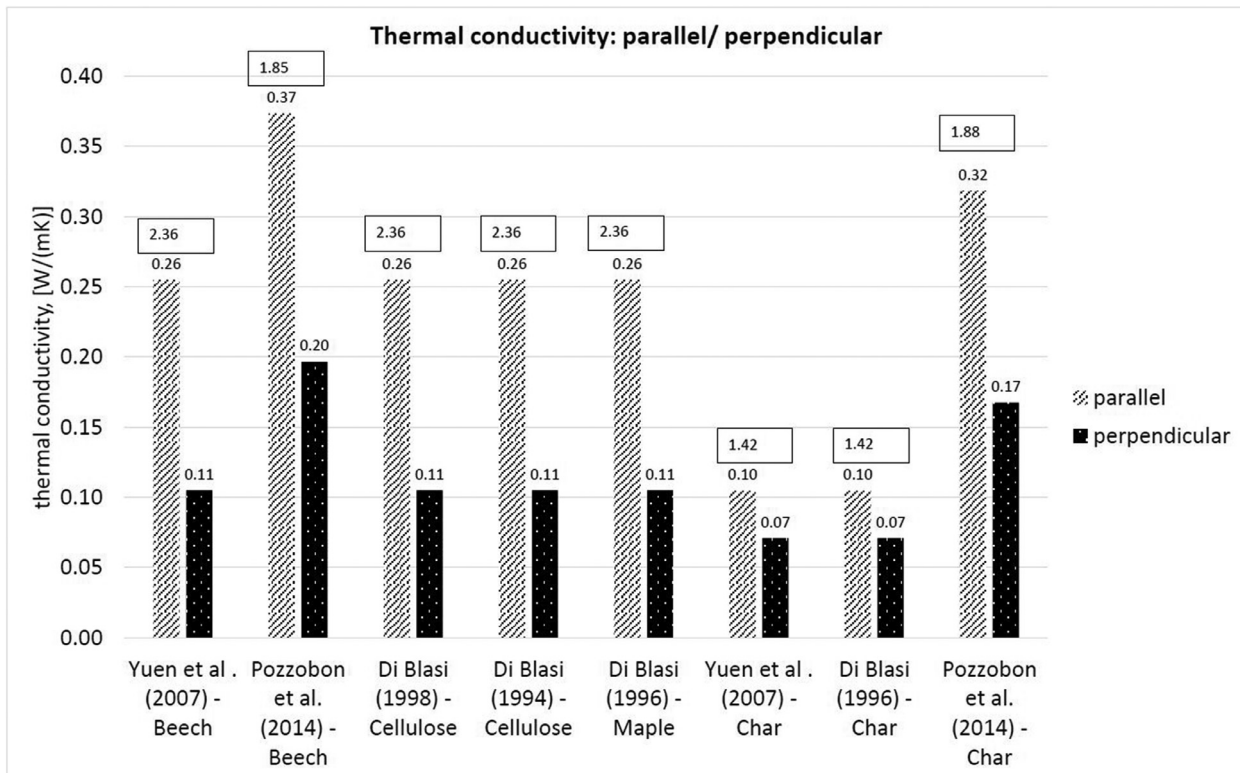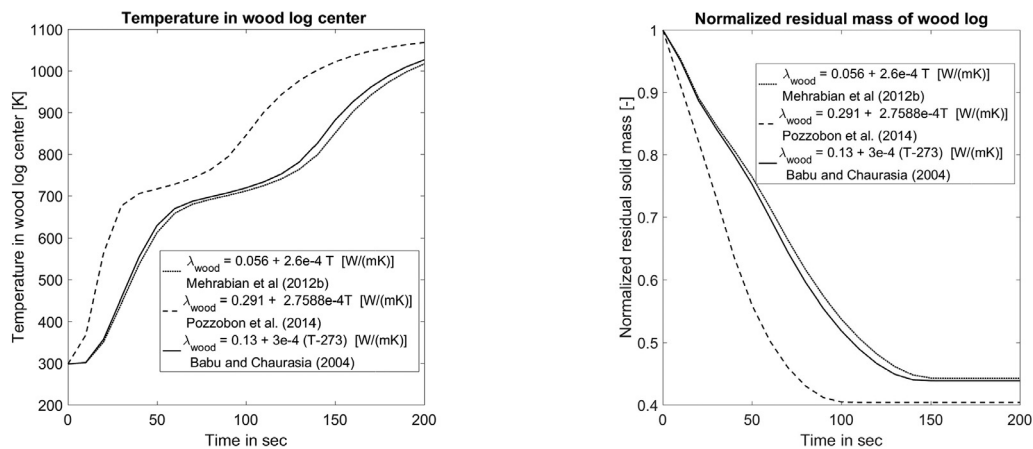

Fig. 14. Thermal conductivities parallel and perpendicular to the fiber direction. The numbers in the boxes represent the ratio between the two thermal conductivities.

(a) Influence of thermal conductivity of wood on core temperature profile.

(b) Influence of thermal conductivity of wood on normalized residual mass and overall conversion time.

Fig. 15. Different temperature functions of thermal conductivity are compared. Their influence on normalized residual mass, conversion time and core temperature are compared. The thermal conductivity changed from the one for wood to the one for char as a linear function of the degree of conversion.

phase conductivity in relation to the influence of the solid phase conductivity on the temperature history in the wood log is less important.

In Fig. 15, the temperature function for the thermal conductivity of wood has been modeled as linearly conversion-dependent. The dashed line in Fig. 15 corresponds to the thermal conductivity of Pozzobon et al. [62], who modeled beech. Babu and Chaurasia [48] did not explicitly mention which wood species was modeled, but compared with the results by Scott et al. [118] and Pyle and Zaror [119], who were using maple and pine, respectively. Their thermal conductivity is presented by the solid line. Again, the weakness in their model is that they used the same properties for comparing hardwood and softwood experiments. The dotted line corresponds to the thermal conductivity used by Mehrabian et al. [10], who modeled poplar. In all three cases, hardwood was modeled, although the applied values differed quite a bit. One can also clearly see that by considering the increasing influence of formed char, permanent gas and tar, the heat transfer inwards slows done, as all these products have lower thermal conductivities compared to wood. A very reasonable finding is also that the residual solid mass is lowest at the highest heating rate (dashed line). In this case, the char yield decreases as the produced gaseous products increase. It is therefore clear that the thermal conductivity has a significant influence on the prediction of product yields, as well as the overall devolatilization time, ranging from approximately 100 s (dashed) to 140 s (dotted) for beech wood modeling when the thermal conductivity is a function of temperature and degree of conversion. After having reached the temperature plateau at roughly 680 to 700 K, the residual heating-up seems to be slower than the initial one (from start until the plateau). The reason for this is that the second increase is occurring after devolatilization has proceeded, so therefore only char, permanent gas and tar are left, all of which have lower thermal conductivities than wood. Accordingly, by only looking at the temperature increase, one can clearly identify three different stages: the first stage is related to the pre-devolatilization heating of the wood, as the thermal conductivity of wood dominates the heat transfer; in the second stage, the actual devolatilization, the endothermic reactions of primary devolatilization, dominate the temperature profile, and the plateau is formed. The third stage in the temperature increase is slower than the initial temperature increase, which is due to the lower thermal conductivities of char, tar and permanent gas, which dominate the post-devolatilization heating process.

In Fig. 16, it is shown how the temperature-dependent thermal conductivities of char influence the temperature history in the center of a wood log, in addition to the overall conversion time.

A low thermal conductivity (line marked with × in Fig. 16) yields a significantly larger amount of residual solid, which seems reasonable as the temperature increases very slowly and remains at around typical pyrolysis temperatures ($<$ 500 °C) for longer times (compare line marked with × and line marked with +). Such a slower heating enhances char formation instead of the formation of permanent gas and tar. It can also be seen that initially neither the temperature profile nor the mass loss vary significantly by choosing different thermal conductivities of char. This seems reasonable, as at earlier conversion times the degree of thermal conversion is limited; thus, the influence of the thermal conductivity of wood dominates over the influence of the thermal conductivity of char. In this comparison, the thermal conductivity of wood has been the same for all four test cases.

It is shown in Fig. 16 that the applied thermal conductivities of char used in current models differ significantly. It is interesting that two temperature-dependent descriptions of thermal conductivity of char actually predict that thermal conductivity decreases as temperature increases [35,48,58]. As can be seen, this temperature dependency gives high discrepancy compared to what is obtained by a constant thermal conductivity or when increasing the thermal conductivity of char with increasing temperature.

After devolatilization reactions have been enhanced significantly at temperatures at approximately 700 K, the difference in the evolution of temperature and residual mass increases, thereby highlighting that the increased presence of char makes an accurate prediction of its thermal conductivity necessary.

Pozzobon et al. [62] were the only ones modeling thermal conductivity of char as a function of T^4. However, the overall validity of this function describing the thermal conductivity of wood has only been tested in a temperature range of 20 to 600 °C [120], which is rather low for gasification and combustion conditions. This significant change in thermal conductivity with respect to temperature is also the reason why it is found that using constant values, commonly around 0.1 W/(mK) [40−43,46,47,52−56,59,61] is yielding false prediction of the temperature history within the wood log, which can consequently affect product yield predictions.

4.6.6. Heat capacity

A wide range of different specific heat capacities of wood, char, ash and pyrolysis gases are used in the literature. The figures below
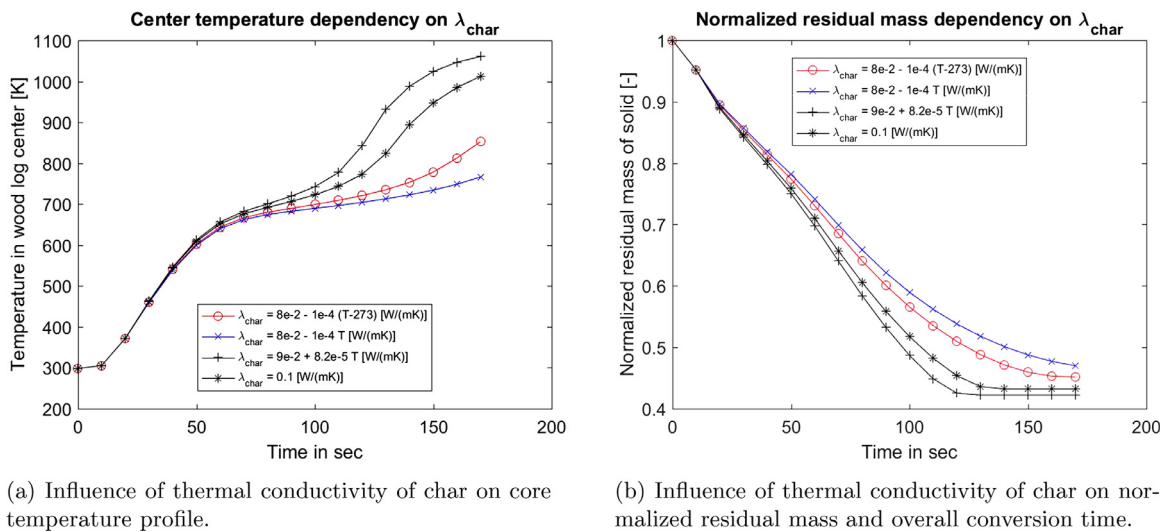
(a) Influence of thermal conductivity of char on core temperature profile.

(b) Influence of thermal conductivity of char on normalized residual mass and overall conversion time.

Fig. 16. Different temperature functions of thermal conductivity of char are compared. Their influence on normalized residual mass, conversion time and core temperature are compared. The thermal conductivities were taken from what is used in current models [34,35,48,58]. Furthermore, it was modeled how a commonly chosen constant value for the thermal conductivity of char differs from temperature-dependent thermal conductivities. Again the authors' model was applied.

aim to illustrate the values used, not only for different wood species, but also for char and gases.

The following plots highlight that the choice of wood species is expected to have a significant impact on the choice of specific heat capacity, but only a limited amount of different values is commonly used in models.

Based on Fig. 17, it is suggested that a linear temperature dependency is a common modeling approach for describing the changing specific heat capacity of the virgin wood. It was found that the linear correlation applied by Bryden et al. [42] for oak wood leads to a significant increase of specific heat capacity as temperature increases. Devolatilization is expected to be finished at < 500 °C, and in such a range the values for specific heat capacity can still increase up to approximately 3000 J/kgK, which is considered very high. A higher specific heat capacity of approximately 3500 J/kgK for modeling oak has also been used [59]. This value exceeds all the other data found in literature and seems non-physically high. It is also expected that by pre-defining constant values for specific heat capacity, errors in the modeling results are significant, because in Fig. 17 it is obvious that constant values are commonly well below what is predicted from temperature dependencies. It is also concluded that the choice of specific heat capacity for wood species is ambiguous, in some modeling works [42] the same temperature dependency for both softwood and hardwood is used.

Furthermore, the same linear dependency applied by Mehrabian et al. [7,10] for poplar modeling has been used by Grønli and Melaaen [22,40] for modeling Norwegian spruce. Biswas and Umeki [1] have also used the same correlation when modeling the Katsura tree, which is classified as hardwood. As far as models based on pine wood are concerned, the choice of specific heat capacities is very random, since the specific heat capacity has been set to 1255.5 J/kgK [42] or 1150 J/kgK [59] in some works, which is significantly lower than other values, such as 1950 J/kgK [34].

From Fig. 18, it can be seen that the influence of specific heat capacity of wood on the temperature evolution and mass loss curve is less significant than the influence of thermal conductivity. It seems that the product yields with respect to solid residue are not significantly affected, even though the conversion time deviates, being shortest by choosing a lower constant value for the specific heat capacity of wood. Both temperature dependencies increase linearly, and there is hardly any difference between the two with respect to the modeling of the wood log center temperature and mass loss

behavior. It is therefore concluded that the choice of a specific heat of wood is not the most sensitive parameter affecting accuracy of a model. A similar behavior is also expected for the specific heat of char.

It is obvious that a broad range of specific heat capacities of char is used in current models, having a maximum value of 2870 J/kgK at 890 K and a minimum value of 1225 J/kgK at the same temperature. Commonly linear temperature dependencies for specific heat capacities are modeled, which is assumed to be mainly due to their simplicity with respect to implementation in numerical codes. The inconsistency in the chosen value for specific heat capacity of char leads to the conclusion that this property is considered a main source of error in current models.

It has to be pointed out that the produced char yield, its composition and therefore also its properties are expected to vary depending on operational conditions. Accordingly, one expects a broad range of values. It also has to be pointed out that the parent fuel can also affect the composition of the produced char; hence, one expects that this leads to a broad variation in values for specific heat capacities for char. Nevertheless, the main reason for such an ambiguous choice of values as shown in Fig. 19 is expected to be due to the general lack of data based on a detailed analysis of the char produced from different wood species. Therefore, future research should focus more on collecting detailed data on specific heat capacities of char, depending on varying operational conditions and parent fuels.

Larfeldt et al. [41] provided the only model where specific heat capacities for wood and char were calculated from thermal diffusivity. The relation between thermal diffusivity and specific heat capacity was such that

$$\alpha = \frac{k_{\text{eff}}}{c_{P,s}\rho_s + \epsilon_g c_{P,g}\rho_g^g} \approx \frac{k_{\text{eff}}}{c_{P,s}\rho_s}. \tag{47}$$

The final approximation suggests that the influence of the gas phase can be neglected in the definition of the thermal diffusivity since the solid phase dominates over the contribution of the gas phase. We have shown that applying constant values in a model affects the accuracy of the modeling results. Still setting constant values for specific heat capacity for wood species, char and gases is a common modeling approach [34,37,39,51−53,56,60,61,64].
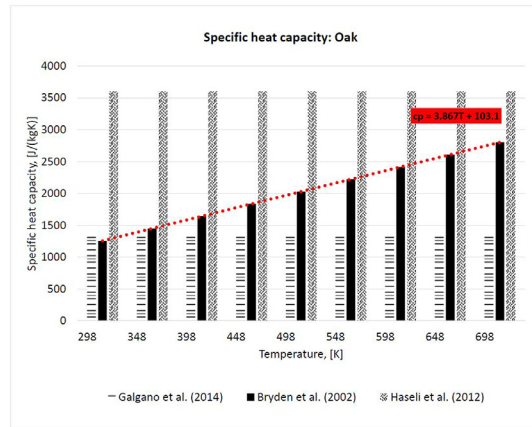
When analyzing the specific heat capacities of gases, the span of values is significant. Moreover, it is also shown in Fig. 20 that the influence of increasing temperature on the specific heat capacity is
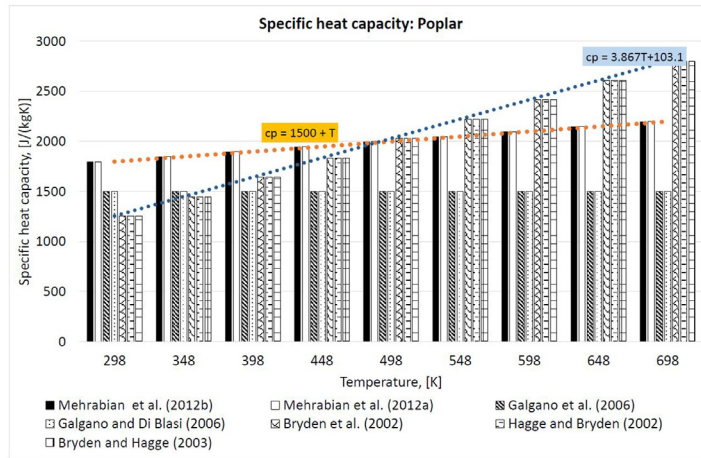
(a) Specific heat capacities for poplar wood.
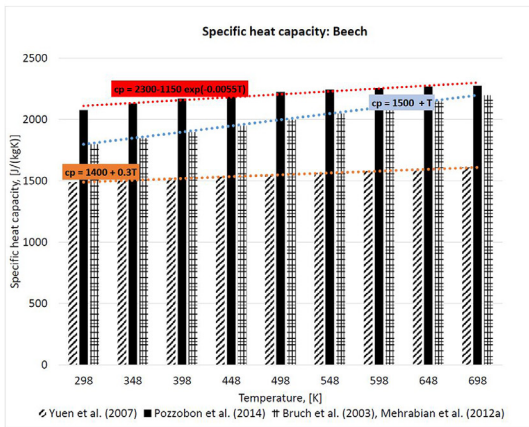
(b) Specific heat capacities for beech wood.
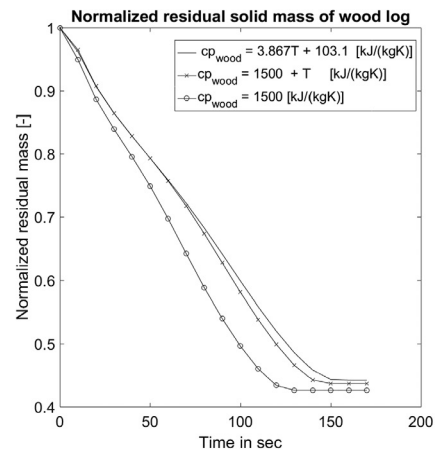

(c) Specific heat capacities for oak wood.

Fig. 17. Specific heat capacities for commonly applied wood species. These figures aim to show that the specific heat capacities of wood are expected to vary depending on the wood species, and that modeling specific heat capacities as temperature-dependent or constant, can have influence on the modeling results.

hardly considered in any model. The highest constant value applied, 2400 J/kgK [42,43,47,54] exceeds the lowest constant value by 1300 J/kgK [37−39,41,49,52,53,56] so it is also assumed that the modeling results are affected by the choice of specific heat

capacities. Yet, the overall influence of the specific heat capacity of gases is negligible compared to the influence of specific heat capacities of solids, since the effective specific heat capacity influencing the heat equation is mass-averaged. For this reason, the higher mass
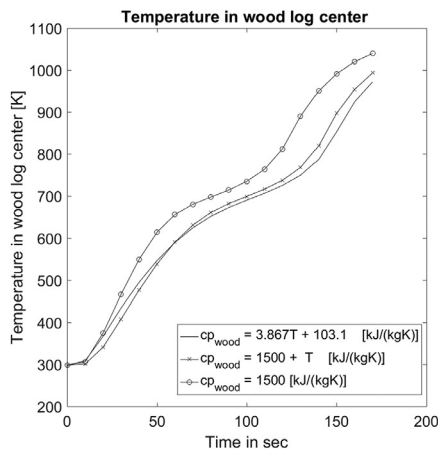
(a) Influence of specific heat capacity of wood on core temperature evolution.

(b) Influence of specific heat capacity of wood on normalized residual solid mass.

Fig. 18. Different temperature functions for the specific heat capacity of wood are compared. Their influence on normalized residual solid mass, conversion time and core temperature are also compared. The values of specific heat capacity have been taken from reference literature [33] and models [10,37].
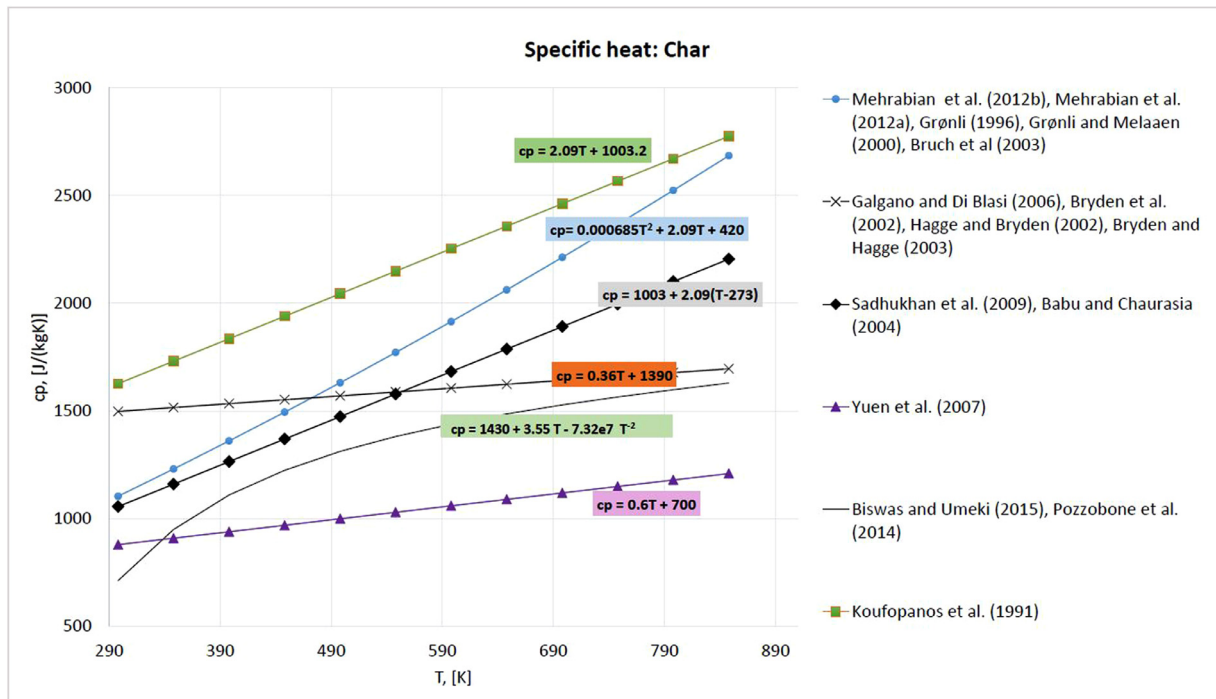
Fig. 19. Specific heat capacities of char. The applied specific heat capacities of char of different models are compared here. Temperature-dependent values are shown.
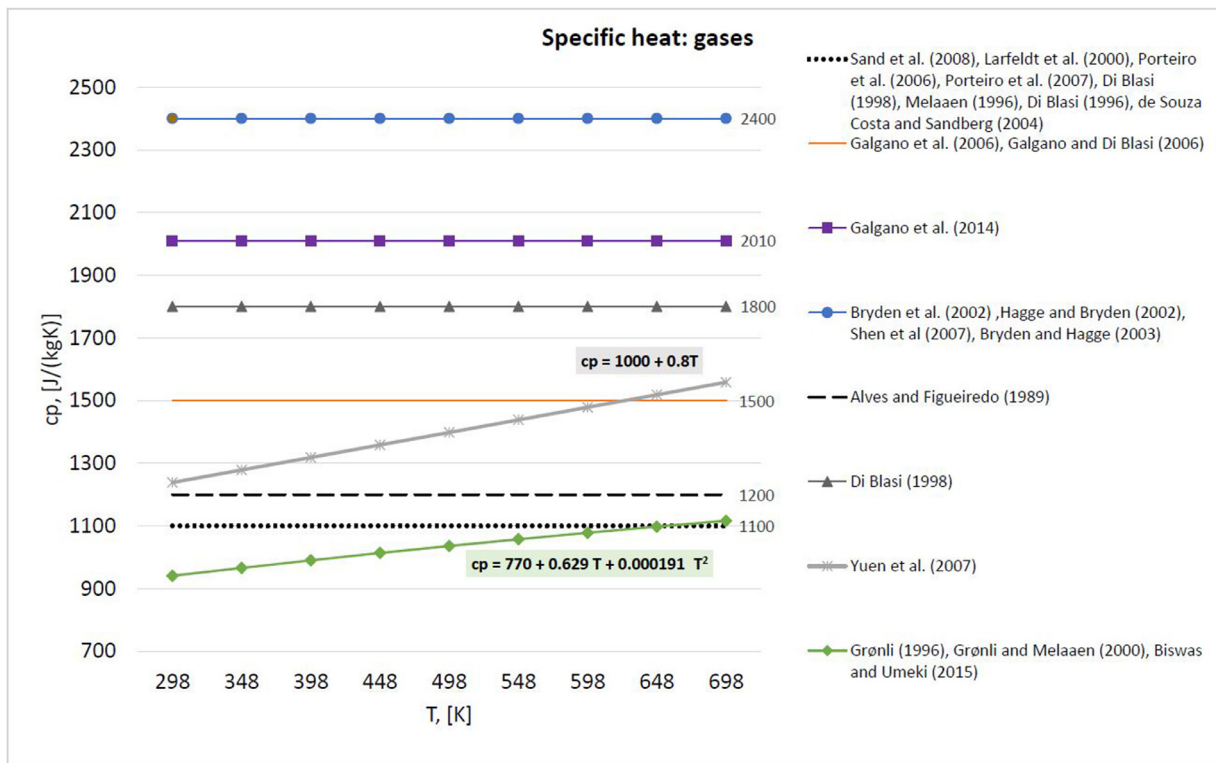

Fig. 20. Specific heat capacity of gases. The applied specific heat capacities used in different models are compared here. Constant values are compared against temperature-dependent values.

of the solids leads to a higher influence on the specific heat capacities.

Furthermore, the specific heat capacity of gases should consider the composition of the gas phase. Detailed knowledge of this composition cannot be easily acquired, since the reacting wood already includes a broad range of chemical compounds. As detailed knowledge on gas phase composition is commonly not included in current numerical models, a corresponding value for specific heat capacity of the gas mixture is also related to approximations.

4.6.7. Permeability

The gas flow inside the wood particle is strongly affected by the wood structure, which consists of a large number of small pores. The pore walls act as a barrier for the bulk flow moving from one neighboring pore to another [56]. The permeability is much lower in radial and tangential directions than along the wood grain.

One expects differences in permeability, not only between virgin wood and char, but also between hardwood and softwood. It can be seen from Fig. 2 that softwoods have slightly lower densities, as the plotted range is from 330 - 620 kg/m^3, while hardwoods have higher densities, ranging from 370 to 770 kg/m^3. It has to be pointed out that some wood species within these two groups can be either below or above the range limits mentioned here, though most of the species will have densities within these limits. Accordingly, it can be assumed that softwoods have either more pores or a larger pore size, since both would contribute to lower apparent wood densities. Thus, one would assume that the permeabilities of softwood are higher than the permeabilities of hardwoods.

As can be seen from Fig. 21 only limited conclusions can be drawn in case of softwoods, as very few models were based on softwoods and included the influence of convection on heat and mass transfer; and thus had to provide information on permeabilities. As previously mentioned, it is concluded that the choice of permeability is still related to a high uncertainty, which can also be seen from the large spread of data points in Fig. 21. Bryden et al. [42] used the same permeabilities for softwood and hardwood. One reason for this might be that the overall availability of data on wood permeabilities is rather limited. However, it can still be seen that the lowest permeability for hardwood is as low as approximately 10^{-17} m^2, which is much lower than what has been used for modeling softwoods. This agrees with a previous theoretical conclusion, that flow is more facilitated in softwoods. With respect to char permeabilities, however, no significant differentiation between hardwood and softwood derived chars can be found in the literature. Still, it can clearly be seen that due to an increasing porosity in char compared to wood, the permeability of char is much higher than the permeability of virgin woods.

A reasonable choice of permeability is needed in order to correctly compute the pressure field in the interior of the wood particle. Furthermore, it has to be pointed out that due to the anisotropy of wood, it is recommended to at least develop a 2D model, because different values for permeability with respect to the fiber direction can then be applied. It is consequently assumed that the pressure in the interior of the wood particle can be predicted more accurately and consequently also the velocity field. This has not been a primary concern in past research, even though it is assumed that the correct prediction of the pressure results in a good prediction of crack formation. Such an accurate prediction of the physical change of the wood particle can affect the modeling results of overall conversion times and product compositions as well as temperature history.

However, it has been found that the choice of permeability is a major uncertainty of thermal degradation and combustion models for wood particles. It has also been the case in a number of works [39] that the permeability was simply defined by fitting the modeling results to the experiments. If so, the physical validity of the used permeability cannot be taken for granted.

(a) Permeabilities for hardwoods, parallel and perpendicular to the fiber direction.

(b) Permeabilities for chars derived from hardwoods, parallel and perpendicular to the fiber direction.

(c) Permeabilities for softwoods, parallel and perpendicular to the fiber direction.

(d) Permeabilities for chars derived from softwoods, parallel and perpendicular to the fiber direction.
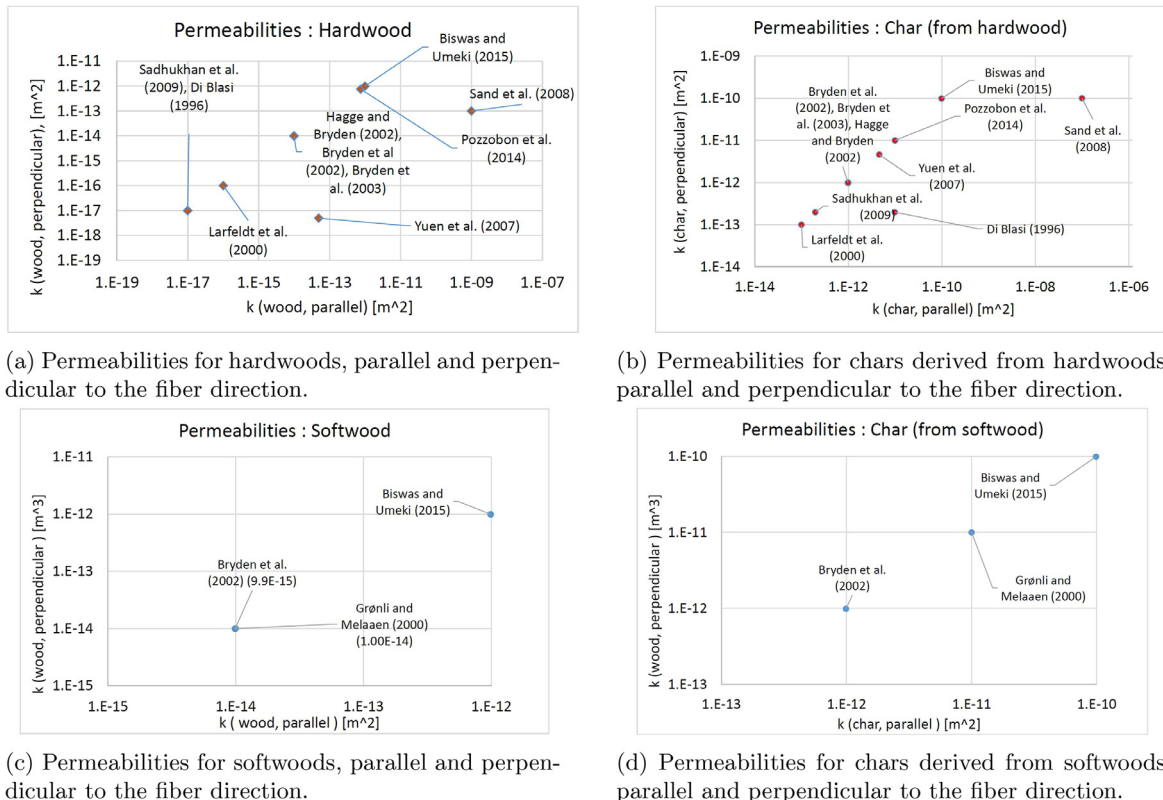
Fig. 21. Different permeabilities applied for modeling convection within the porous structure of wood and the char layer that is forming around it due to ongoing devolatilization.

4.6.8. Shrinkage modeling

The ratio between the decreased dimension and the initial dimension is what is defined as shrinkage [43]. Shrinkage during devolatilization varies with respect to the direction in the wood log. Because of this, shrinkage can only be accurately replicated in a 3D model, while 1D models instead focus on shrinkage in only one preferential direction, e.g. commonly radially in the case of cylindrical wood logs or particles. Such a simplifying assumption is commonly done in a number of 1D models, e.g. [1,43,61]. Then again, none of these works focuses explicitly on the distortion of a wood particle during volumetric shrinkage. Therefore, future research is recommended to focus on such physical changes in wood particles to help identify the extent to which they affect heat and mass transfer and the structure and shape of wood logs.

There are two different and broadly used approaches for modeling the shrinkage of a particle during devolatilization. The first shrinkage model was introduced by Di Blasi [37], and is based on three parameters. The main assumption of this model is that the volume first occupied by the solid is linearly reduced with the wood mass, while it is increased by the increasing char mass. The correlation describing to what extent the volumetric shrinkage is increasing linearly with the char mass is described by the first shrinkage factor, α. Also, the gas volume contribution to the entire volume changes during devolatilization. The gas phase volume includes two contributions by itself, which are the initial gas phase volume and the fraction β, describing which amount of the solid volume is added to the gas phase volume due to conversion reactions. The third parameter of the shrinkage model, γ, accounts for internal structural changes, such as a porosity increase as devolatilization proceeds [20]. Accordingly, these three parameters are not related to the common definition of shrinkage factors as described by Hagge and Bryden [43]. A significant uncertainty of this three-parameter model is that the choice of values for the three parameters is rather ambiguous. They are not derived from any experiments, but are chosen to fit the model to the experimental data. Additionally, it is not yet known whether these three parameters are affected by intra-dependencies or not, even though the current version of the shrinkage model assumes that α, β and γ are independent from each other [18].

Hagge and Bryden [43] used a one-parameter approach for modeling shrinkage. The basic idea of this model is the constant intrinsic densities of char and wood, and shrinkage is assumed to linearly depend on the degree of conversion of the solid. This does not entirely agree with experiments, in which it was shown that shrinkage commences later than the mass loss during devolatilization reactions [121,122]. In order to express this correlation, the shrinkage factor is introduced, which can mathematically be expressed as [43]

$$f = \frac{\text{current dimension}}{\text{original dimension}} = \frac{\Delta y}{\Delta y_0}. \tag{48}$$

However, this equation outlines that cracking is commonly not considered when discussing shrinkage factors, and it further highlights that in most works such shrinkage factors are related to a certain direction, e.g. radial or longitudinal. For example, Eq. (48) only considers shrinkage across the grains, since Δx and Δz remain unchanged. A disadvantage of this shrinkage consideration is actually that the shrinkage factors have been experimentally obtained by Bryden and Hagge [47]. The factors were related to the final char dimensions, which are provided in the final shrinkage values. A simplifying assumption for deriving a suitable mathematical expression for shrinkage from measured values is therefore obtained by assuming that the char dimensions decrease, but that there is no fragmentation [47]. Accordingly, one can conclude that for the restricted modeling of shrinkage during devolatilization, the mentioned simplifying assumption yields an acceptable mathematical description of shrinkage. Even though the mathematical derivation of shrinkage

is acceptable, the validity of the overall description of shrinkage is restricted because of the experimentally derived values for shrinkage factors, suggesting that these are only valid in a limited range of operational conditions.

The one-parameter model has been applied in many different works [1,5,8,43,44,47,52,53,58,62]. Sadhukhan et al. [58] found that particle shrinkage during devolatilization led to a reduced heat transfer area. As a result, it was found that more heat, mainly obtained from exothermic secondary tar reactions, was kept inside the particle, resulting in a higher center temperature of the particle than the temperature at the surface.

The most simplifying assumption, however, is that shrinkage can be neglected, and that the particle volume therefore stays constant during drying and devolatilization [22,36,39,40,63]. Nonetheless, it is assumed that this assumption is not very realistic, since wood loses roughly 80% of its organic mass during devolatilization; hence, such a significant conversion of the solid to gas phase is assumed to have a significant influence on the physical structure of a wood particle. A critical aspect of neglecting shrinkage in the model is that the validation of the model against experiments is highly inaccurate, as shrinkage will always occur in an experimental investigation on the thermal conversion of wood samples. However, a suitable assumption for an acceptable validation was presented by Grønli and Melaaen [40], as they neglected shrinkage in their devolatilization model, but compared the results against experiments of spruce wood, which was heated in parallel with the grain. The reasoning is that in the axial direction only, a low shrinkage is expected, and it is most reasonable to compare the obtained experimental results with a non-shrinkage model.

Shrinkage modeling is usually highly dependent on pre-defined shrinkage parameters. The derivation of those parameters, commonly either experimental or based on assumptions, is a main weakness of current models, as it cannot be easily and flexibly changed to different operational conditions and wood species.

5. Homogeneous gas phase reactions

The released permanent gases, including released combustible gases obtained from char conversion, enter into the freeboard (which is the gas phase area above the wood log), where they are eventually oxidized. The consideration of this homogeneous gas phase reaction is very significant, as the temperature increase resulting from the oxidation further heats up the wood log, so that drying, devolatilization and char conversion reactions can proceed. Accordingly, a discussion of those reactions is required in connection with a discussion of the thermal degradation of a solid wood particle in a combustion unit. Please note that gas phase combustion is also discussed in connection with a relevant application in the chapter on small-scale furnace modeling, where particularly turbulence and combustion models are discussed.

The relevant reactions of homogeneous gas phase reactions are [23]

$$CO + 0.5O_2 \rightarrow CO_2, \tag{R6}$$

which is commonly considered in the freeboard of current domestic wood heating appliances [50,51,123−126]. In some cases, the complexity of the homogeneous reaction model is further enhanced by also considering CO_2 dissociation [124]. This reaction is only relevant at very high temperatures though. Hydrogen oxidation;

$$H_2 + 0.5O_2 \rightarrow H_2O \tag{R7}$$

has also been modeled in small-scale wood heating appliances [50,51,124−127], since it is expected that hydrogen is one of the main compounds of the volatiles released during the devolatilization of a wood particle. The increasing importance of H_2 with respect to increasing temperature has been discussed earlier [19], and as such,

it seems reasonable that a high temperature conversion processes, such as that occurring in e.g. wood stoves, requires the explicit consideration of this homogeneous gas phase reaction.

Regarding combustion of methane it can be modeled in two different ways, either as a full oxidation [50,51,127];

$$CH_4 + 2O_2 \rightarrow CO_2 + 2H_2O \qquad (R8)$$
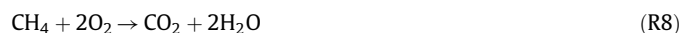
or as a partial oxidation, as is done by Porteiro et al. [124];

$$CH_4 + \frac{3}{2} O_2 \rightarrow CO + 2 H_2O. \qquad (R9)$$

Huttunen et al. [126] also described incomplete oxidation of methane to carbon monoxide, similar to what is shown in equation (R9).

In addition to modeling light hydrocarbon oxidation, such as the oxidation of methane, more complex hydrocarbon structures than methane can also be included in homogeneous gas phase modeling, e.g. [124]

$$C_6H_6 + \frac{15}{2} O_2 \rightarrow 6 CO_2 + 3 H_2O, \qquad (R10)$$
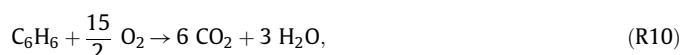
which is modeling the combustion of heavy hydrocarbons released from a wood particle undergoing thermal conversion.

In addition to the previous reactions, the water-gas-shift reaction

$$CO + H_2O \rightarrow CO_2 + H_2 \qquad (R11)$$

is also of interest [50,51,126], as it can be important for staged combustion units that have more gasifier-like conditions in the primary stage.

Only in a limited number of works has a differentiation in homogeneous gas phase modeling been done by modeling saturated and unsaturated hydrocarbons. Saturated hydrocarbons contain only single bonds, while unsaturated hydrocarbons can also contain double or triple bonds. Tabet et al. [128] assumed that the released saturated hydrocarbons (CH_{X_1}) decompose to unsaturated hydrocarbons (CH_{X_2}), which then react to CO. This CO is then combusted to CO_2. In addition, nitrogen containing species are released from the degrading wood particle, and consequently, NO_x formation has to be modeled.

5.1. NO_x formation

So far, none of the described reactions consider the influence of nitrogen-containing gas phase species. The influence of fuel-bound nitrogen is relevant when modeling thermal wood degradation and combustion, as the parent fuel contains a certain amount of nitrogen. The nitrogen released from the wood during devolatilization and char conversion is not considered in any of the single particle models. Not even the detailed Ranzi scheme [27] can describe the release rate of either NH_3 or HCN from wood, which will be the main precursors for NO_x (from fuel-bound nitrogen). Some researchers developed post-processing [129] models for NO_x formation. This simplification can be justified because NO_x reactions have very little influence on the combustion nor the fluid itself.

Due to the relatively complicated formation mechanisms of NO_x, it is generally required to use detailed reaction kinetics in order to obtain reasonably accurate predictions of the NO_x formation. With respect to modeling of detailed gas phase reactions, it is, however, a common approach to reduce the actual number of reactions and species. This reduction has to be based on the relevant conditions and accuracy requirements. This reduction of a detailed mechanism to a skeletal mechanism can be a very efficient approach to reduce complexity and computational cost of a model, but still obtain a high enough accuracy when it comes to model predictions. Bugge et al. [13,130] compared a detailed reaction mechanism including 81 species and 1401 reactions with more simplified skeletal mechanisms, developed by Løvås et al. [131], with only 49 species and 36 species. The detailed mechanism fully describes the interaction

between nitrogen species and hydrocarbons. One main finding was that the results of the skeletal mechanism including 49 species was close to the results of the detailed mechanism including 81 species, whereas the mechanism including 36 species deviated significantly from the results of the other two reaction mechanisms. In the case of 36 species, the formation of NO_2, HCN, NO, NH_3 and N_2O was over-predicted [13]. In fact, the skeletal mechanism including 36 species agreed with the detailed mechanism including 81 species only at very high temperatures (about 1073 K), while at lower temperatures (about 873 K) NO_x was over-predicted. In previous work, where Bugge et al. [132] only tested a mechanism with 36 species, they found that the prediction of prompt NO_x was overestimated by 20 times with this skeletal mechanism. Thermal NO_x was entirely negligible since the temperatures in the stove were below 1700 K which indicates that the Zeldovich mechanism does not significantly contribute to the NO_x formation.

However, there are also other modeling approaches on how NO_x prediction originating from fuel-bound nitrogen can be modeled, without requiring a detailed reaction scheme. Huttunen et al. [126] assumed that half the nitrogen in the permanent gas phase is NH_3, which is a precursor for NO_x, originating from fuel-bound nitrogen. The rest is assumed to be N_2. Furthermore, it is assumed that the nitrogen in pyrolysis gases and char is proportional to the amount of char and volatiles in wood and therefore also their ratio. However, basing NO predictions on this approximation resulted in predicted emission levels that where five to ten times smaller compared to what was found in experiments. Accordingly, such a gross simplification of the evolution path for nitric oxides, cannot yield accurate results, even though it has not been tested if better results can be obtained when modeling HCN and NH_3 as NO precursors [126].

Reviewing homogeneous gas phase modeling has clearly shown that simplifications are not only required for chemical and physical processes in the interior of the wood log, but are also a significant aspect for the development of efficient gas phase models. This highlights that a computationally efficient simulation tool for wood heating appliances does not solely rely on a numerically efficient and accurate solid phase model, but also highly depends on the numerical efficiency of the gas phase model. The complexity of a model can for example be reduced by reducing the number of homogeneous gas phase reactions by lumping heavy and light hydrocarbons into two representative species. A higher number of homogeneous gas phase reactions is expected to result in a stiffer system of equations. For a numerically efficient simulation tool, it is required to reduce the number of stiff equations, such that the computational cost is balanced with accuracy. This principle accounts for the devolatilization modeling of wood, as well as the homogeneous reactions of the released volatiles species.

5.2. Theory of soot formation and its modeling

There is only a limited amount of works available that discuss soot formation from biomass conversion processes, either experimentally or by modeling. Yet, it is clear that soot formation is a key aspect of an accurate wood heating appliances simulation tool, as soot in the flame intensifies radiant heat transfer between gases and wall such that the gas temperature decreases [126]. The parent fuel will have a significant influence on the soot production; therefore, soot formation models for liquid and gaseous hydrocarbon fuels are not applicable for biomass.

Wood smoke which is responsible for a high number of deaths per year, has soot as a primary contributor, and further includes ash and volatiles. Soot is built up by two components; organic and black soot. Black soot contains furthermore two components; elemental soot and condensed organic compounds [133−135].

The most common description of soot formation is with acetylene as a precursor. Acetylene (C_2H_2) enhances the formation of

increasingly larger ring structures. The process starts with the abstraction of H from the ring structure by a free H. The products of the initial step are therefore H_2 and an aromatic radical. The aromatic radical will then react with C_2H_2. An additional C_2H_2 will then react, and the reaction will lead to cyclization and the formation of more connected aromatic ring structures [21]. This reaction sequence is commonly shortened to "hydrogen-abstraction-carbon-addition"-route (HACA) . The reaction products will be PAH, which contains one to four-aromatic-ring-structures. According to the Frenklach model, the soot precursors subsequently start to nucleate and size growth occurs, which suggests that nucleation occurs through an association of four-aromatic-ring species. First soot precursors are formed, and this initializing stage is followed by nucleation and surface growth. Larger spherical particles are formed, which then cluster together and by agglomeration form chains [136]. However, as the particle grows, the forming particles are also affected by oxidation reactions [21]. Accordingly, both formation and consumption are relevant and define the final soot yield.

However, with respect to soot formation from degrading wood, soot can be synthesized via an additional reaction pathway [137,138], in which it is suggested that biomass devolatilization fragments react further. This formation mechanism of soot has been found relevant for species adsorbed onto the soot particle, as they seem to be intermediates between small oxygenated biomass devolatilization compounds and the large structures of soot.

It is suggested that cyclopentadiene (CPD) can be a precursor for an additional PAH formation route [136]. Cyclopentadiene is formed via primary reactions of phenols (therefore lignin compounds), in which CO is eliminated from the initial chemical structures in wood, such that CPD is formed, as well as its methyl derivatives [139–141]. Further pyrolysis of CPD then leads to the formation of benzene, toluene, indene and naphtalene [142–145]. In a more simplified explanation, one can mention the following steps as part of the second soot-formation route; wood degrades into decomposition products (mostly from lignin), that can then continue reacting according to the traditional HACA-soot-formation root, or form oxygen-containing aromatic species and char. The oxygen-containing aromatic species can further react and form soot.

Most interesting is that the original formation pathway of HACA does not consider oxygen-containing PAH, as it only considers PAH based on four-aromatic-ring structures. When modeling the second reaction pathway, one can also accurately consider C/O ratios in the soot. It was also generally found that PAH formation and destruction is very sensitive to the C/O ratio in the parent fuel and the temperatures of the thermal conversion processes. Furthermore, with respect to common temperatures in combustion units (1220 K), it was also found that such high temperatures, as well as the time during which the temperature remains at such a high level, influence the PAH/soot formation [146]. An additional influence on soot formation is the ratio of O_2 / CO_2 in the combustion atmosphere, since this ratio has a significant influence on the temperature profile of the particle, which can then affect the amount of soot formed [147]. Most interesting, however, is that Wijayanta et al. [148] claimed that biomass soot formation modeling can be based on previous modeling work done on soot formation from coal. One would not expect this, since there is a significant difference in the composition of wood and coal; hence, C/O and C/H ratios are assumed to be different, which is expected to have some effect on soot formation. Wijayanta et al. [148] developed a soot formation model for biomass, in which 276 species were involved, and 2158 conventional gas phase reactions were modeled, in addition to 1635 heterogeneous surface reactions. They based their soot model on previous work done by Ergut et al. [149] on soot formation from coal conversion. Ergut et al. [149] assumed an atmospheric pressure, which would make the model suitable for modeling soot formation in domestic wood heating appliances, where no significant pressure increase is expected. In their model, pyrene, naphtalene, methylnaphtalene and phenol are present in negligible amounts, while most of the species that can react and form soot are CO, CO_2, CH_4, acetylene, ethylene and C_2, in addition to C_3 alkanes. To some reduced extent benzene and toluene are considered, but much less significant compared to the previously mentioned species. To a certain degree, it can therefore be concluded that the influence of biomass fragments on soot formation and the influence of CO elimination from phenol compounds is not considered at all in their model, which again highlights that it might be suitable for coal, but one expects it to exhibit higher discrepancies for wood soot formation modeling. By considering such a detailed description of soot formation, as done by Wijayanta et al. [148], they were able to identify the influence of temperature on soot formation. It was found that PAHs formation increases as the temperature rises from (1073–1473 K), but again decreases at higher temperatures (1678–1873 K). Within the first temperature range, it is assumed that the temperature influences the conversion kinetics of hydrocarbon polymerization for PAH formation. It is interesting to note that no soot was found at temperatures below 1473 K, because at these temperatures the oxidation reactions of soot and PAH are faster than soot growth. Within the second temperature range, temperatures are high enough to enhance PAH oxidation reactions, this is due to enhanced OH radial formation at these temperatures. It was also found that the pressure in a reactor system has an insignificant influence on soot formation reactions.

With respect to furnace modeling, primarily small-scale heating appliances, soot formation has only been considered very limitedly in current models. Bugge et al. [13,130,132] used the Moss and Brookes soot model [150], in which the primary precursors for soot formation are acetylene and ethylene. Brookes and Moss [150] focused on jet diffusion flames burning methane at elevated or atmospheric pressure. The purpose was to discuss how flame radiative heat losses and soot production rate are linked. Their modeling followed the conventional HACA pathway of soot formation. Because this work is not linked to detailed information on soot formation from biomass, it is considered to go beyond the scope of this work, and is therefore not discussed in more detail here.

Huttunen et al. [126] modeled soot formation according to two different models, whereby one was developed by Magnussen and Hjertager [151] and Tesner et al. [152], while the other one was developed at Brigham Young University [153]. However, Huttunen et al. [126] stated that for solid fuel combustion, the Brigham Young University model is more suitable, and was consequently linked in their model to the TULISIJA code. Magnussen and Hjertager [151] also did not focus on soot formation from the thermal conversion of wood, but predicted soot formation from C_2H_2 diffusion flames. Soot formation in this work occurred stepwise, in which the first stage was the formation of radical nuclei, while the second stage was soot formation from these nuclei. Soot combustion in their work was modeled in regions, where the local mean soot concentration dropped below the concentration of oxygen. Because the focus of this work is again gaseous fuels, it is concluded that a detailed discussion of this soot formation model goes beyond the scope of this review paper, and the same reason for neglecting a detailed discussion can be applied to the model by Tesner et al. [152]. They also discussed soot formation from a C_2H_2 diffusion flame. It was claimed that soot particles are formed due to branched-chain processes and the destruction of active particles on the surface of the formed soot particle [152].

Due to the limited number of works currently available in the open literature, it is not yet clear how soot and PAH formation are influenced by different wood species. Most of the works are on liquid or gaseous fuels, while wood has not been investigated intensively. So far, most of the available works concerning soot formed during thermal conversion of wood have been performed on pine wood [136,148]. Furthermore, none of the works focused on soot

formation from large wood logs. Nevertheless, it is expected that the size of the woody particle has an influence on soot formation, as it has been pointed out by Liu et al. [147] that the temperature history of the particle influences soot formation. Since entirely different temperature histories are expected for large and small particles, it is clear that the particle size has an influence. It is also expected that particle shape has an impact on soot formation, as the external surface area of the particle exposed to heat also has an influence on the heating history of the wood particle. Future research is therefore recommended to confront these unknown components of soot formation occurring during thermal wood conversion in small-scale wood heating appliances.

6. Small-scale furnace modeling

Only a limited amount of works has been done on small-scale furnace modeling [13,14,50,51,123,125−128,130,132,154,155]. The most challenging difficulty of current works is the enormous computational effort of common CFD models, since a very fine mesh is required, where steep gradients can be expected and very detailed reaction mechanisms are needed to model combustion chemistry sufficiently well [124]. In the following chapter, the current state-of-the-art of small-scale heating appliances modeling is reviewed in order to identify the most important features of small-scale furnace simulation tools, and to discuss the most common approximations and assumptions current models are based on. Furthermore, the most important modeling results are outlined. However, one has to acknowledge that both the development of precise models, as well as the accurate performance of experiments, is difficult. With respect to experiments, it has to be emphasized that due to the mostly discontinuous feeding system of small-scale boilers or stoves, a stable reaction environment can not be obtained. For example, by opening the heating unit during discontinuous feeding, the air-fuel ratio, which has to be controlled in well-defined experiments, can vary significantly [124]. Furthermore, 100% constant feed rates can hardly be managed, even in automatically fed pellet boilers. Accordingly, even with respect to the validation of modeling results, it has to be considered that errors can arise on both the experimental and modeling side.

Table 6 outlines that a simulation tool for real-world small-scale heating appliances has to include certain modeling aspects in order to accurately model a given reactor configuration. First, a model has to include a description of the solid bed, which will be thermally converted to gaseous products and ash. The solid phase conversion defines the volatiles release rate to the gas phase. The solid bed model describes the drying of moist wood, together with wood devolatilization, where most of the combustible gases are released, as well as char conversion. The char can be converted through gasification, oxidation, or a combination of the two. The extent to which these two reaction paths occur is dependent on the operational conditions of the furnace. As outlined in the previous section on particle degradation modeling (Section 4), also with respect to the bed model in domestic combustion units, chemical processes related to the thermal conversion of wood have to be simplified significantly in order to be used in an efficient simulation tool for engineering applications, such as optimization and design of heating appliances. Not only is the thermal conversion of a single particle a model requirement, but also the accurate description of the influence of various wood particles on each other is needed for a detailed bed model. It should also be mentioned that another requirement for the accurate modeling of heating appliances is the ability of the bed model to account for the wood species of interest. A flexible bed model, which allows for a detailed characterization of the parent fuel, is mostly achieved by splitting wood into its pseudo-components.

Also presented in Table 6 is the second chief feature of a domestic heating unit model is the gas phase model, which must contain a

Table 6

Chief features required for model development of small-scale heating appliances. This table lists the most important features of a model.[a] implies that the bed model was decoupled from the gas phase model, as the temperature at the boundaries of the wood log were set to constant values. [b] RSM refers to Reynolds-Stress Model, [c] refers to the Eddy Dissipation Model (EDM), [d] refers to the Eddy Break-Up model (EBU), [e] refers to the Eddy Dissipation Concept (EDC), [f] refers to probability density function modeling approach. The references refer to current state-of-the-art models, that included certain key aspects of a specific feature. "*Theoretical model*" implies that model development was based on theoretical knowledge of the processes and was purely mathematically modeled. This required that transport equations were solved. "*Empirical model*" models have been derived mainly from data obtained from experiments. "*Semi-empirical model*" is used to categorize models that are not based on solving transport equations, but are related to simplified mathematical expressions that are commonly related to measurements.

Chief features	Key aspects of the features
Bed model	1) Detailed characterization of wood species (hemicellulose, cellulose, lignin)
	2) Dimensionality
	2.1) 1D, e.g. [14,50,51,124,126,127,154]
	2.2) 2D
	2.3) 3D
	3) Shape of wood particle
	4) Drying model
	4.1) Empirical model, e.g. [14,154]
	4.2) Theoretical model, e.g. [50,51,123,124,127,128]
	4.3) Semi-empirical model, e.g. [126,127]
	5) Devolatilization model
	5.1) Empirical model, e.g. [14,154]
	5.2) Theoretical model, e.g. [50,51,123,124,127,128]
	5.3) Semi-empirical model, e.g. [126,127]
	6) Char conversion model
	6.1) Empirical model, e.g. [14,154]
	6.2) Theoretical model, e.g. [50,51,123,124,127,128]
	6.3) Semi-empirical model, e.g. [126]
	7) Particle-particle-contact
	7.1) Heat transfer
	7.2) Mass transfer
Bed model boundary conditions	1) Heat and mass transfer coefficients
	1.1) Blowing effect of leaving gases
	2) Emissivity of wood particle
	3) Structural changes affecting gas release and heat transfer
	4) Coupling gas-phase and solid-phase:
	4.1) Coupled, e.g. [14,50,51,124,127,128,154]
	4.1) Decoupled [a], e.g. [123,126]
Gas phase model	1) Turbulence model
	1.1) Standard k-ϵ, e.g. [123−126,128]
	1.2) Realizable k-ϵ, e.g. [13,14,130,132,154]
	1.3) RSM [b], e.g. [125]
	1.4) Low-Reynolds-number-model, e.g. [50,51,125,127]
	1.5) RNG k-ϵ model, e.g. [126,127]
	2) Combustion model
	2.1) EDM [c], e.g. [154]
	2.2) EBU [d]
	2.3) EDC [e], e.g. [13,50,51,125,127,130,132]
	2.4) PDF [f], e.g. [128]
	2.5) Finite-Rate-Eddy-Dissipation, e.g. [14,124]
	3) Radiation model
	3.1) Discrete ordinate model (DOM), e.g [13,14,123−125,127,128,130,132,154].
	3.2) Discrete transfer method by Lockwood and Shah, also referred to as DTRM, e.g. [50,51,126]
	4) Gas phase kinetics

(continued)

Table 6 (*Continued*)

Chief features	Key aspects of the features
	4.1) Detailed mechanism, e.g. [13,130,132]
	4.2) Simplified mechanism, e.g. [14,50,51,123−128,154]
	5) Soot modeling, e.g. [13,126,132]
	6) Particle entrainment, e.g. [124]
	7) Ash deposit formation, e.g. [154]
Furnace boundary conditions	1) Furnace wall emissivity
	2) Heat storage in the furnace wall
	3) Heat transfer to the surrounding room
	4) Primary air supply / Secondary air supply
	5) Glass window: radiation losses
	6) Furnace geometry

detailed descriptions of homogeneous gas phase reactions, see Section 5, turbulence, turbulent combustion and radiation. Gas phase kinetics are subject to gross simplifications, since not all chemical species released from the wood log can be modeled due to efficiency requirements of the simulation tool. Furthermore, not all evolution paths of all emissions are yet fully understood.

A third chief feature in the modeling of a small-scale combustion unit, also listed in Table 6, is an accurate coupling between the solid and gas phases, as the two phases significantly interact. Accordingly, heat and mass transfer from one phase to the other need to be accounted for in great detail. Blowing effects of leaving volatiles from the wood particle will reduce the heat and mass transfer of the gas phase back to the solid phase, see Section 4.1.1, which can affect conversion times and product yields.

A fourth main feature listed in Table 6 is an accurate description of furnace geometry and furnace wall material properties, both of which have a significant effect on temperature history within a combustion chamber. The material properties of furnace walls, which are also recommended to include the presence of any glass windows, significantly affect the temperature in the combustion chamber, as well as heat transfer into the room surrounding the heating unit. Moreover, an accurate description of flow fields entering and leaving a computational domain is required to precisely model emission products and quantities.

Based on the above, one can conclude that a number of different features must be included in a model in order to yield an accurate real-world simulation tool. In the following sub-sections, this will be discussed in more detailed for the particular application of boilers or stoves.

6.1. Boiler

6.1.1. Bed model

Empirical bed models [154] are a well-established concepts for fixed bed modeling of wood log-fired boilers and wood pellet boilers. The release of volatiles in these models is based on the main compounds of wood, which are C, H and O. This means that the presence of S, N and Cl, initially found in the wood material, is commonly neglected.

Accordingly, such a simplified bed model cannot account for the formation of either NO_x or ash vapor precursors. There is a number of works in which these minor constituents of wood are neglected, e.g. [123,127]. Typical volatile species that are included in the models are; CH_4, CO, CO_2, H_2 and H_2O [154], with the release rate depending on the local fuel composition and stoichiometric air ratio. Furthermore, char can react (gasification) with CO_2 to form CO, and with O_2 (oxidation) to form CO_2 or CO, that reacts with O_2 in the gas phase to form CO_2. The main problem with this model, which is also applied in [14], is that the temperature dependency of the CO/CO_2 is

neglected. Another weakness of such empirical models is that the accuracy of the modeling results are totally dependent on the accuracy and applicability of the experimental data used to build the empirical model. One should therefore be very cautious not to use an empirical model for cases that are different from the experimental setup for which the model was designed. If used for the right conditions, however, empirical bed models may yield high accuracy results at an affordable cost.

In comparison to the empirical model approach discussed above, there are other bed models based on a theoretical understanding of the chemical and physical processes occurring during the thermal conversion of wood and the mathematical description of those processes. Porteiro et al. [124] developed a 1D transient particle model and applied it to the simulation of a domestic wood pellet boiler. More information on this model can be found elsewhere [52,53] (also in Section 4 of this review paper), and is not repeated here. In the following we will describe how their bed model interacts with the gas phase above the bed. They modeled pellets [124], and as the pellets became very small, they leave the bed and get entrained into the gas phase, where a Lagrangian particle approach is used to track the particle transport. The Damköhler number is defined as the ratio between the time scales for chemical reactions and convective transport. For a pellet boiler, the Damköhler number is large, and hence, the bed can be approximated as a well-stirred reactor. This means that all particles can be assumed to be surrounded by the same gas species concentrations [124]. This is not the case, however, for wood logs, where the Damköhler number is much smaller.

Another bed modeling approach is based on the approximation of constant load operation, which indicates that wood and oxidizer flow rates and compositions are not allowed to change during the entire model scenario [123]. It is accentuated that this simulated test case can hardly be maintained in the entire transient thermal conversion cycle in a combustion unit due to inevitable fluctuations. However, if the purpose of the model is to gain fundamental understanding of the processes in the combustion chamber, the effect of this assumption is negligible.

Splitting the wood log in constant layers in which the three conversion stages, drying, devolatilization and char conversion occur is another simplifying assumption [123]. The thickness of the different layers is set based on the ultimate analysis of wood, the need to maintain a constant burnout of the wood log and the motivation to predict a reasonable temperature in the combustion zone, as a large amount of char is assumed to lead to too high temperatures. Accordingly, it is suggested that the bed model is consequently somewhat fitted to what has been observed in experiments and what can theoretically be expected from the combustion of wood logs in combustion units. Even when splitting the wood log into three layers, the wood log was not fully resolved for [123] and no mass transfer phenomena of the volatiles within the wood log were modeled. As a result, the volumetric mass sources entering the CFD simulation are only kinetically controlled, and thus only the temperature at the wood log surface defines the mass release rate of volatiles. In this work,was CO_2 also considered to be the only oxidation product, which is another simplifying assumption of that solid phase model [123] that is considered a weakness. Considering that the formation of CO from char would lead to a different heat release rate, a different temperature profile and gas species concentrations entering the CFD gas phase model via boundary conditions can be expected. The deviation between the experimental results and the modeling results [123] highlights that this consideration of CO formation does not yield accurate predictions of CO levels.

A common simplifying assumption of the solid phase model of a wood heating appliances simulation is the decoupling of the bed model from the results of the gas phase model [123]. This setting suggests that there is only a forward coupling between the bed model and the gas phase model. However, this approximation

entirely neglects that the temperature in the combustion zone is fluctuating and accordingly, a varying heat transfer to the wood log surface is assumed to also affect the thermal conversion of the wood log and therefore the volatiles release- and char conversion rates. For this reason, it is considered to be one of the main error sources in the simulation of wood fired combustion units. It is recommended to base the coupling on a dynamic interaction between results of the gas phase model and results of the bed model [124]. In such a case, the bed model is also influenced by variations of the operational conditions of the combustion unit.

6.1.2. Gas phase model

In this section, the most relevant aspects of the gas phase model are discussed. This includes the turbulence model, the combustion model and the radiation model. Gas phase kinetics have already been discussed in the chapter on homogeneous gas phase modeling, Section 5.

Turbulence model

The realizable k-ϵ model is used in some boiler simulations [154], but the standard k-ϵ model is more common [123,124].

The motivation for choosing the standard k-ϵ turbulence model is its robustness, the fact that it is computationally efficient, and that it still leads to a reasonable accuracy. Near the walls of the furnace, standard wall functions are applied [123]. Since computational cost is a primary aspect of the applicability of a simulation tool, the choice of the standard k-ϵ model seems reasonable, but the realizable version is recommended due to better accuracy for more complicated flow patterns.

Combustion model

Some researchers [154] coupled turbulence and combustion with the Eddy Dissipation Model (EDM). Buchmayr et al. [156] claim that EDM with a two-step methane combustion mechanism is used quite frequently, despite the disadvantage that the EDM (also valid for the Eddy Break-Up model, EBU) cannot consider detailed chemistry. On the other hand, they are very fast, which makes them attractive for engineering applications. The EDM (and EBU) will result in elevated reaction rates, since the reaction rates only depend on turbulent mixing [156].

The effect of neglecting detailed chemistry is that the gas temperature tends to be over-predicted. This is due to the fact that for global chemical reactions there are no radicals in the gas phase, where the radicals carry chemical energy that could otherwise be converted to heat. Furthermore, multi-step chemistry such as that relevant in the evolution path of nitric oxides cannot be accounted for.

The Finite-Rate-Eddy-Dissipation modeling approach, which was used by Porteiro et al. [124], calculates the Arrhenius expression as well as the Eddy dissipation rate, and the smaller of the two is chosen to model the reaction rates in the species equations. It is assumed that this combustion modeling approach can predict what happens in a combustion chamber in great detail. Close to the bed, where the flame is located and very high temperatures can be measured (about 1000 °C), the reaction kinetics are very fast, and accordingly, the mixing between volatiles and oxygen will control combustion reactions. Close to the water pipes and the furnace wall, temperatures will be significantly lower, so the kinetics will be the controlling factor for combustion reactions. More general information on various turbulent combustion models can be found elsewhere [157]. One can conclude that the choice of combustion model depends significantly on the purpose of the simulation tool, with either being a fast tool or a more accurate one.

Radiation model

Most commonly, the discrete ordinate model (DOM) is used for modeling the radiative heat transfer in boilers [123,124,154]. When modeling the DOM, the radiative transfer equation is solved for a limited number of distinct solid angles. One thereby models the transport of radiative intensity in a sector that is defined by the solid angle. The value of the intensity is influenced by both the position vector and the direction vector [123]. DOM is commonly used since it can be applied over the full range of optical thicknesses [158], which can also be done by the Discrete Transfer Radiation Model (DTRM) [159]. The DTRM is based on the assumption that radiation exiting a surface element within a range of certain solid angles can be clustered together and modeled as a single ray. Nonetheless, one needs to take into consideration that both DOM and DTRM are computationally more expensive than other radiation models, such as the P–1 model and the Rosseland model, with the latter being the most computationally effective [158]. DTRM becomes disproportionately expensive, if there are too many surfaces that rays must be traced from. This implies that especially for boilers with complex installations in the interior of the combustion chamber, a denser grid has to be used and the DTRM is considered too computationally expensive, as tracing the rays through a large number of control volumes increases the computational effort.

When applying a less expensive radiation model, other restrictions become important. The P–1 model is restricted to an optical thickness larger than 1, while the Rosseland model is restricted to an optical thickness larger than 3 [158]. In the P–1 model, the radiative heat flux vector in a gray medium is approximated [160,161], whereas in the Rosseland radiation model, intensity is assumed to be the intensity of a black body at the gas temperature [160]. One advantage of the Rosseland model is its efficiency, while a main disadvantage is that it cannot account for particle effects. For a pellet-fired furnace, where particles may be entrained in the gas flow during the last phases of burnout, or where the nucleation of ash vapors in the cooler furnace regions can lead to particle formation, the influence of the radiation exchange between particles and gases may be significant. This highlights that particularly the P–1 model and the DOM are relevant for wood heating appliance modeling due to their ability to handle embedded particles. However, even though the DOM is computationally more expensive, it is able to consider semi-transparent walls, e.g. glass, which makes it suitable for a furnace modeling where the radiant heat losses via the glass window have a significant effect on the temperature within the combustion chamber [158]. The potential of considering the glass window in a radiation model can be a criterion of exclusion for other less expensive models. Considering all these aspects, it is concluded that the DOM considers most of the key aspects of a suitable radiation model, which belongs to one of the chief features of a realistic simulation tool. This discussion of radiation modeling does not only apply to domestic boiler modeling, but is also valid for the domestic stove modeling discussed in the following section. Most commonly, the properties of the gases (absorption/ emissivity) are modeled by the Weighted-Sum-Of-Gray-Gases (WSGG) model, e.g. [124]. However, no simulation tool for domestic boilers included the absorption and emissivity characteristics of soot, even though the influence of most of the volatile species products is considered by implementing the WSGG model. A future field of research is therefore the full and accurate consideration of the role of soot in combustion units, which therefore also requires the accurate adjustment of the properties of gas including soot.

6.1.3. Boundary conditions of boiler

To reduce the computational cost of a simulation, it is a common approximation to not simulate the entire boiler [124]. The water side of the boiler can be modeled by convective heat transfer, with a constant heat transfer coefficient. This simplification reduces the

computational cost significantly and it yields good results. At the boundaries of the furnace modeling domain, where heat is transferred to the heat exchanger surfaces, the grid has to be refined in order to be able to handle the steep temperature gradients [123]. Furnace wall emissivities are normally set to constant values, such as 0.8 [124] or 0.9 [123]. There is currently no model available that considers the change of emissivity and heat transfer of the furnace walls, due to ash vapor condensation and particle deposition. This is therefore recommended to be investigated further in future research.

6.1.4. Most important modeling results

Scharler et al. [154] found that an optimization of the secondary air nozzles, in addition to a reduction in the number of installed air nozzles yield an improved mixing between flue gas and secondary air, which resulted in a significantly better burnout of CO. Porteiro et al. [124] were able to detect a strong recirculation zone with their model. The recirculation zone is essential, since it stabilizes the flame. In their prediction, the flame occupied two-thirds of the combustion chamber. Another advantage of their model is that a very good prediction of NO_x and an overall good agreement of the CO prediction between the model and measured values [162,163] was achieved. Furthermore, they found that the operational conditions of the furnace had negligible effects on NO_x formation, and all modeled cases resulted in a more or less constant NO_x yield [124].

In other works, the predicted CO deviated significantly from what had been experimentally measured. As pointed out earlier, the choice of kinetics of homogeneous and heterogeneous reactions is assumed to be one main source of error [123] with respect to these predictions.

Overall, the number of works on small-scale-boiler modeling (scale of smaller 30 kW), is very limited. Future research is therefore encouraged to increase the focus on such small-scale boiler units, since those small units are related to high emission levels.

6.2. Stoves

6.2.1. Bed model

Empirical models are also commonly used for wood log modeling in domestic wood stoves [14]. Details on the model of Scharler et al. [14] have been discussed in the boiler section, and the same model has been used for wood log modeling in stoves where a bed of two non-touching wood logs was modeled. Touching wood logs imply that heat and mass transfer from and to the wood log surface were hindered. However, such a blockade to transport phenomena has not been modeled in any of the reviewed works.

When modeling small-scale wood stoves fired by wood logs, it is also a common approach to derive volumetric mass source terms entering the gas phase model without actually fully discretizing and solving a bed model [13,132]. The volatiles release of six non-touching wood logs in the combustion chamber was modeled in these specific cases. The released gas composition was either based on Norwegian spruce [13,132] or demolition wood pellets [130]. The wood consumption rate has to be obtained experimentally for the model, and accordingly, the wood consumption rate is given under fixed operational conditions of the furnace, which therefore limits the applicability of the model to one specific time of a particular test case. Furthermore, the consumption rate depends on the wood species tested. If the wood consumption rates are only known for a limited number of test cases and wood species, the flexibility of the bed model is restricted. However, since the main purpose of the work of Bugge et al. [13,132], was to gain a fundamental understanding of NO_x formation mechanisms from fuel-bound nitrogen, it is assumed that relevant knowledge can be gained from this model, even though no detailed bed model has been developed.

Another bed model discussed in the available open-literature restricts the active area to the external surface of the wood log, while the interior of the wood log was not discretized and modeled [127]. Devolatilization was modeled with a one-step global reaction mechanism, which was based on literature data [51,164] linking the composition of the gaseous mixture to the wood consumption. Char gasification was treated in a similar manner. Coupling between the gas phase model and the bed model was done with mass and heat source terms at the interface between them.

In some works, the solid phase model was assumed to be quasi-steady-state [126−128]. These models are based on the assumption that only one specific stage of combustion can be described by the model, where a constant burning rate is given and the stage is related to a slow shrinkage of the wood log. It is said that the time scale for wood degradation can be expressed with the time of shrinkage, which is in the range of minutes. This is very long compared to gas phase reactions, which have time scales in the order of seconds, so the solid degradation process can hence be assumed to be steady state [127]. The model can be considered as a computationally efficient modeling approach, but does entirely neglect secondary reactions of the leaving tar, as well as the cooling of exiting water vapor or volatiles. The assumption of immediately leaving gaseous products of wood conversion is assumed to be related to significant errors as far as emission predictions are concerned.

Tabet et al. [128] modeled a bed composed of a single wood log. They described the solid bed by three layers that represent drying, devolatilization and char conversion. The wood log was 50 cm long, and each layer had a height of 4 cm. This suggests that the sizes of the layers do not change, suggesting that they maintain the exact same thickness throughout the conversion. Accordingly, this assumption is limited to a conversion stage where conversion can be considered to be a quasi-steady-state. Furthermore, this assumption restricts its application to a specific stage in thermal conversion, making it unsuitable to model an entire combustion cycle.

Steady-state assumptions were also performed by Huttunen et al. [126], though that overall approach for the bed model was slightly different from previous modeling approaches. Huttunen et al. [126,155] developed a model for wood log drying, devolatilization and char conversion, and coupled it to a CFD model by using the TULISIJA-code (more background information on the code itself can be found elsewhere [165,166]). Huttunen et al. [126,155] developed their solid bed model in two steps, in which the first stage was only discussing the volatile composition and release rate, whereas the second stage focused on char conversion modeling. They made two different models (the first-generation pyrolysis model and the second-generation pyrolysis model) for devolatilization and drying. In the first-generation pyrolysis model, the drying and devolatilization rates were based on the energy equation describing heat storage, conduction and convection in the interior of the wood log, and in addition also energy sources originating from drying and devolatilization. The equations were based on a radiative heat flux to the surface of the wood log, which in their model was defined to be uniform. The disadvantage of this model is that it is not time-dependent, which is a problem if e.g. ignition is supposed to be considered. In the second-generation pyrolysis model, the drying and devolatilization rates were modeled differently and were said to depend on the penetration velocity of the temperature zone into the wood log. Limitations of the second-generation pyrolysis model are that it is only applicable in a certain range of radiation temperatures and log diameters. The rate of evaporation and devolatilization is proportional to the penetration velocity of a certain temperature zone, where the penetration velocity includes the influences of a constant and $1/\sqrt{t}$, with t being time [126]. Huttunen et al. [126] coupled the pyrolysis model to the flow model by inserting its results (mass, energy fluxes, etc.) in the evolution equations as source terms.

For wood log modeling in wood stoves, there are also more comprehensive models available in open-literature. These models include models with fully discretized wood logs that also contain a detailed description of chemical and physical processes related to thermal wood conversion [50,51]. These models have been discussed in detail with respect to single particle models (Section 4). Galgano et al. [50,51] show that the flow field is closely connected to the temperature and the species distribution released from the wood.

6.2.2. Turbulence model

Knaus et al. [125] implemented the standard k-ϵ model, the Reynolds stress model (RSM) and the low Reynolds number k-ϵ model suggested by Lam and Bremhost [167]. They tested two cases, whereof one was an isothermal case (no combustion) and the second one was the combustion case. In the isothermal case, they investigated the prediction of recirculation zones by the different turbulence models and found that the standard k-ϵ model correctly predicts location and strength of the recirculation zone, whereas the RSM gives more accurate results. However, these two previously mentioned models are only applicable at high Reynolds numbers. It was found that there might also be zones of low Reynolds numbers. This justifies use of the low Reynolds number k-ϵ model. Another problem is the influence of the walls on the free flow. It was found that it cannot be adequately modeled with standard wall functions applied in the k-ϵ model and RSM in such narrow geometries. This underlines the fact that the low Reynolds number k-ϵ has some significant advantages [125].

Comparing the standard k-ϵ model and the RNG-k-ϵ model show that the choice of turbulence models has a significant effect on predictions of both temperature and emission levels [126]. The RNG k-ϵ model predicts lower turbulent viscosity and a longer turbulent time scale than the standard k-ϵ model.

For high Reynolds numbers, the RSM is known to yield more accurate results than any k-ϵ model. This does, however, come at the cost of more CPU load. In wood stoves, the Reynolds number is typically rather low, and the extra CPU cost of the RSM model will therefore not necessarily pay off. The RNG k-ϵ model has not been proven to perform significantly better than the standard k-ϵ model, maybe with the exception of rotational flows. A better choice is then to use the realizable k-ϵ model, which lately has shown to yield improved results for a large number of different flows. Unless one really feels that a low Reynolds number k-ϵ model is required, the realizable model seems to be the preferred option for wood stove simulations.

By using the RNG k-ϵ model instead of the low Reynolds number model of Chien it was found that the flame ignite earlier, leading to higher temperatures in front of the wood log [127].

Due to its impact on the level of temperature fluctuations, the choice of turbulence model can have a significant effect on modeling of NOx emissions. Hill [168] studied the effect of either considering or neglecting fluctuations of temperature and species and found that this could yield differences in NOx emissions up to 600%. The relevance of the turbulence model for the accuracy of the predictions of NOx emissions has so far only been studied for pulverized coal combustion, where entrainment of converting fuel particles is significant [168], which means that the turbulence is of significance not only for homogeneous gas phase reactions, but also for particle-gas heat transfer and therefore particle conversion. It has not yet been studied how important the turbulence model is for large wood log conversion, where turbulence is mainly influencing homogeneous burnout of combustible gases.

6.2.3. Combustion model

Knaus et al. [125] as well as many other researchers [13,50,51, 127,132] coupled turbulence and combustion modeling via EDC. Very few models [128] used a pre-assumed probability density function approach. With respect to wood stove applications also the Eddy Dissipation / Finite Rates Kinetics Combustion Model has been applied [14]. This approach will yield relatively accurate results with global chemical kinetics as it accounts for both kinetically and mixing controlled combustion. If detailed chemistry is required, the EDC model is the more appropriate choice. The increased accuracy does come at the expense of somewhat higher computations costs. All wood stove models focusing on NO$_x$ are based on the EDC.

6.2.4. Radiation model

In case of wood stove modeling, the Discrete Ordinates Method (DOM) is commonly applied [13,14,125,127,128,132], as it is also for boiler modeling. Some researchers [50,51,126] used a discrete transfer model, originally suggested by Lockwood and Shah [169] for modeling radiation, which is previously discussed but referred to as DTRM. In work by Huttunen et al. [126], the local absorption coefficient of the gas phase was calculated based on the Weighted Sum of Grey Gases (WSGG) approach while the absorption of the soot was added on top of this. A similar approach has also been used by others [170,171]. The detailed discussion on advantages and disadvantages of various radiation models presented with respect to the boiler model, Section 6.1.2, can be applied to stove modeling as well, due to similarities between these two heating appliances.

6.2.5. Boundary conditions of the wood stove

The importance of the consideration of the glass window of a wood stove as part of the boundary conditions of the stove on temperature predictions has been outlined in a number of works [13,132]. However, the influence of a glass window and the radiative heat loss due to it, are not captured by current models, since the glass window, like any other furnace wall, is commonly assigned the same constant temperature as any other furnace wall [13,127,132]. Some works define stove boundary conditions based on purely experimentally derived values [126,165,166]. There is clearly room for significant improvements here. This should be done by including the transparency of the window and by accounting for heat transfer to the surroundings through all furnace walls. In addition, the air inlets should not be placed at the inlet to the furnace, but rather at the position where the air enters the stove itself. This means that the air transport channels leading to the furnace must be meshed and simulated. A reasonable pressure difference should then be applied between the inlet and the outlet to drive the draft. In this way, the total airflow to the furnace and distribution between the different inlets would automatically be correct.

6.3. Detailed comparison of wood stove models

In addition to the models discussed in the previous sub-sections, also more case specific models may be included to yield more accurate wood stove simulations. In the current section, a number of such case specific models for wood log combustion will be discussed. Important aspects of a reliable simulation tool for wood stoves are explained in more detail in Table 7.

Table 7 outlines which aspects are considered by the currently available models. The aim is to identify the completeness of current models in order to understand which aspects of furnace modeling cannot yet be described. Reviewing the current state-of-the-art has shown that modeling CO and to some extent also NO$_x$ emissions is a main feature of current models. Even though a deeper understanding of the evolution paths of different gas phase species is recommended in order to optimize gas phase kinetics, the principle implementation of the gas phase reactions and the corresponding predictions of emission levels are rather well-established. In contrary, many aspects related to the bed model are either entirely neglected or not accurately accounted for in current models.

The first aspect 1) refers to models that include detailed descriptions of chemical and physical processes related to thermal

Table 7
Aspects for a real world simulation tool for wood stoves. The table marks which aspects of an advanced simulation tool have or have not been considered in current models.

No. in Fig. 6	Aspect								
	Ref.	[132]	[13]	[14]	[154]	[128]	[127]	[50,51]	[126]
1)	Detailed solid phase model	–	–	–	–	–	–	✓	–
2)	Bark layer	–	–	–	–	–	–	–	–
3)	Stack of logs	✓	✓	✓	✓	–	–	–	✓
4)	Logs in contact	–	–	–	–	–	–	–	–
5)	Transient log model	–	–	✓	✓	–	–	✓	–
6)	Log shape	brick	brick	irrr.	irr.	irr.	cyl.	cyl.	brick
7)	Log size	NA	NA	NA	NA	NA	ø 12−21 cm 1.5 m long	ø 12−21 cm 1.5 m long	5 x 5 x 30 cm
8)	Modeling of pseudo-components	–	–	–	–	–	–	–	–
9)	Ignition principle	–	–	–	–	–	–	–	–
10)	Multi−cycles	–	–	–	–	–	–	–	–
11)	Soot modeling	✓	✓	–	–	–	–	–	✓
12)	Prediction of recirculation zones	NA	NA	NA	NA	✓	✓	✓	NA
13)	Radiation loss through glass	–	–	–	–	–	–	–	–
14)	Air flushing of glass window	✓	✓	✓	✓	✓	–	–	–
15)	Stove walls modeled	–	–	✓	✓	–	–	–	–
16)	Heat transfer to room	–	–	✓	✓	–	–	–	–

"irr." is the abbreviation for irregular, "cyl." is the abbreviation for cylindrical and "brick" is the abbreviation for brick−shaped. "NA" means not announced. If "Prediction of recirculation zones" is marked as "NA", this indicates that this aspect might have been modeled, but was not discussed in the paper at all.

conversion of wood and that include evolution equations for wood mass, char mass, gas species and temperature. It also implies that the interior of the wood log has been fully discretized. As can be seen from Table 7, only a limited number of works includes such a detailed description of the solid fuel. The main reason for this is the increased computational cost that results from a comprehensive bed model.

The second aspect 2) clearly shows that none of the currently available models considers the influence of bark. The elemental composition of bark, however, differs significantly from the elemental composition of the wood. This may have a significant effect on conversion reactions, since the bark contains a higher amount of inorganics that can catalytically influence the conversion reactions. Especially, when ash formation is a major concern of a model, bark has to be considered, as it contains a significantly higher ash content than the inner wood [172].

Modeling stacks of logs (point 3) is a more realistic assumption, even though it is not assumed to have a significant influence on the modeling results if the wood logs are not touching. If the stacked wood logs in the combustion unit touch (point 4 in Table 7), which has not been modeled so far, there will be a reduction of mass and heat transfer to and from the blocked wood surfaces. Accordingly, depending on the position in a wood stack and depending on the degree of contact between wood logs, different boundary conditions for the wood log models have to be used. This is expected to influence conversion times, and product release rates. So far none of the wood stove models, has taken the complexity of in-contact stacking of wood logs into consideration. A transient log model (point 5) can be applied for the entire thermal conversion process, also including initial heating and ignition of the wood logs, the stage of more or less stable devolatilization and char conversion rates, as well as the final stage where only residual char is converted to ash. Some of the models available in the current literature only focus on one specific stage in the thermal conversion of the wood log, where constant thermochemical degradation and combustion can be assumed [126−128]. The aspect of transient log models is furthermore closely linked to modeling of ignition principle (aspect 9). It was found that unless a dynamic coupling between gas phase and bed model, considering the influence of a higher heat flux back to the bed model to due flame establishment, was done, the ignition principle was not

fully accounted for. Furthermore, if the aim is to model a multi-cycle, ignition modeling is essential. However, as can be seen from Table 7 also none of the current models was extended over more than a single combustion cycle.

When pseudo-components are modeled (point 8), wood is split into hemicellulose, cellulose and lignin and therefore enables the user to adjust the corresponding mass fractions with respect to the applied wood species. If only wood (the mixture of all main pseudo-components) is simulated, the aspect is marked as "not considered (−)" in Table 7. Splitting the wood into its pseudo-components, which results in a higher flexibility of the model since different wood species can easily be modeled, is not common for wood log conversion modeling in wood stoves.

Only Bugge et al. [13,132] explicitly mentioned the relevance of glass windows on the energy equations of the stove, since the glass window can be linked to significant heat losses. Still, even in their work, the glass was treated as an optically thick isothermal wall. Expanding the computational domain to also including the stove walls in an energy balance, such that the heat transfer to the surrounding room can be modeled, has only been done by Scharler et al. [14,154].

Soot is only considered in models developed by Bugge et al. [13,132] as well as Huttunen et al. [126]. Furthermore, the validity of the soot models and chemical kinetics used in these works, and their ability to accurately predict the correct level of soot, still has to be proven.

This discussion outlines that with respect to wood stove modeling, a significant number of chief aspects required for a realistic simulation tool, have not yet been considered in current models.

7. Bed models in grate furnace modeling

This section focuses on fuel bed modeling in large-scale grate furnaces. Yin et al. [173] stated in their review paper that there are two common approaches to modeling biomass conversion in a large-scale grate furnace fuel bed. These approaches are listed and briefly described in Table 8.

The main challenges for current bed models are the inhomogeneity and complexity of the wood bed, and the fact that this demands detailed multi-dimensional models. In order to capture the

Table 8
General modeling approaches used for woody biomass conversion in the fuel bed in grate furnaces.

Approach	Short description
Approach 1	The bed model is measurement-based as well as experience-based. The inlet conditions for the freeboard model are taken from measurements. The prescribed combustion rate is dependent on the position on the grate and can be obtained from heat and mass balances of fuel and primary air. Outputs of the bed model are temperature, species concentration and velocity profiles, which enter the freeboard [a] model [173].
Approach 2	Separate models for solid bed and gas phase are developed. In the most advanced case the bed models deliver the inlet conditions for the CFD model and radiative heat transfer from the freeboard back to the fuel bed model is also modeled, resulting in a dynamic coupling between the two models [174]. In a more simplified approach, the two models can also be decoupled, and therefore the degree of coupling can vary.

[a] Freeboard refers to the gas phase above the fuel bed.

structural changes of the bed due to thermal conversion, as well as phenomena occurring in connection to those changes, such as channeling, multi-dimensional models are more accurate. But, multi-dimensional simulations are also associated with higher computational costs. For efficient large-scale grate furnace simulation tools, simplifications of the fuel bed are therefore required. These simplifying assumptions are the primary difference between single particle modeling and fuel-bed modeling in large-scale grate furnaces.

The main disadvantage of today's independent modeling approaches for the solid bed and freeboard is that in order to describe flow, turbulence and heat transfer in two separate sub-models, a number of simplifications are required (e.g. for temperature and velocity profiles at the interface between the gas phase and bed model) [174]. The bed shape is also usually geometrically simplified, e.g. evened out. Due to these simplifications, no overall valid

model is commonly developed, but rather models that only apply to certain furnace types. This is due to the fact that a lot of simplifying assumptions are based on measurements in specific plants with different grates. Furthermore, experiments for validation of the output from the bed, which enters the gas phase, can hardly be done, because experiments at the interface between the two phases are very challenging [174]. Fig. 22 shows the theoretical coupling between the freeboard and fuel bed that is required for an accurate CFD simulation of the grate furnace.

Table 9 outlines the current state-of-the-art of solid bed models applied in large-scale grate furnace simulations. Only grate furnace bed models using woody biomass have been included. Biomass types other than wood have not been considered.

Ash-related problems are vast, and can range from affecting particulate emissions, to causing internal plant problems related to slagging, deposit formation and corrosion. The enhanced ash melting behavior of a fuel in particular can lead to problems in a grate furnace [172]. Wood has a rather low ash content, while herbaceous biomass has a high ash content that can affect the furnace operation. It is expected that it is crucial to account for the ash for accurate modeling predictions if herbaceous biomass is converted, while it is less relevant for wood conversion. The modeling of fine particulate formation and ash deposit formation, with a special focus on grate furnaces, is not frequently done in current models [154]. Because a biomass is thermally converted on the grate, ash-forming vapors are released [154]. As the flue gas containing ash vapors cools, fine particles can be formed due to nucleation or condensation processes. Ash vapors can condense on these particles. However, in addition to condensation on the particles, ash vapors can also condense on the boiler walls [154]. These ash vapors contain sulfur and chlorine, which means that condensation on the furnace walls can lead to corrosion. One can clearly see that depending on operational conditions, and therefore temperatures in the furnace, as well as the biomass type, the importance of ash vapor condensation varies significantly.
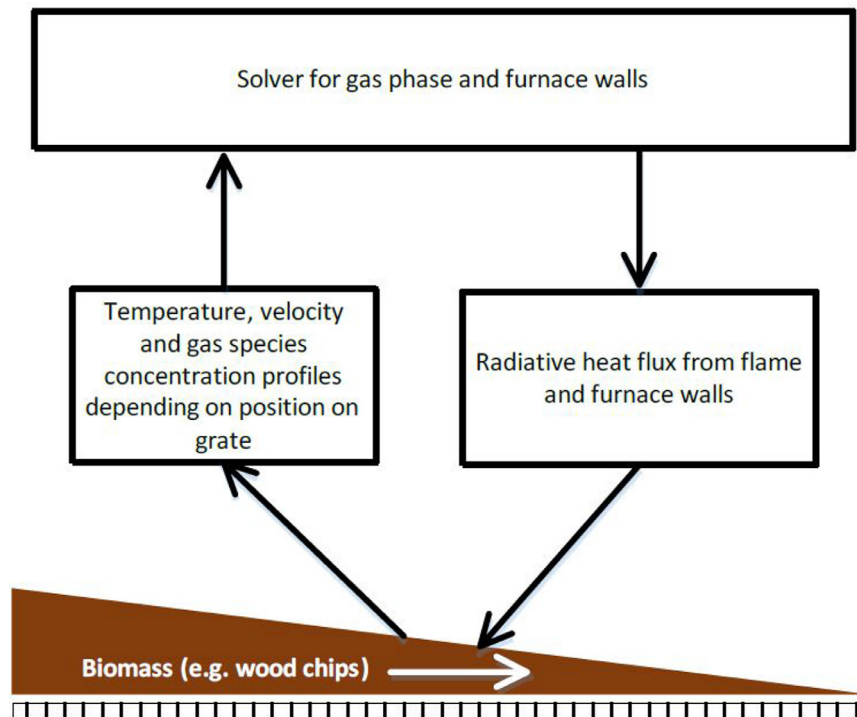

Fig. 22. Coupling between gas phase and solid phase. The brown triangle illustrates the fuel bed on the grate. The bed height decreases along the grate as the degree of conversion increases. The combustion gas exits the solid phase and enters the freeboard, while the radiative heat fluxes emitted by the flame and the furnace walls heat up the biomass on the grate.

Table 9

Bed models applied in current woody-biomass-grate-fired furnace models. The bed models are sorted by increasing complexity. The models are categorized by the "Approach type" listen in Table 8. "Empirical" indicates that main data entering the model has been taken from experiments. The fourth column lists the literature, parameters have been taken from. "Separate sub-models" outlines that a model has been developed for the bed model and another model has been developed for the gas phase. "Conversion from literature" indicates that conversion parameters were required in the model and those were taken from literature.

Author & year	Ref.	Bed model type	Empirical	Conversion from literature	Separate sub-models	Approach type
Griselin and Bai (2000)	[175]	Empirical B.M.	✓	NA	–	1
Klason & Bai (2006)	[16]	Empirical B.M.	✓	[176]	–	1
Scharler et al. (2000)	[177]	Empirical B.M.	✓	[178]	–	1
Scharler and Obernberger (2000)	[17]	Empirical B.M.	✓	[178–180]	–	1
Scharler and Obernberger (2002)	[181]	Empirical B.M.	✓	[178]	–	1
Scharler et al. (2004)	[182]	Empirical B.M.	✓	[178,183]	–	1
Costa et al. (2014)	[184]	Empirical B.M.	✓	[185]	–	1
Rajh et al. (2016)	[186]	Empirical B.M.	✓	NA	–	1
Wurzenberger et al. (2002)	[45]	Transport equations	–	–	✓	2
Bruch et al. (2003)	[46]	Transport equations	–	–	✓	2
Huttunen et al. (2004)	[187]	Three zone B.M.	–	–	✓	2
Zhang et al. (2010)	[3]	FLIC [b]	–	–	✓	2
Boriouchkine et al. (2012)	[188]	Transport equations	–	–	✓	2
Kurz et al. (2012)	[174]	One single 3D CFD code	–	[189]	✓	2
Chen et al. (2015)	[190]	FLIC [c]	–	–	✓	2

[a] FLIC is the abbreviation for "FLuid dynamic Incinerator code".

One of the most detailed bed models available today solves a 3D CFD code for both the solid and gas phase by only adjusting the transport equations with respect to the volume fraction occupied by the solid matrix [174]. This highlights the fact that the bed model and the gas phase model are closely linked, and that the interaction between these two phases is dynamic. The model is steady-state and accounts for freeboard and bed modeling based on a multiphase approach. The principle of the multi-phase approach is that the physics and the reactions of both the solid and gas phase are considered simultaneously. Drying is based on a pure thermal model. Detailed reactions describing devolatilization and char conversion are included in the model. A simplifying approximation of the model is that the detailed gas phase composition is not fully modeled, instead, volatile species mass fractions are approximated based on experimentally defined relations. Experimental relations suggested by Thunman et al. [189] were then used, in addition to the elemental mass balance in order to calculate the mass fractions of a total of five different volatile species. The particle mixing model accounts for the influence of grate movement, which is causing a stronger mixing in the bed. The corresponding particle mixing coefficient is experimentally obtained [191], and it is affected by the physical properties of the biomass in the fuel bed, the type of grate installed in the furnace and the operation conditions of the furnace. The simulation results gave too high temperatures compared to experiments. This deviation is most likely due to the wall boundary conditions, which are set to be adiabatic. Another reason for over-predictions of temperatures was found to be the inaccurate prediction of secondary air penetration. The model under-predicted the penetration depth of the air from the secondary air nozzles [174].

The FLuid dynamic Incinerator Code (FLIC), where transport equations are solved in 2D [3,190], is less complex than the 3D model discussed above. Two sub-models, where one accounts for the fuel bed (FLIC) while the other handles the gas flow in the freeboard above the bed, are the basis of this model. The two sub-models are dynamically coupled via the boundary conditions, but the fuel bed is only heated by radiation from the gas phase. Devolatilization is described with a one-step global model, and the permanent gas phase is composed of C_2H_4, CO_2 and H_2O. As products of char conversion, CO as well as CO_2, are formed [3].

FLIC is based on solving transport equations for both the entire bed and the freeboard [191]. The equations in the bed are solved in 2D. The solid fuel conversion is split into four sub-processes, namely drying, devolatilization, combustion of the volatiles in the gaseous phase and char gasification. The model is steady-state, and it is assumed that the conversion front moves downward from the top of the bed at the same constant speed. During drying, the fuel is heated by radiation, but also the dry primary air flow from below the grate drives moisture out of the bed. Gas combustion is considered to take place in the voids of the bed. The burning of the volatiles is dependent on kinetics, as well as the mixing rate with the under-fire air. One current restriction to the FLIC model is that it is not possible to solve the velocities of the bed, but instead a horizontal movement of the bed is predefined. The vertical component of movement is obtained from the solid-phase continuity equation [191].

Due to channeling, the temperature profile across the bed is highly non-uniform. It is assumed that channeling inhibits mixing between combustible gases and air, and results in a lower combustion efficiency of hydrocarbons, thus increasing the C_xH_y emissions. Only a limited amount of work has yet been done concerning

modeling of channeling. Hermansson and Thunman [192] modeled channeling and the shrinkage of a bed in a grate furnace. However, they only discussed char conversion in the bed model (excluding drying and devolatilization), their model was therefore not included in Table 9. It was found that the shrinking of the bed is not smooth. The reasons for this are uneven fuel consumption across the bed and the influence of the moving grate, as well as the non-spherical particle shape. The particles have a rough surface; therefore, particles will not smoothly slide down in the bed as the thermal conversion of the bed proceeds. Hermansson and Thunman [192] recommended describing shrinkage as a combination of continuous bed shrinkage and occasional collapses due to porosity growth.

Using the FLIC model for simulating a wood chip boiler predicted that char conversion starts in the middle of the moving grate [3]. High CO contents were found next to the bed, and CO levels were reduced significantly as mixing with secondary air increased. Experiments showed that volume fractions of CO and NO in the flue gas experienced significant fluctuations, ranging from 313 to 781 mg/m^3 and 27.8 to 65.1 ppmv, respectively. Modeling results were within these ranges, being 403.5 mg/m^3 and 40.6 ppmv, respectively [3]. For validation, one has to keep in mind that near the bed, detailed measurements cannot be obtained mainly due to unavoidable unsteady phenomena, mostly due to the riddling of the fuel on the grate, which is enhanced by grate movement and sudden collapses of channel-structures in the bed, thus leading to fluctuations in measurements [174].

The influence of flue gas recirculation can also be captured with this simulation tool, built up by a combination of FLIC and Fluent [190]. The CO reduction when modeling a test case without flue gas recirculation has been shown to be significant compared to a test case considering flue gas recirculation. This behavior can also be replicated by the model [190]. As a rather cold flue gas was recirculated, this flue gas also reduced the flame temperature, resulting in lower peak flame temperatures and higher gas volumes being transported through the combustion chamber, resulting in an enhanced CO formation. However, the advantage of such a recirculation is that the temperature reduction leads to less NO$_x$ formation as the thermal NO$_x$ formation route is decelerated. However, the reduction potential found in experiments and simulation was small, as the main source of NO$_x$ is not the thermal formation route, but rather fuel-bound nitrogen [190].

It is concluded that the 2D-FLIC code in connection with Fluent for free board handling is able to correctly simulate the combined phenomena of heat transfer, homogeneous and heterogeneous kinetics and fluid flue for a moving grate-boiler.

A 1D bed model solving for governing equations for energy of solid and gas phase and gas species was developed for a biomass boiler, where the fuel enters a conical grate from below [188]. The fuel is then transported outwards, with rings that rotate either clockwise or counterclockwise. The fuel bed of biomass in grate furnaces is highly heterogeneous. Even though detailed evolution equations were solved [188], devolatilization was simplified compared to what has been found in single particle modeling. Devolatilization was based on earlier single particle modeling work by Alves and Figueiredo [34]. In comparison to their work, only the devolatilization reactions of cellulose and hemicellulose were modeled [188] instead of modeling six independent parallel reactions as suggested by Alves and Figueiredo [34]. In order to compensate for the higher computational cost of solving a higher number of transport equations, the model was reduced to 1D. Since transport equations for the bed and the gas phase are modeled, they dynamically interact [188]. The model was able to clearly identify the influence of the particle size on the overall conversion process [188]. Smaller particles ignite faster and absorb radiative heat more efficiently. However, the simulations also gave temperature oscillations, which can be explained by an easier cooling of smaller particles compared to large particles. As reactions in the

solid particle are enhanced, heat release starts and the temperature of the particle rises, which enhances the temperature difference between the solid phase and the gas phase. Consequently, re-radiation losses of the particle will be enhanced, cooling the particle and resulting in the observed temperature oscillation [188].

The bed modeling of grate furnaces is also done by developing single particle models and coupling them to a bed model. Most of these bed models, based on explicit particle models, are based on thermally thin particles [108,193−195], while it is assumed that for wood chips or pellets forming the bed, the intraparticle temperature gradient also has to be considered. Models based on the assumption of thermally thick particles in beds [45,46] were already discussed in Section 4. The bed models were 1D, assuming that only the gradients in the direction of the bed height were relevant. This is also the direction of the primary air flow. Next, the gas phase in the bed was solved in Cartesian coordinates, whereas the single particles were described by 1D spherical coordinates [45,46]. Therefore, the bed model is discretized by the so-called "1D + 1D"-grid [45]. One of these particle models [45] is based on the assumption of constant operational conditions, which as a consequence lead to the simplification of a pseudo-steady-state. Another simplifying assumption of the model is that one assumes the bed surface temperature to be constant over the entire length of the grate. This is considered to be a gross simplification, since it is well known that the temperature of the bed drops as the degree of conversion proceeds, and that the temperature of the ash near the ash outlet is lower. The reason for this simplification is that the bed model and the gas phase model were not modeled as dynamically coupled, and therefore independent boundary conditions for the bed model are set that do not vary depending on the gas phase modeling results. This is a gross simplification, since the interaction between the two phases influenced by the operational conditions of the furnace are entirely neglected [45].

A rather intermediately complex bed model splits the bed into three zones, in which drying, devolatilization and char conversion, respectively, are described [187]. The bed model is 1D, leading to reduced computational costs. The surface layer of the bed in the drying zone is affected by radiative heat, while the length of the drying zone is made dependent on the temperature. As long as the temperature is below the ignition temperature, the drying layer is still present. As soon as the temperature increases over this critical ignition temperature, the devolatilization zone is reached. The ignition temperature is user-defined, thereby suggesting that the geometrical dependencies of different conversion layers and the propagation speeds of these layers are solely dependent on a fixed temperature defined by the user of the model [187]. This is clearly a gross simplification of the model, thus reducing its flexibility to certain wood species and operation conditions. The ignition velocity influencing the bed conversion and gas release from the bed has been taken from literature data found for batch combustion, and is a function of particle diameter, moisture content (dry basis), ignition temperature, initial temperature, particle density and specific heat [196]. This is assumed to introduce some error to the model, since a grate furnace does not have an exact counter-flow of ignition front and airflow, as in the batch case. It is assumed that by using this literature data, the ignition velocity will be under-predicted, but then again the length of the devolatilization zone is made dependent on the ignition velocity [196], hence influencing the prediction of the volatiles release rate. An advantage over most other models is that this model allows for volatile consumption within the bed. This is assumed to affect the fractions of released gases from the bed model entering the free board.

The models of lowest complexity are empirical models, which have the primary advantage of being related to low computational costs, since they do not solve a high number of governing transport equations. A well-established empirical 1D bed model has been developed by Scharler et al. [17,177,181,182]. The model is based on

experimental results that showed that linear correlations between the release rates of H_2O, C, H, N and O from the woody fuel can be found. This leads to the simplification that only a single parameter (e.g. the release of C) has to be known to mathematically describe fuel consumption. This parameter is obtained from test runs where samples are taken at different locations on the grate. Furthermore, conversion parameters have to be known, which are required to model the concentration of gas phase species at a certain location. These conversion parameters are either taken from literature or based on experience/ assumptions. When modeling NO_x formation in a biomass grate furnace, the empirical bed model is recommended to be improved by a more fundamental model based on transport equations [182], even though such a development has to be balanced with the computational effort.

It is not common for empirical models to include a dynamic coupling between the bed and the free board. It is very often only forward coupling that is done [177,181,182]. Such a decoupling of bed and gas phase models [16,17,175,177,181,182] is clearly a gross simplification, since changes in operating conditions will affect conversion in the fuel bed and therefore also conditions in the freeboard, which is not accounted for if decoupling is done.

Some empirical 1D bed models do, however, include a dynamic coupling between the bed and the gas phase [186]. The dynamic coupling is then done with the radiative heat flux emitted by the flame and the furnace walls, which heats up the fuel bed, as well as the mass flux of combustible gases from the fuel bed into the gas phase. Yet, the fuel conversion, being influenced by these radiative heat fluxes, as well as the primary air flow and recycled flue gas flow through the bed, is only described with an empirical 1D bed model. The output of this model entering the gas phase includes temperature and velocity profiles of the exiting volatiles, in addition to species concentration profiles.

The model of lowest complexity is the zero dimensional time-independent scheme [184] that splits the bed into two zones [197]. This model has not been added to Table 9, since it cannot be categorized by one of the approaches listed in Table 8. The furnace operates under steady conditions. The two zones are drying and conversion (devolatilization and char conversion), and in each of these zones mass and energy balances have to be solved. In the conversion section, it is assumed that a mixture of 11 species is present in the gas phase and the species exiting the fuel bed are in a thermochemical equilibrium. The empirical bed model, as well as the zero dimensional time-independent scheme, are acceptable engineering tools if the focus of the studies lies in an analysis of the freeboard processes and optimization in the freeboard region. These models, however, might not be suitable for primary air zone optimization [184].

It was found that a major part of the bed models in large-scale grate furnaces is empirical [16,17,175,177,181,182,184,186]. This finding was confirmed by Yin et al. [173], claiming that such experience- and measurement- based models are attractive due to their robustness. Due to their reduced computational time, these models are still important for engineering applications.

In conclusion, it can be stated that detailed thermal degradation and the combustion of single particles forming the bed are not commonly done with respect to grate furnace modeling. This was also found by Hajek and Jurena [198], who stated that current works model a homogeneous isotropic packed bed rather than individual particles of fuel.

8. Conclusion and recommendation

Single particle degradation models, simulations of small-scale heating appliances and bed models of large-scale grate furnaces have been reviewed in this work. A short introduction to wood chemistry is given. This is considered to be essential in order to understand the complexity of the challenges related to devolatilization and the char

conversion modeling of wood. Physical differences of wood logs, pellets and briquettes are subsequently mentioned to outline the diversity of the reacting wood type. Following this introduction, particle degradation modeling with interface or mesh-based models is discussed and the main assumptions and simulation results are outlined. Interface-based models are commonly used if reduced computational cost is essential while mesh-based models are more detailed and include more physics, such as the gas phase flow and pressure solutions inside the wood particle. Secondary tar reactions are also commonly implemented in mesh-based models. For engineering applications, the interface-based models provid accurate predictions of mass and energy fluxes, which are the main coupling to gas phase modeling. An emphasis was also placed on discussing the complexity of the models with respect to dimensionality, outlining that mainly 1D models have been developed so far.

Different drying models were discussed in this paper, and it was found that a combination of the equilibrium model and the thermal drying model is a suitable choice for accurately describing drying in both low and high-temperature conditions, thus covering a broad temperature range. Kinetic rate drying models are typically found to be significantly less CPU intensive though.

Especially with respect to the quantitative determination for the heat of reactions of devolatilization, no common consensus exists. The same kinetic data for gasification and oxidation reactions are often used, since limited data can be found in the literature. The available kinetic data for heterogeneous reactions is therefore not able to account for the varying char reactivity dependent on the operational conditions the char has been formed in, and the wood species the char has been derived from.

The second part of the paper focuses on small-scale heating appliances. The chief features and their main aspects were listed and it is not surprising that an accurate bed model and its coupling to the gas phase can have a significant influence on the accuracy of the gas phase simulations.

The third part of the paper focuses on the bed model of large-scale grate furnaces. It was found that a number of simplifications are necessary to keep the model numerically efficient. The complexity of the bed model covers a broad span, ranging from purely empirical models, to advanced 3D CFD codes based on multi-phase approaches.

A list of the 11 most relevant recommendations for future development is presented below. These recommendations will yield more reliable simulation tools for both single particle degradation and small- and large-scale furnaces:

1. When using the thermal drying model, the evaporation temperature is recommended to be modeled as pressure-dependent, since it is expected that the internal wood particle pressure will significantly exceed atmospheric pressure, such that the assumption of drying at 373 K can result in false predictions.
2. Determine the influence of inorganics on the conversion of the solid phase.
3. Determine the volatile species composition for different wood species and conversion rates. As a consequence it is also possible to model ash deposit formation more accurately and predict ash-related internal furnace problems, and influence of ash deposit formation on the thermal efficiency of a furnace.
4. Define reaction pathways and determine precisely the products and reaction kinetics for gasification and oxidation reactions of char derived from wood devolatilization. In addition it is recommended to model char conversion as pressure dependent. This will result in a more accurate description of heat release as well as a more detailed modeling of reaction products that enter the gas phase model.

5. Development of multi-dimensional single particle models such that the diversity of wood particles can accurately be replicated. Multi-dimensional models would also account for anisotropy of the solid and non-homogeneous boundary conditions of a large particle, such as a wood log.

6. Development of a comprehensive, but numerically efficient single particle model that can accurately describe gas phase movement in the interior of the particle, therefore also accounting for internal pressure-related structural changes of the particle. Accurate internal pressure predictions require detailed knowledge of permeabilities of different wood species. Therefore, the database of experimentally defined permeabilities needs to be enlarged in the future.

7. Determination of soot formation reactions related to wood conversion processes, since significant influences on soot formation are expected, dependent on whether liquid, solid or gaseous hydrocarbons are reacting.

8. Develop a detailed model accounting for the NO_x formation, mainly due to fuel-bound nitrogen in large-scale grate furnaces as well as boilers and stoves, which balances a detailed description of the multi-step chemical evolution path and computational cost.

9. Development of a more realistic description of the wood log bed model in a small-scale heating appliance, accounting for touching of wood logs, bark-containing wood and the transient character of thermal wood conversion, which also includes initial heat-up and ignition. This is assumed to lead to a more accurate description of CO and unburnt hydrocarbon emissions.

10. Expand the computational domain of small-scale heating appliances, such that radiative and convective heat transfer into the surrounding room can be accurately modeled. This is assumed to be necessary if the purpose of the simulation tool is the optimization of small-scale heating appliances, since a stable heat release to the room is a chief feature.

11. Consideration of the influence of different materials used in the furnace on radiative heat losses, e.g. glass windows. Only in this case can the small-scale heating unit be fully optimized.

Acknowledgements

References

[1] Biswas AK, Umeki K. Simplification of devolatilization models for thermally-thick 1 particles: Differences between wood logs and pellets. Chemical Engineering Journal 2015;274:181–91.

[2] Basu P. Chapter 1 - Introduction. In: Basu P, editor. Biomass Gasification, Pyrolysis and Torrefaction. Second ed., Boston: Academic Press; 2013. p. 1–27.

[3] Zhang X, Chen Q, Bradford R, Sharifi V, Swithenbank J. Experimental investigation and mathematical modelling of wood combustion in a moving grate boiler. Fuel Processing Technology 2010;91(11):1491–9.

[4] Sousa N, Azevedo JLT. Model simplifications on biomass particle combustion. Fuel 2016;184:948–56.

[5] Ström H, Thunman H. A computationally efficient particle submodel for CFD-simulations of fixed-bed conversion. Applied Energy 2013;112:808–17.

[6] Daouk E, Van de Steene L, Paviet F, Salvador S. Thick wood particle pyrolysis in an oxidative atmosphere. Chemical Engineering Science 2015;126:608–15.

[7] Mehrabian R, Scharler R, Obernberger I. Effects of pyrolysis conditions on the heating rate in biomass particles and applicability of TGA kinetic parameters in particle thermal conversion modelling. Fuel 2012;93:567–75.

[8] Ström H, Thunman H. CFD simulations of biofuel bed conversion: A submodel for the drying and devolatilization of thermally thick wood particles. Combustion and Flame 2013;160(2):417–31.

[9] Gómez MA, Porteiro J, Patiño D, Míguez JL. Fast-solving thermally thick model of biomass particles embedded in a CFD code for the simulation of fixed-bed burners. Energy Conversion and Management 2015;105:30–44.

[10] Mehrabian R, Zahirovic S, Scharler R, Obernberger I, Kleditzsch S, Wirtz S, et al. A CFD model for thermal conversion of thermally thick biomass particles. Fuel Processing Technology 2012;95:96–108.

[11] Buczyński R, Weber R, Szlek A. Innovative design solutions for small-scale domestic boilers: Combustion improvements using a CFD-based mathematical model. Journal of the Energy Institute 2015;88(1):53–63.

[12] Skreiberg Ø, Seljeskog M, Georges L. The process of batch combustion of logs in wood stoves - transient modelling for generation of input to CFD modelling of stoves and thermal comfort simulations. Chemical Engineering Transactions 2015;43:433–8.

[13] Bugge M, Skreiberg Ø, Haugen NEL, Carlsson P, Seljeskog M. Predicting NO_x emissions from wood stoves using detailed chemistry and computational fluid dynamics. Energy Procedia 2015;75:1740–5.

[14] Scharler R, Benesch C, Neubeck A, Obernberger I. CFD based design and optimisation of wood log fired stoves. In: Proceedings of 17th European Biomass Conference and Exhibition. Hamburg, Germany; 2009. p. 1361–7.

[15] Chaney J, Liu H, Li J. An overview of CFD modelling of small-scale fixed-bed biomass pellet boilers with preliminary results from a simplified approach. Energy Conversion and Management 2012;63:149–56.

[16] Klason T, Bai XS. Combustion process in a biomass grate fired industry furnace: a cfd study. Progress in Computational Fluid Dynamics, An International Journal 2006;6(4-5):278–86.

[17] Scharler R, Obernberger I. Numerical modelling of biomass grate furnaces. In: Proceedings of the 5th European Conference on Industrial Furnaces and Boilers. Porto, Portugal: Rio Tinto, Portugal; April 2000. p. 1–17.

[18] Anca-Couce A. Reaction mechanisms and multi-scale modelling of lignocellulosic biomass pyrolysis. Progress in Energy and Combustion Science 2016;53:41–79.

[19] Neves D, Thunman H, Matos A, Tarelho L, Gómez-Barea A. Characterization and prediction of biomass pyrolysis products. Progress in Energy and Combustion Science 2011;37(5):611–30.

[20] Di Blasi C. Modeling chemical and physical processes of wood and biomass pyrolysis. Progress in Energy and Combustion Science 2008;34(1):47–90.

[21] Borman GL, Ragland KW. Combustion Engineering. McGraw-Hill series in mechanical engineering. First ed., Singapore: McGraw-Hill; 1998.

[22] Grønli MG. A theoretical and experimental study of thermal degradation of biomass [PhD thesis]. Trondheim: Norwegian University of Science and Technology; 1996.

[23] Kaltschmitt M, Hartmann H, Hofbauer H. Energie aus Biomasse: Grundlagen, Techniken und Verfahren. Second ed., Berlin: Springer; 2009.

[24] Patil RA. Cleavage of acetyl groups for acetic acid production in kraft pulp mills. Maine: University of Maine; 2012 Electronic theses and dissertations paper 1857 (2012).

[25] Adam M, Ocone R, Mohammad J, Berruti F, Briens C. Kinetic Investigations of Kraft Lignin Pyrolysis. Industrial & Engineering Chemistry Research 2013;52 (26):8645–54.

[26] Anca-Couce A, Obernberger I. Application of a detailed biomass pyrolysis kinetic scheme to hardwood and softwood torrefaction. Fuel 2016;167:158–67.

[27] Ranzi E, Cuoci A, Faravelli T, Frassoldati A, Migliavacca G, Pierucci S, et al. Chemical kinetics of biomass pyrolysis. Energy & Fuels 2008;22(6):4292–300.

[28] Mohanty AK, Misra M, Hinrichsen G. Biofibres, biodegradable polymers and biocomposites: An overview. Macromolecular Materials and Engineering 2000;276-277(1):1–24.

[29] Spiridon I, Popa VI. Chapter 13 - Hemicelluloses: Major Sources, Properties and Applications. In: Belgacem MN, Gandini A, editors. Monomers, Polymers and Composites from Renewable Resources. 1st ed. Amsterdam: Elsevier; 2008. p. 289–304.

[30] Obernberger I, Thek G. Physical characterisation and chemical composition of densified biomass fuels with regard to their combustion behaviour. Biomass and Bioenergy 2004;27(6):653–69.

[31] Döring S. Chapter 2: Biomass types for pellet production. In: Power from Pellets: Technology and Applications. -ed Berlin, Heidelberg: Springer Berlin Heidelberg; 2013. p. 13–30.

[32] NS 4414. Ns 4414 - ved til brensel i husholdninger. 1997.

[33] Simpson W, TenWolde A. Wood Handbook - Wood as an Engineering Material. General technical report FPL–GTR–113. Physical properties and moisture relations of wood. Forest Products Laboratory, U.S. Department of Agriculture; 1999. p. 3.1–3.24.

[34] Alves SS, Figueiredo JL. A model for pyrolysis of wet wood. Chemical Engineering Science 1989;44(12):2861–9.

[35] Koufopanos C, Papayannakos N, Maschio G, Lucchesi A. Modelling of the pyrolysis of biomass particles. studies on kinetics, thermal and heat transfer effects. The Canadian Journal of Chemical Engineering 1991;69:907–15.

[36] Di Blasi C. On the influence of physical processes on the transient pyrolysis of cellulosic samples. Fire Safety Science 4 1994: 229–40.

[37] Di Blasi C. Heat, momentum and mass transport through a shrinking biomass particle exposed to thermal radiation. Chemical Engineering Science 1996;51(7):1121–32.

[38] Melaaen MC. Numerical analysis of heat and mass transfer in drying and pyrolysis of porous media. Numerical Heat Transfer, Part A: Applications 1996;29(4):331–55.

[39] Di Blasi C. Physico-chemical processes occurring inside a degrading two-dimensional anisotropic porous medium. International Journal of Heat and Mass Transfer 1998;41(24):4139–50.

[40] Grønli MG, Melaaen MC. Mathematical Model for Wood Pyrolysis - Comparison of Experimental Measurements with Model Predictions. Energy & Fuels 2000;14(4):791–800.

[41] Larfeldt J, Leckner B, Melaaen MC. Modelling and measurements of the pyrolysis of large wood particles. Fuel 2000;79(13):1637–43.

[42] Bryden KM, Ragland KW, Rutland CJ. Modeling thermally thick pyrolysis of wood. Biomass and Bioenergy 2002;22(1):41–53.

[43] Hagge MJ, Bryden KM. Modeling the impact of shrinkage on the pyrolysis of dry biomass. Chemical Engineering Science 2002;57(14):2811–23.

[44] Thunman H, Leckner B, Niklasson F, Johnsson F. Combustion of wood particles - A particle model for Eulerian calculations. Combustion and Flame 2002;129(1-2):30–46.

[45] Wurzenberger J, Wallner S, Raupenstrauch H, Khinast J. Thermal conversion of biomass: comprehensive reactor and particle modeling. AIChE J 2002;48:2398–411.

[46] Bruch C, Peters B, Nussbaumer T. Modelling wood combustion under fixed bed conditions. Fuel 2003;82(6):729–38.

[47] Bryden KM, Hagge MJ. Modeling the combined impact of moisture and char shrinkage on the pyrolysis of a biomass particle. Fuel 2003;82(13):1633–44.

[48] Babu BV, Chaurasia AS. Heat transfer and kinetics in the pyrolysis of shrinking biomass particle. Chemical Engineering Science 2004;59:1999–2012.

[49] de Souza Costa F, Sandberg D. Mathematical model of a smoldering log. Combustion and Flame 2004;139(3):227–38.

[50] Galgano A, Di Blasi C. Coupling a CFD code with a solid-phase combustion model. Progress in Computational Fluid Dynamics 2006;6:287–302.

[51] Galgano A, Di Blasi C, Horvat A, Sinai Y. Experimental validation of a coupled solid- and gas-phase model for combustion and gasification of wood logs. Energy & Fuels 2006;20(5):2223–32.

[52] Porteiro J, Míguez JL, Granada E, Moran JC. Mathematical modelling of the combustion of a single wood particle. Fuel Processing Technology 2006;87(2):169–75.

[53] Porteiro J, Granada E, Collazo J, Patiño D, Morán JC. A Model for the Combustion of Large Particles of Densified Wood. Energy & Fuels 2007;21(6):3151–9.

[54] Shen DK, Fang MX, Luo ZY, Cen KF. Modeling pyrolysis of wet wood under external heat flux. Fire Safety Journal 2007;42(3):210–7.

[55] Yuen RKK, Yeoh GH, de Vahl Davis G, Leonardi E. Modelling the pyrolysis of wet wood I. three-dimensional formulation and analysis. International Journal of Heat and Mass Transfer 2007;50(21–22):4371–86.

[56] Sand U, Sandberg J, Larfeldt J, Bel Fdhila R. Numerical prediction of the transport and pyrolysis in the interior and surrounding of dry and wet wood log. Applied Energy 2008;85(12):1208–24.

[57] Yang YB, Sharifi VN, Swithenbank J, Ma L, Darvell LI, Jones JM, et al. Combustion of a single particle of biomass. Energy& Fuel 2008;22:306–16.

[58] Sadhukhan AK, Gupta P, Saha RK. Modelling of pyrolysis of large wood particles. Bioresource technology 2009;100(12):3134–9.

[59] Haseli Y, van Oijen JA, de Goey LPH. A simplified pyrolysis model of a biomass particle based on infinitesimally thin reaction front approximation. Energy & Fuels 2012;26(6):3230–43.

[60] Galgano A, Di Blasi C, Ritondale S, Todisco A. Numerical simulation of the glowing combustion of moist wood by means of a front-based model. Fire and Materials 2014;38(6):639–58.

[61] Kwiatkowski K, Bajer K, Celińska A, Dudyński M, Korotko J, Sosnowska M. Pyrolysis and gasification of a thermally thick wood particle - Effect of fragmentation. Fuel 2014;132:125–34.

[62] Pozzobon V, Salvador S, Bézian JJ, El-Hafi M, Maoult YL, Flamant G. Radiative pyrolysis of wet wood under intermediate heat flux: Experiments and modelling. Fuel Processing Technology 2014;128:319–30.

[63] Seljeskog M, Skreiberg Ø. Batch combustion of logs in wood stoves - Transient fuel models and modelling of the fuel decomposition and products composition as input to CFD gas phase calculation. First International workshop on CFD and Biomass Thermochemical conversion. Leipzig, Germany; 2014. p. 39–44.

[64] Ding Y, Wang C, Lu S. Modeling the pyrolysis of wet wood using FireFOAM. Energy Conversion and Management 2015;98:500–6.

[65] Basu P. - pyrolysis. In: Basu P, editor. Biomass Gasification, Pyrolysis and Torrefaction. 2nd ed., Boston: Academic Press; 2013. p. 147–76.

[66] Plötze M, Niemz P. Porosity and pore size distribution of different wood types as determined by mercury intrusion porosimetry. European Journal of Wood and Wood Products 2011;69(4):649–57.

[67] Kansa EJ, Perlee HE, Chaiken RF. Mathematical model of wood pyrolysis including internal forced convection. Combustion and Flame 1977;29:311–24.

[68] Galgano A, Di Blasi C. Modeling wood degradation by the unreacted-core-shrinking approximation. Industrial & Engineering Chemistry Research 2003;42(10):2101–11.

[69] Galgano A, Di Blasi C. Modeling the propagation of drying and decomposition fronts in wood. Combustion and Flame 2004;139(12):16–27.

[70] Spolek GA, Plumb OA. Capillary pressure in softwoods. Wood Science and Technology 1981;15(3):189–99.

[71] Perre P, Degiovanni A. Control-volume formulation of simultaneous transfer in anisotropic porous-media - simulations of softwood drying at low and high temperature. International Journal of Heat and Mass Transfer 1990;33:2463–78.

[72] Fogler HS. Elements of Chemical Reaction Engineering. New Jersey: Prentice Hall International Editions; 1986.

[73] Bear J, Buchlin JM. Modelling and applications of transport phenomena in porous media. In: Bear J, Buchlin JM, editors. Dordrecht: Kluwer Academic Publishers Dordrecht; 1991.

[74] Park WC, Atreya A, Baum HR. Experimental and theoretical investigation of heat and mass transfer processes during wood pyrolysis. Combustion and Flame 2010;157(3):481–94.

[75] Demirbas A. Hydrocarbons from pyrolysis and hydrolysis processes of biomass. Energy Sources 2003;25(1):67–75.

[76] Moffat RJ, Kays WM. The turbulent boundary layer on a porous plate: Experimental heat transfer with uniform blowing and suction. International Journal of Heat and Mass Transfer 1968;11(10):1547–66.

[77] Fatehi H, Bai XS. A comprehensive mathematical model for biomass combustion. Combustion Science and Technology 2014;186(4-5):574–93.

[78] Lu H, Robert W, Peirce G, Ripa B, Baxter LL. Comprehensive study of biomass particle combustion. Energy & Fuels 2008;22(4):2826–39.

[79] Saastamoinen J, Richard JR. Simultaneous drying and pyrolysis of solid fuel particles. Combustion and Flame 1996;106(3):288–300.

[80] Font R, Marcilla A, Verdu E, Devesa J. Kinetics of the pyrolysis of almond shells and almond shells impregnated with CoCl2 in a fluidized bed reactor and in a Pyroprobe 100. Industrial and Engineering Chemistry Research 1990;29(9):1846–55.

[81] Chan WCR, Kelbon M, Krieger BB. Modelling and experimental verification of physical and chemical processes during pyrolysis of a large biomass particle. Fuel 1985;64(11):1505–13.

[82] Di Blasi C. Modeling and simulation of combustion processes of charring and non-charring solid fuels. Progress in Energy and Combustion Science 1993;19(1):71–104.

[83] Sharma A, Pareek V, Zhang D. Biomass pyrolysis - A review of modelling, process parameters and catalytic studies. Renewable and Sustainable Energy Reviews 2015;50:1081–96.

[84] Di Blasi C. Comparison of semi-global mechanisms for primary pyrolysis of lignocellulosic fuels. Journal of Analytical and Applied Pyrolysis 1998;47(1):43–64.

[85] Ranzi E, Pierucci S, Aliprandi PC, Stringa S. Comprehensive and detailed kinetic model of a traveling grate combustor of biomass. Energy & Fuels 2011;25(9):4195–205.

[86] Hashimoto K, Hasegawa I, Hayashi J, Mae K. Correlations of kinetic parameters in biomass pyrolysis with solid residue yield and lignin content. Fuel 2011;90(1):104–12.

[87] Miller RS, Bellan J. A generalized biomass pyrolysis model based on superimposed cellulose, hemicelluloseand liqnin kinetics. Combustion Science and Technology 1997;126(1-6):97–137.

[88] Wichman IS, Oladipo AB. Examination of three pyrolytic reaction schemes for cellulosic materials. Fire safety science 4 1994: 313–23.

[89] Thurner F, Mann U. Kinetic investigation of wood pyrolysis. Industrial & Engineering Chemistry Process Design and Development 1981;20(3):482–8.

[90] Hajaligol MR, Howard JB, Longwell JP, Peters WA. Product compositions and kinetics for rapid pyrolysis of cellulose. Industrial & Engineering Chemistry Process Design and Development 1982;21(3):457–65.

[91] Di Blasi C. Analysis of convection and secondary reaction effects within porous solid fuels undergoing pyrolysis. Combustion Science and Technology 1993;90(5-6):315–40.

[92] Di Blasi C, Branca C. Kinetics of primary product formation from wood pyrolysis. Industrial & Engineering Chemistry Research 2001;40(23):5547–56.

[93] Nunn TR, Howard JB, Longwell JP, Peters WA. Product compositions and kinetics in the rapid pyrolysis of sweet gum hardwood. Industrial & Engineering Chemistry Process Design and Development 1985;24(3):836–44.

[94] Papari S, Hawboldt K. A review on the pyrolysis of woody biomass to bio-oil: Focus on kinetic models. Renewable and Sustainable Energy Reviews 2015;52:1580–95.

[95] Rath J, Wolfinger MG, Steiner G, Krammer G, Barontini F, Cozzani V. Heat of wood pyrolysis. Fuel 2003;82(1):81–91.

[96] van de Velden M, Baeyens J, Brems A, Janssens B, Dewil R. Fundamentals, kinetics and endothermicity of the biomass pyrolysis reaction. Renewable Energy 2010;35(1):232–42.

[97] Branca C, Albano A, Di Blasi C. Critical evaluation of global mechanisms of wood devolatilization. Thermochimica Acta 2005;429(2):133–41.

[98] Orfão JJM, Antunes FJA, Figueiredo JL. Pyrolysis kinetics of lignocellulosic material - three independent reactions model. Fuel 1999;78(3):349–58.

[99] Manyà JJ, Velo E, Puigjaner L. Kinetics of Biomass Pyrolysis: A Reformulated Three-Parallel-Reactions Model. Industrial & Engineering Chemistry Research 2003;42(3):434–41.

[100] Turner I, Rousset P, Remond R, Perre P. An experimental and theoretical investigation of the thermal treatment of wood (Fagus sylvatica L.) in the range 200 - 260 °C. International Journal of Heat and Mass Transfer 2010;53(4):715–25.

[101] Hosoya T, Kawamoto H, Saka S. Cellulose-hemicellulose and cellulose-lignin interactions in wood pyrolysis at gasification temperature. Journal of Analytical and Applied Pyrolysis 2007;80(1):118–25.

[102] Shafizadeh F. Introduction to pyrolysis of biomass. Journal of Analytical and Applied Pyrolysis 1982;3(4):283–305.

[103] Mamleev V, Bourbigot S, Yvon J. Kinetic analysis of the thermal decomposition of cellulose: The main step of mass loss. Journal of Analytical and Applied Pyrolysis 2007;80(1):151–65.

[104] Seebauer V. Experimentelle untersuchungen zur pyrolyse von kohle und holz. [PhD thesis], Graz: Graz University of Technology; 1999.

[105] Glaister DS. The prediction of chemical kinetic, heat, and mass transfer processes during the one- and two-dimensional pyrolysis of a large wood pellet. Seattle: University of Washington; 1987 Master's thesis.

[106] Levenspiel O. Chapter 25: Fluid-Particle reactions: Kinetics. In: Santor K, editor. Chemical reaction engineering. 3rd ed. New York: John Wiley and Sons, Inc.; 1972. p. 566–88.

[107] Septien S, Valin S, Peyrot M, Dupont C, Salvador S. Characterization of char and soot from millimetric wood particles pyrolysis in a drop tube reactor between 800 °C and 1400 °C. Fuel 2014;121:216–24.

[108] Shin D, Choi S. The combustion of simulated waste particles in a fixed bed. Combustion and Flame 2000;121(1-2):167–80.

[109] Dasappa S, Sridhar H, Paul P, Mukunda H, Shrinivasa U. On the combustion of wood-char spheres in O_2/N_2 mixtures-experiments and analysis. Symposium (International) on Combustion 1994;25(1):569–76.

[110] Fatehi H, Bai XS. Effect of pore size on the gasification of biomass char. Energy Procedia 2015;75:779–85.

[111] Hurt RH, Sarofim AF, Longwell JP. The role of microporous surface area in the gasification of chars from a sub-bituminous coal. Fuel 1991;70(9):1079–82.

[112] Ballal G, Zygourakis K. Evolution of pore surface area during noncatalytic gas-solid reactions. 2. experimental results and model validation. Industrial & Engineering Chemistry Research 1987;26(9):1787–96.

[113] Chi WK, Perlmutter DD. The effect of pore structure on the char-steam reaction. AIChE Journal 1989;35(11):1791–802.

[114] Dutta S, Wen CY. Reactivity of coal and char. 2. in oxygen-nitrogen atmosphere. Industrial & Engineering Chemistry Process Design and Development 1977;16(1):31–7.

[115] Di Blasi C, Buonanno F, Branca C. Reactivities of some biomass chars in air. Carbon 1999;37(8):1227–38.

[116] Lu H. Experimental and modelling investigation of biomass particle combustion [PhD thesis]. Provo, Utah: Brigham Young University; 2006.

[117] Forest Products Laboratory. Wood Handbook - Wood as an Engineering Material. General Technical Report FPL–GTR–190. Madison, Wisconsin: U.S. Department of Agriculture; 1999.

[118] Scott DS, Piskorz J, Bergougnou MA, Graham R, Overend RP. The role of temperature in the fast pyrolysis of cellulose and wood. Industrial & Engineering Chemistry Research 1988;27(1):8–15.

[119] Pyle DL, Zaror CA. Heat transfer and kinetics in the low temperature pyrolysis of solids. Chemical Engineering Science 1984;39:147–58.

[120] Gauthier G. Synthèse de biocarburants de deuxième génération: étude de la pyrolyse à haute température de particules de bois centimétriques. Thèse de doctorat dirigée, Ecole nationale des Mines d'Albi-Carmaux; 2013.

[121] Bellais M, Davidsson KO, Liliedahl T, Sjöström K, Pettersson JBC. Pyrolysis of large wood particles: a study of shrinkage importance in simulations. Fuel 2003;82(12):1541–8.

[122] Paulauskas R, Džiugys A, Striūgas N. Experimental investigation of wood pellet swelling and shrinking during pyrolysis. Fuel 2015;142:145–51.

[123] Athanasios N, Nikolopoulos N, Nikolaos M, Panagiotis G, Kakaras E. Optimization of a log wood boiler through CFD simulation methods. Fuel Processing Technology 2015;137:75–92.

[124] Porteiro J, Collazo J, Patiño D, Granada E, Gonzalez JCM, Míguez JL. Numerical modeling of a biomass pellet domestic boiler. Energy & Fuels 2009;23:1067–75.

[125] Knaus H, Richter S, Unterberger S, Schnell U, Maier H, Hein KRG. On the application of different turbulence models for the computation of fluid flow and combustion processes in small scale wood heaters. Experimental Thermal and Fluid Science 2000;21(1-3):99–108.

[126] Huttunen M, Saastamoinen J, Kilpinen P, Kjäldman L, Oravainen H, Boström S. Emission formation during wood log combustion in fireplaces - part I: volatile combustion stage. Progress in Computational Fluid Dynamics 2006;6(4–5):200–8.

[127] Menghini D, Marra FS. A model of wood logs combustion for CFD simulations. In: Proceedings of 16th European Biomass Conference and Exhibition. Valencia, Spain; 2008. p. 1407–14.

[128] Tabet F, Fichet V, Plion P. A comprehensive CFD based model for domestic biomass heating systems. Journal of the Energy Institute 2016;89(2):199–214.

[129] Zahirovic S. CFD analysis of gas phase combustion and NO_x formation in biomass packed-bed furnaces: a contribution towards quantitative prediction of CO and NO_x emissions [Dissertation]. Graz, Austria: Institut für Prozess- und Partikeltechnik, Graz Univeristy of Technology, Austria; 2008.

[130] Bugge M, Skreiberg Ø, Haugen NEL, Carlsson P, Houshfar E, Løvås T. Numerical simulations of staged biomass grate fired combustion with an emphasis on NO_x emissions. Energy Procedia 2015;75:156–61.

[131] Løvås T, Houshfar E, Bugge M, Skreiberg Ø. Automatic generation of kinetic skeletal mechanisms for biomass combustion. Energy & Fuels 2013;27(11):6979–91.

[132] Bugge M, Haugen NEL, Skreiberg Ø. NO_x emission from wood stoves - a CFD modelling approach. In: Proceedings of 22nd European Biomass Conference and Exhibition. Hamburg, Germany; 2014. p. 676–9.

[133] Penner JE, Chuang CC, Grant K. Climate forcing by carbonaceous and sulfate aerosols. Climate Dynamics 1998;14(12):839–51.

[134] Grant KE, Chuang CC, Grossman AS, Penner JE. Modeling the spectral optical properties of ammonium sulfate and biomass burning aerosols: parameterization of relative humidity effects and model results. Atmospheric Environment 1999;33(17):2603–20.

[135] Cooke WF, Liousse C, Cachier H, Feichter J. Construction of a 1° x 1° fossil fuel emission data set for carbonaceous aerosol and implementation and radiative impact in the echam4 model. Journal of Geophysical Research: Atmospheres 1999;104(D18):22137–62.

[136] Fitzpatrick EM, Jones JM, Pourkashanian M, Ross AB, Williams A, Bartle KD. Mechanistic aspects of soot formation from the combustion of pine wood. Energy & Fuels 2008;22(6):3771–8.

[137] Fitzpatrick EM, Ross A, Jones JM, Willians A. Formation of soot and oxygenated species from wood combustion. European Combustion Meeting 2007. Chania, Greece; 2007.

[138] Fitzpatrick EM, Ross A, Jones JM, Willians A. Smoke produced from combustion of biomass. 15th Biomass Conference and Exhibition. Berlin, Germany; 2007.

[139] Cypres R, Bettens B. Mecanismes de fragmentation pyrolytique du phenol et des cresols. Tetrahedron 1974;30(10):1253–60.

[140] Cypres R, Bettens B. Pyrolyse thermique des [^{14}C] et [^{3}H] ortho et para-cresols. Tetrahedron 1975;31(4):353–7.

[141] Cypres R, Bettens B. La formation de la plupart des composes aromatiques produits lors de la pyrolyse du phenol, ne fait pas intervenir le carbone porteur de la fonction hydroxyle. Tetrahedron 1975;31(4):359–65.

[142] Spielmann R, Cramers CA. Cyclopentadienic compounds as intermediates in the thermal degradation of phenols. kinetics of the thermal decomposition of cyclopentadiene. Chromatographia 1972;5(12):295–300.

[143] Mulholland JA, Lu M, Kim D-H. Pyrolytic growth of polycyclic aromatic hydrocarbons by cyclopentadienyl moieties. Proceedings of the Combustion Institute 2000;28(2):2593–9.

[144] Lu M, Mulholland JA. PAH growth from the pyrolysis of CPD, indene and naphthalene mixture. Chemosphere 2004;55(4):605–10.

[145] Melius CF, Colvin ME, Marinov NM, Pit WJ, Senkan SM. Reaction mechanisms in aromatic hydrocarbon formation involving the C_5H_5 cyclopentadienyl moiety. Symposium (International) on Combustion 1996;26(1):685–92.

[146] Koziński J, Saade R. Effect of biomass burning on the formation of soot particles and heavy hydrocarbons. an experimental study. Fuel 1998;77(4):225–37.

[147] Liu F, Guo H, Smallwood G, Gülder O. The chemical effects of carbon dioxide as an additive in an ethylene diffusion flame: Implications for soot and NO_x formation. Combustion and Flame 2001;125(1-2):778–87.

[148] Wijayanta AT, Alam MS, Nakaso K, Fukai J, Shimizu M. Optimized combustion of biomass volatiles by varying O_2 and CO_2 levels: A numerical simulation using a highly detailed soot formation reaction mechanism. Bioresource Technology 2012;110:645–51.

[149] Ergut A, Granata S, Jordan J, Carlson J, Howard JB, Richter H, et al. PAH formation in one-dimensional premixed fuel-rich atmospheric pressure ethylbenzene and ethyl alcohol flames. Combustion and Flame 2006;144(4):757–72.

[150] Brookes SJ, Moss JB. Predictions of soot and thermal radiation properties in confined turbulent jet diffusion flames. Combustion and Flame 1999;116(4):486–503.

[151] Magnussen BF, Hjertager BH. On mathematical modeling of turbulent combustion with special emphasis on soot formation and combustion. Symposium (International) on Combustion 1977;16(1):719–29.

[152] Tesner PA, Smegiriova TD, Knorre VG. Kinetics of dispersed carbon formation. Combustion and Flame 1971;17(2):253–60.

[153] Brown AL, Fletcher TH. Modeling soot derived from pulverized coal. Energy & Fuels 1998;12(4):745–57.

[154] Scharler R, Benesch C, Schulze K, Obernberger I. CFD simulations as efficient tool for the development and optimization of small-scale biomass furnaces and stoves. In: Proceedings of 19th European Biomass Conference and Exhibition. Berlin, Germany; 2011. p. 4–12.

[155] Huttunen M, Saastamoinen J, Kilpinen P, Kjäldman L, Oravainen H, Boström S. Emission formation during wood log combustion in fireplaces - part II: char combustion stage. Progress in Computational Fluid Dynamics 2006;6(4–5):209–16.

[156] Buchmayr M, Gruber J, Hargassner M, Hochenauer C. A computationally inexpensive CFD approach for small-scale biomass burners equipped with enhanced air staging. Energy Conversion and Management 2016;115:32–42.

[157] Veynante D, Vervisch L. Turbulent combustion modeling. Progress in Energy and Combustion Science 2002;28(3):193–266.

[158] Fluent Inc. Choosing a radiation model. https://www.sharcnet.ca/Software/Fluent6/html/ug/node583.htm; 2006 [accessed: March 2, 2017].

[159] Fluent Inc. Discrete transfer radiation model (DTRM) theory. https://www.sharcnet.ca/Software/Fluent6/html/ug/node579.htm; 2006 [accessed: March 2, 2017].

[160] Fluent Inc. Rosseland radiation model theory. https://www.sharcnet.ca/Software/Fluent6/html/ug/node578.htm; 2006 [accessed: March 2, 2017].

[161] Fluent Inc. P-1 radiation model theory. https://www.sharcnet.ca/Software/Fluent6/html/ug/node577.htm; 2006 [accessed: March 2, 2017].

[162] Granada E, Lareo G, Míguez JL, Moran J, Porteiro J, Ortiz L. Feasibility study of forest residue use as fuel through co-firing with pellet. Biomass and Bioenergy 2006;30(3):238–46.

[163] Patiño D, Moran J, Porteiro J, Collazo J, Granada E, Míguez JL. Improving the cofiring process of wood pellet and refuse derived fuel in a small-scale boiler plant. Energy & Fuels 2008;22(3):2121–8.

[164] Bryden KM, Ragland KW. Numerical modeling of a deep, fixed bed combustor. Energy & Fuels 1996;10(2):269–75.

[165] Kilpinen P, Ljung M, Bostrom S, Hupa M. Final report of the tulisija programme 1997 -1999. Tech. Rep. Abo Akademi Unversity, Tulisija Coordination; 2000.

[166] Kilpinen P, Ljung M, Bostrom S, Hupa M. TULISIJA technical review, 1997 - 1999. Tech. Rep. Abo Akademi Unversity, Tulisija Coordination; 2000.

[167] Lam CKG, Bremhorst K. A modified form of the k-epsilon model for predicting wall turbulence. ASME Transactions Journal of Fluids Engineering 1981;103:456–60.

[168] Hill S, Smoot L, Smith P. Prediction of nitrogen oxide formation in turbulent coal flames. Proceedings of the Combustion Institute 1985;20(1):1391–400.

[169] Lockwood FC, Shah NG. A new radiation solution method for incorporation in general combustion prediction procedures. Symposium (International) on Combustion 1981;18(1):1405–14.

[170] Coppalle A, Vervisch P. The total emissivities of high-temperature flames. Combustion and Flame 1983;49(1):101–8.

[171] Taylor PB, Foster PJ. Some gray gas weighting coefficients for CO_2-H_2O-soot mixtures. International Journal of Heat and Mass Transfer 1975;18(11):1331–2.

[172] Biedermann F, Obernberger I. Ash-related problems during biomass combustion and possibilities for a sustainable ash utilisation. In: Proceedings of the International Conference 'World Renewable Energy Congress (WREC)'. Aberdeen, Scotland: Elsevier Ltd., Oxford, UK; May 2005.

[173] Yin C, Rosendahl LA, Kær SK. Grate-firing of biomass for heat and power production. Progress in Energy and Combustion Science 2008;34(6):725–54.

[174] Kurz D, Schnell U, Scheffknecht G. CFD simulation of wood chip combustion on a grate using an Euler-Euler approach. Combustion Theory and Modelling 2012;16(2):251–73.

[175] Griselin N, Bai XS. Particle dynamics in a biomass fired furnace predictions of solid residence changes with operation. IFRF Combustion Journal 2000 (October).

[176] Lindsjö H, Bai XS, Fuchs L. Numerical and experimental studies of NO_x emissions in a biomass furnace. International Journal on Environmental Combustion Technologies 2001(2):93–113.

[177] Scharler R, Obernberger I, Längle G, Heinzle J. CFD analysis of air staging and flue gas recirculation in biomass grate furnaces. In: Proceedings of the 1st World Conference on Biomass for Energy and Industry. Sevilla, Spain; June 2000. p. 1935–9.

[178] Keller R. Primärmaßnahmen zur NO_x Minderung bei der Holzverbrennung mit dem Schwerpunkt der Luftstufung. forschungsbericht nr. 18. Tech. Rep. ETH Zürich, Switzerland: Laboratorium für Energiesysteme; 1994.

[179] Weissinger A, Obernberger I. NO_x reduction by primary measures on a travelling - grate furnace for biomass fuels and waste wood. In: Proceedings of the 4th Biomass Conference of the Americas. Oakland, USA: Elsevier Science Ltd., Oxford, UK; September 1999. p. 1417–25.

[180] Skreiberg Ø. Theoretical and experimental studies on emissions from wood combustion. Tech. Rep. ITEV Report 97:03. Trondheim, Norway: The Norwegian University of Science and Technology; 1997.

[181] Scharler R, Obernberger I. Deriving guidelines for the design of biomass grate furnaces with CFD analysis - a few mutlifuel-low-NO_x furnace as example. In: Proceedings of 6th European conference on industrial furnaces and boilers. Portugal; April 2002. p. 227–41.

[182] Scharler R, Widmann E, Obernberger I. CFD modelling of NO_x formation in biomass grate furnaces with detailed chemistry. In: Proc. of the Internat. Conf. Science in Thermal and Chemical Biomass Conversion. Victoria, Vancouver Island, BC, Canada; 2004. p. 284–300.

[183] Obernberger I, Widmann E, Scharler R. Entwicklung eines Abbrandmodells und eines NO_x-Postprozessors zur Verbesserung der CFD-simulation von Biomasse-Festbettfeuerungen. berichte aus energie-und umweltforschung no. 31/(2003). Tech. Rep. Vienna, Austria: Ministry for Transport, Innovation and Technology; 2003.

[184] Costa M, Massarotti N, Indrizzi V, Rajh B, Yin C, Samec N. Engineering bed models for solid fuel conversion process in grate-fired boilers. Energy 2014;77:244–53.

[185] Yin C, Rosendahl L, Clausen S, Hvid SL. Characterizing and modeling of an 88 mw grate-fired boiler burning wheat straw: Experience and lessons. Energy 2012;41(1):473–82.

[186] Rajh B, Yin C, Samec N, Hriberšek M, Zadravec M. Advanced modelling and testing of a 13 MW_{th} waste wood-fired grate boiler with recycled flue gas. Energy Conversion and Management 2016;125:230–41.

[187] Huttunen M, Kjäldman L, Saastamoinen J. Analysis of grate firing of wood with numerical flow simulation. IFRF Combustion Journal 2004 (Article no. 200401).

[188] Boriouchkine A, Zakharov A, Jämsä-Jounela SL. Dynamic modeling of combustion in a biograte furnace: The effect of operation parameters on biomass firing. Chemical Engineering Science 2012;69(1):669–78.

[189] Thunman H, Niklasson F, Johnsson F, Leckner B. Composition of volatile gases and thermochemical properties of wood for modeling of fixed or fluidized beds. Energy & Fuels 2001;15(6):1488–97.

[190] Chen Q, Zhang X, Zhou J, Sharifi VN, Swithenbank J. Effects of flue gas recirculation on emissions from a small scale wood chip fired boiler. Energy Procedia 2015;66:65–8.

[191] Yang YB, Goh YR, Zakaria R, Nasserzadeh V, Swithenbank J. Mathematical modelling of MSW incineration on a travelling bed. Waste Management 2002;22(4):369–80.

[192] Hermansson S, Thunman H. CFD modelling of bed shrinkage and channelling in fixed-bed combustion. Combustion and Flame 2011;158(5):988–99.

[193] Liu S-l, Amundson NR. Stability of adiabatic packed bed reactors. an elementary treatment. Industrial & Engineering Chemistry Fundamentals 1962;1(3):200–8.

[194] Eigenberger G. On the dynamic behavior of the catalytic fixed-bed reactor in the region of multiple steady states -i. the influence of heat conduction in two phase models. Chemical Engineering Science 1972;27(11):1909–15.

[195] Di Blasi C. Dynamic behaviour of stratified downdraft gasifiers. Chemical Engineering Science 2000;55(15):2931–44.

[196] Saastamoinen J, Taipale R, Horttanainen M, Sarkomaa P. Propagation of the ignition front in beds of wood particles. Combustion and Flame 2000;123(1-2):214–26.

[197] Deydier A, Marias F, Bernada P, Couture F, Michon U. Equilibrium model for a travelling bed gasifier. Biomass and Bioenergy 2011;35(1):133–45.

[198] Hajek J, Jurena T. Modelling of 1 MW solid biomass combustor: Simplified balance-based bed model coupled with freeboard CFD simulation. Chemical Engineering Transactions 2012;29:745–50.